

**A COMPARISON OF CONVENTIONAL AND UNCONVENTIONAL
REDUCTANTS THROUGH CHARACTERIZATION AND REACTIVITY TESTS
ON SOLID STATE CHROMITE REDUCTION FOR APPLICATION IN THE
SOUTH AFRICAN FERROCHROME INDUSTRY**

Aaron Chiwoko – Student No: 784933

A research report submitted to the Faculty of Engineering and the Built Environment, of the University of the Witwatersrand, in partial fulfilment of the requirements for the degree of Master of Science in Engineering.

School of Chemical, Metallurgy and Materials Engineering

DECLARATION

I declare that this research report is my own, unaided work. It is being submitted for the Degree of Masters of Science at the University of the Witwatersrand, Johannesburg.

It has not been submitted before for any degree or examination in any University.

Aaron Chiwoko

_____ Day of _____ 2018

ABBREVIATIONS, ACRONYMS AND NOMENCLATURE

Abbreviations, Acronyms and Nomenclature	Description
AAS	Atomic Absorption Spectroscopy
Ab	Air Basis
AC	Alternate Current
BSE	Backscattered Electrons
CCr	Charge Chrome
CRI	Coke Reactivity Index
CRP	Coke Reactivity Potential
CSN	Crucible Swelling index
CSR	Coke Strength after Reaction
CV	Calorific Value
Db	Dry Basis
DC	Direct Current
deg C	Degrees Celsius
DOM	Degree of Metallisation
DOR	Degree of Reduction
EDS	Energy Dispersive Spectrometer
EPA	Environmental Protection Agency
FC	Fixed Carbon
FeSiCr	Ferrochrome- Ferrosilicon Chrome
FSI	Free Swelling Index
GDP	Growth Domestic Product
H, M, & LCFeCr	High, Medium & Low Carbon Ferrochrome
H/C	Hydrogen Carbon Ratio
HGI	Hardgrove grindability index
Hrs	Hours
I ₄₀ , I ₁₀	IRSID Indices (Institute de Recherche Sidérurgique)

Abbreviations, Acronyms and Nomenclature	Description
ICCP	International Coal And Coking Programme
ICPOES	Inductively Coupled Plasma Optical Emission Spectrometer
LG6	Lower Group Six Chromite
ΔG	Gibbs Free Energy of Formation
Θ	Angle Between Incident & Diffracted Beam
K	Rate Constant
M ₁₀ , M ₂₅ and M ₄₀	Micum Indices
NMR	Nippon Steel Corporation
O/C	Oxygen Carbon Ratio
PGM's	Platinum Group Metals
PSD	Particle Size Distribution
Ro, max	Maximum Vitrinite Reflectance
Rr%	Random Reflectance
SAF	Submerged-arc Furnaces
SE	Secondary Electrons
SEM	Scanning electron Microscope
SRC	State Reduction of Chromite
SSCC	Semi-soft Coking Coal
T	Temperature
T	Time
TEM	Transmission Electron Microscope
TGA	Thermogravimetric Analysis
UG2	Upper Group Two Chromite
VM	Volatile Matter
XRD	X-ray Diffraction
XRF	X-Ray Fluorescence
Λ	X-Ray Wavelength
σ	Standard Deviation

ABSTRACT

Reductants form a significant portion of the production costs during ferroalloys processing. Consequently, the need arises to cut costs and drive profitability through raw materials optimization, *viz*, reductants. Unconventional reductants are expected to have a high reactivity and fixed carbon content, but their current availabilities are low. Innovation together with substitution has become a necessity to ensure sustainability and competitiveness of processing operations. The main objective of this research was to study and compare the reactivity of commonly used reductants and that of readily available, new sustainable carbon materials as potential reductants for the reduction of natural chromite at steady state. The selected reductants comprise of conventional Reductants A (Market Coke), B and B1 (Trial Market Cokes), C (Industrial Char) and unconventional Reductant D (Charcoal).

This investigation was undertaken by initially characterizing the reductants with the use of advanced analytical techniques including proximate, ultimate, particle size distribution and petrography and then to determine the merits and demerits of each in typical ferrochrome processes. This was followed by reactivity tests in the solid state at temperatures ranging from 1100°C, 1200°C, 1300°C to 1400°C and over a 4 hour period. A thermo-gravimetric analysing (TGA) furnace was used with tests undertaken under inert atmosphere in order to determine the practical performance and application of each reductant. Data collected from a series of TGA furnace campaigns was utilised to determine the reactivity of the selected reductants. Analytical methods of chemical speciation, XRD and SEM-EDS were applied to confirm the extent of chromite reduction.

The outcome of this research project indicated that the best reductants according to overall mass loss were D (122.03%), C (112.97%), A

(91.61%), B (90.51%) and B1 (80.72%), consecutively in reducing order. Whilst the unconventional Reductant D was shown to be most reactive and having the highest mass loss at test temperatures 1100°C -1300°C, all conventional reductants performed better than the unconventional reductant at 1400°C. At this temperature, Reductant B had the highest mass loss of 51.5% followed by Reductants A (47.7%), B1 (44.1%), C (40.5%) and lastly D with 31.7%. Only Reductants D and C in most instances reached saturation within the test period (4 hours). Substantial reduction of Cr_2O_3 and FeO occurred (%DOR for FeO, 72.03% and Cr_2O_3 , 67.96 %) as shown by the analysis of chemical phases present. This had the iron-chrome and chrome-iron phases dominating.

It is hoped that the outcomes of this research will establish the relevancy of new unconventional reductants as benchmarked against the current reductant products used in ferrochrome processing. Finally, this study has developed a procedure for the ranking of reductant reactivity.

**In Memory of My Daughter Tanatswa-Rufaro Nicole for truly
showing me What *'The Secret of Life'* is about?**

ACKNOWLEDGEMENTS

I hereby acknowledge the following people and/or institutions

- ✓ Professor Rosemary Falcon for the support, guidance and supervision of this research project
- ✓ Mintek (Pyrometallurgy Division) for provision of test work and analytical facilities and Exxaro (Mineralogy) for analytical facilities
- ✓ Ms Grethe Naude (Mineralogist), Victor Mwamba (Metallurgical Engineer) and other colleagues in Metallurgy for their support

TABLE OF CONTENTS

DECLARATION	i
ABBREVIATIONS, ACRONYMS AND NOMENCLATURE	ii
ABSTRACT.....	iv
ACKNOWLEDGEMENTS	vii
TABLE OF CONTENTS.....	viii
LIST OF FIGURES	xii
LIST OF TABLES.....	xv
1. INTRODUCTION.....	1
1.1. Research Significance	2
1.2. Problem Statements and Research Motivation	3
1.3. Research Objectives.....	3
2. LITERATURE REVIEW	5
2.1. SA Ferroalloys Production	5
2.1.1. Typical Smelting Technologies.....	5
2.1.2. Chromite Ore and Typical ferrochrome Reduction Process ...	9
2.2. Reductants Application in Ferroalloys Production.....	19
2.2.1 Coal.....	19
2.2.2 Graphite and Semi-graphite	30
2.2.3 Natural Coke and Natural Char	30
2.2.4 Coke (Metallurgical and Market).....	31
2.2.5 Typical Carbon Reductant Characteristics for the Metallurgical Industry (Quality, Reactivity, Strength, CRI, CSR)	32
2.3. Ferrochrome Reductant Characterization and Reactivity Tests..	34
2.3.1 Reductant Characterization.....	34

2.3.2	South African Coal Properties Affecting Coking and Coke Properties.....	39
2.3.3	Reactivity Tests.....	42
3.	METHODOLOGY.....	46
3.1.	Equipment.....	46
3.2.	Materials.....	48
3.2.1	Chromite ore.....	48
3.2.2	Reductants.....	48
3.3.	Sample Preparation.....	49
3.4.	Reductant Reactivity Tests.....	51
3.5.	Reactivity mechanism and characterization.....	52
3.6.	Analytical Techniques.....	55
3.6.1	Reductant Characterization Tests.....	55
3.6.2	Chromite Ore and Reactivity Test Products.....	57
4.	RESULTS.....	59
4.1.	Physico-Chemical Characterization of Raw Materials.....	59
4.1.1	Chromite Ore Chemical and Physical Analyses.....	59
4.1.2	Reductants Chemical and Physical Analyses.....	61
4.1.3	Reductants Petrography.....	63
4.1.4	Optical Light Microscopy.....	67
4.2.	Isothermal Thermogravimetric Analysis - Reactivity Tests.....	69
4.2.1	TGA Feed Material and Furnace Preparation.....	70
4.2.2	Reductant A – TGA Reactivity Curves.....	71
4.2.3	Reductant B – TGA Reactivity Curves.....	74
4.2.4	Reductant B1 – TGA Reactivity Curves.....	76
4.2.5	Reductant C – TGA Reactivity Curves.....	78

4.2.6	Reductant D – TGA Reactivity Curves	81
4.3.	TGA Test Product Analyses – (Chemical, XRD and SEM)	83
4.3.1	Reductant A Product – (Chemical, XRD)	83
4.3.2	Reductant B Product – (Chemical, XRD, SEM).....	86
4.3.3	Reductant B1 Product Analysis – (Chemical).....	88
4.3.4	Reductant C Product – (Chemical, XRD)	89
4.3.5	Unconventional Reductant D Product – (Chemical, XRD, SEM)	90
5.	DISCUSSION	95
5.1.	Chromite Reduction and Metallisation	97
5.1.1	Degrees of Reduction and Metallisation by Speciation	99
5.2.	Comparison of Reactivity at 1100°C, 1200°C, 1300°C & 1400°C...	103
5.2.1	Comparison of Reductant Reactivity at 1100°C	104
5.2.2	Comparison of Reductant Reactivity at 1200°C	107
5.2.3	Comparison of Reductant Reactivity at 1300°C	110
5.2.4	Comparison of Reductant Reactivity at 1400°C	114
5.3.	Comparison between Speciation and Quantitative XRD Results....	117
5.3.1	Comparison between Speciation and Quantitative XRD Results for Iron and Chromium.....	118
5.4.	Comparison of SEM-EDS for Selected 1400°C Products	119
5.5.	Factors Affecting Metallisation and Reduction Degree	120
5.5.1	Effect of Temperature on %DOR and%DOM.....	120
5.5.2	Effect of Reductant Rank on % DOR and %DOM.....	121
5.5.3	Effect of Reductant Quality (Fixed Carbon, Ash and volatiles).	123

5.6. Relationship of Reductant Characterization, Reactivity and Product Analysis.....	125
6. CONCLUSIONS	128
6.1. Characterization of Selected Reductants.....	128
6.2. Reactivity Tests	129
6.3. Relevancy and Sustainability Of Reductants Currently In Use For The Ferrochrome Process In South Africa.....	131
7. RECOMMENDATIONS	134
7.1. Further Investigations in Unconventional Reductants.....	134
7.2. Cost Implications	134
7.3. Process Innovation	135
8. REFERENCES.....	138
9. APPENDICES	148
9.1. Appendix A: Chrome Ore Samples.....	148
9.2. Appendix B: Reductant Samples	149
9.3. Appendix C: TGA Furnace Feed Material Charge Calculation..	151
9.4. Appendix D: Reductant Characterization Results	154
8.5 Appendix E: TGA Raw Data	159
8.6 Appendix F: TGA Product Analysis Results.....	163

LIST OF FIGURES

Figure 2.1: A Schematic Reaction Diagram in Submerged-Arc Furnace for Chromite Smelting (Source: Holappa and Xiao, 2004).	7
Figure 2.2: Typical DC- Arc Furnace (Source: www.bateman-dc.com).....	8
Figure 2.3 : The Ellingham diagram (ΔG^0) for some oxides corresponding to the reaction of type $2x/y \text{ Me} + \text{O}_2 (\text{g}) + \text{C} \rightarrow 2/y \text{ Me}_x + \text{O}_y$ (Calculated by HSC Chemistry 7 – (Source: Gasik M, 2013)	13
Figure 2.4: Coalification series: atomic ratios H/C vs. O/C (Source: Habashi, 1998).....	21
Figure 2.5 : Chrome Ore Reactivity at 1300°C (Source: Barnes et al., 2015).....	43
Figure 3.1: Schematic Thermogravimetric analysis setup (Source: Barnes and Eric, 1995).....	46
Figure 3.2: Photographic image of the thermogravimetric setup (Mintek, 2016).....	47
Figure 4.1: Unconventional Reductant D Particle-4 Photo micro-graphs (500x magnification objective).....	66
Figure 4.2: Cell Wall and Macro-pores Distribution in a Section of Reductant B (20x magnification objective).....	68
Figure 4.3: Cell Wall and Macro-pores Distribution in a Section of Reductant D at 20 μm (500x magnification objective).....	69
Figure 4.4: Temperature Profile of the TGA Furnace (hot zone is shown by the solid red line).....	71
Figure 4.5: TGA Curves for Reductant A at 1100°C to 1400°C	72
Figure 4.6 : Differential Time Analysis Graph - Reductant A (1100°C to 1400°C).....	73
Figure 4.7: TGA Curves for Reductant B from 1100°C to 1400°C.	74
Figure 4.8: Differential Time Analysis Graph - Reductant B (1100°C to 1400°C).....	75
Figure 4.9 : TGA Curves for Reductant B1 from 1100°C to 1400°C	76
Figure 4.10: Differential Time Analysis Graph - Reductant B1 (1100°C to 1400°C).....	77

Figure 4.11: TGA Curves for Reductant C at 1100°C to 1400°C.	78
Figure 4.12: Differential Time Analysis Graph - Reductant C (1100°C to 1400°C).....	80
Figure 4.13 : TGA Curves for Reductant D from 1100°C to 1400°C.	81
Figure 4.14: Differential Time Analysis Graph - Reductant D (1100°C to 1400°C).....	82
Figure 4.15: XRD Pattern for Reductant-A 1400°C Test Product	85
Figure 4.16: XRD Pattern for Solid-State Reduction of Chromite with Reductant B at 1400°C	87
Figure 4.17: Backscattered Electron Image of Reduced Chromite with Reductant B at 1400°C (<i>1-8 are the phases identified</i>)	88
Figure 4.18: XRD Pattern for Solid-State Reduction of Chromite with Reductant C at 1400°C.....	90
Figure 4.19: XRD pattern for solid state reduction of chromite using Reductant D at 1400°C	92
Figure 4.20: Backscattered electron image of reduced chromite with Reductant D at 1400°C (<i>9-16 are the phases identified</i>).....	93
Figure 5.1: Reductants A, B, B1, C and D Isotherms at 1100°C – First Stage.	104
Figure 5.2: Reductants A, B, B1, C and D Isotherms at 1100°C – Second Stage.	105
Figure 5.3: Reductant A, B, B1, C and D Change in Mass at 1100°C. ..	106
Figure 5.4: Reductants A, B, B1, C and D Isotherms at 1200°C – First Stage.	107
Figure 5.5: Reductants A, B, B1, C and D Isotherms at 1200°C – Second Stage.	108
Figure 5.6: Reductant A, B, B1, C and D Change in Mass at 1200°C. ..	109
Figure 5.7: Reductants A, B, B1, C and D Isotherms at 1300°C – First Stage	111
Figure 5.8: Reductants A, B, B1, C and D Isotherms at 1300°C – Second Stage.	112
Figure 5.9: Reductants A, B, B1, C and D Change in Mass at 1300°C..	113

Figure 5.10: Reductant A, B, B1, C and D Isotherms at 1400°C – First Stage.	114
Figure 5.11: Reductant A, B, B1, C and D Isotherms at 1400°C – Second Stage	115
Figure 5.12: Reductant A, B, B1, C and D Change in Mass at 1400°C..	117
Figure 5.13: Reductant Changes in %DOR and %DOM with Temperature	120
Figure 5.14: Changes in %DOR and %DOM with Reductant Rank.	122
Figure 5.15: Changes in %DOR and %DOM with Reductants Ash, Volatiles and Fixed Carbon Content	123
Figure 9.1 : Chromite Ore Concentrate Particle Size Distribution (<i>Source: Mintek 2015</i>).....	148
Figure 9.2 : Reductant Samples – As Received.....	149
Figure 9.3 : Reductants Particle Size distribution, (Mintek 2016).....	150
Figure 9.4: Photomicrographs of Conventional Reductants (A) coarse circular. (B), coarse lenticular and (C) medium ribbon anisotropic carbon, as indicated by the boxed areas.	154
Figure 9.5: Photomicrographs of Unconventional Reductant (D) Particle 1(A, B, C & D).	155
Figure 9.6: Photomicrographs of Unconventional Reductant (D) Particle 2(A, B, C & D).	156
Figure 9.7: Photomicrographs of Unconventional Reductant (D) Particle 3(A, B, C & D).	157

LIST OF TABLES

Table 1.1 : The General Market for Chrome Ore (adapted from Chrome Development Association in Barnes <i>et al.</i> , 2015).....	2
Table 2.1 : Typical UG2, MG2 and LG6 Chromite Ore Compositions in Mass %. (Adapted from Cramer <i>et al.</i> , 2007).....	10
Table 2.2 : Comparison of key characteristics of coal macerals (<i>Source: Lu et al. 2013</i>).....	24
Table 2.3 : Petrographic classification of coal for coking technology (<i>Source: Gibson, 1979</i>).....	25
Table 2.4 : Desirable properties of coking coals (<i>Source: Mitchell 1999a</i>)	27
Table 2.5 : Coal quality parameters for coke making (<i>Sanders et al., 2010</i>)	28
Table 2.6: Electrical, Mechanical and Thermal Properties (<i>Source: Speight, 2013</i>).....	36
Table 2.7: Reductant Proximate Analysis (<i>Source: Nurmukhanbhetov et al., 2013</i>).....	44
Table 3.1: Typical Reaction Mix of Reductant and Chromite Ore	50
Table 3.2: Final Test Work Matrix (Solid State Chromite Reduction)	52
Table 4.1: Bulk chemical composition of UG2 Chromite (mass %).	60
Table 4.2 : UG2 Concentrate Fe and Cr Speciation Analysis (mass %) ..	60
Table 4.3: Reductants Proximate Analysis (air dried – Mass %).	61
Table 4.4: Reductants Ultimate Analysis (air dried - mass %)	61
Table 4.5: Reductant Ash Chemical Composition (mass %).	62
Table 4.6: Reductant Random Reflectance Data.....	65
Table 4.7: Macro-porosity and Compactness (Reductants A, B & C).	67
Table 4.9 : Reduced Material Metallic Content –Reductant A (mass %)..	84
Table 4.10: Product Phases Relative Abundance - Reductant A.	85
Table 4.11: Reduced Material Metallic Content – Reductant B (mass %) 86	
Table 4.12: Product Crystalline Phases Relative Abundance - Reductant B.	87

Table 4.14: Reduced Material Metallic Content – Reductant B1 (mass %).	89
Table 4.15: Reduced Material Metallic Content – Reductant C (mass %)	89
Table 4.16 : Reduced Material Metallic Content – Reductant D (mass %)	91
Table 4.17: Product Crystalline Phases Relative Abundance -Reductant D	92
Table 4.18: The SEM Phases Chemical analysis	94
Table 5.1 : Iron Speciation (mass% Fe ^x) and %DOR and %DOM.	101
Table 5.2: Chromium Speciation (mass% Cr ^x) and %DOR and %DOM.	102
Table 5.3: XRD and speciation compositions of Iron (1400°C).	118
Table 5.4: XRD and speciation compositions of Chromium (1400°C)....	118
Table 5.5: Chemical Analysis of Phases Present (mass %)	119
Table 5.6: Reductant Fixed Carbon, %DOR and %DOM (mass %)	124
Table 9.1 : Typical Reaction Mix of Reductant and Chromite Ore	151
Table 9.2: Typical Reaction Outputs Calculated	153
Table 9.3: 1100°C TGA Test Raw Data	159
Table 9.4: 1200°C TGA Test Raw Data	160
Table 9.5: 1300°C TGA Test Raw Data	161
Table 9.6: 1400°C TGA Test Raw Data	162
Table 9.7: TGA Products Chemical Speciation Results (% mass- Oxides)	163
Table 9.8: TGA Products Chemical Speciation Results (Oxides)	164
Table 9.9: TGA Products XRD results (mass %)	165
Table 9.10: TGA Products Chemical Analysis of SEM Phases Present (mass %)	166
Table 9.11: TGA Products Iron Speciation (mass %) and %DOR & %DOM for repeats	166
Table 9.12: TGA Products Chromium Speciation (mass %) and %DOR & %DOM for repeats	166

1. INTRODUCTION

South Africa possesses the largest chrome resources in the world (over 70%). However, over the past ten years, the country has dropped from being the world's leading ferrochrome producer with China taking over this position (Oberholzer and Daly, 2014). This has been attributed to decreased cost competitiveness and shortages in electricity supplies in South Africa which have resulted in an increase in raw chrome ore rather than processed chrome exports. The ore exports are mainly to China and this has ironically helped the Chinese ferrochrome industry grow to surpass the South African industry. The ferrochrome industry has been known and confirmed to contribute significantly to the country's employment (200 000 jobs sustained), foreign earnings (6 Billion US\$) and GDP (7 Billion US\$) with 90% of technology and equipment sourced locally (Ruiters, 2012).

The ferrochrome industry is important to the steel manufacturing process with the ferrochrome alloys, such as charge ferrochrome, ferrosilicon chrome (FeSiCr), High, Medium and Low Carbon ferrochrome (H, M, & LCFeCr) being the most important alloying elements during the manufacturing of the various stainless steel grades (see Table 1.1). The elements impart different qualities to steel ranging from corrosion resistance (Chrome), ductility (Carbon/Silicon) and acid/alkali corrosion resistance. Increasing stainless steel demand translates to demand for ferroalloys.

Reductants form a significant portion of the production costs during ferroalloy processing. The Macquarie Research Report summarises the South African ferroalloy production costs for 2013, showing that reductants represent 17% of costs, after electricity and chrome ore at 25% and 24%, respectively (Oberholzer and Daly, 2014). Consequently, the need arises to cut costs and drive profitability through raw materials optimization and

reductants more specifically. Such factors put great emphasis on quality requirements for the reductants used by ferroalloy producers with, typically, carbon reducing agents and electric power accounting for 30-60% of production costs in the ferroalloys processes (Strakhov, 2009).

Table 1.1 : The General Market for Chrome Ore (adapted from Chrome Development Association in Barnes *et al.*, 2015)

CHROME ORE MARKET		
5%	90%	5%
Refractories & Foundries	Metallurgical Industry	Chemicals
Iron & Steel Cement Glass Ceramics Machinery Others	Stainless steel Alloyed steel Non-ferrous alloys	Leather tanning Plating Metal Wood Preservative Pigments Others

According to Myrvågnes and Lindstad (2007), reductant resource materials are limited, with the most common for ferroalloys production being:

- ✓ Coal;
- ✓ Coke;
- ✓ Char;
- ✓ Anthracite;
- ✓ Woodchips; and
- ✓ Bio-carbon in the form of charcoal

The specification of the product and its purity factor limit the number of coal types that can be used. In addition, the process requires a reductant with specific reactivity and physical strength, further limiting the use of readily available carbonaceous materials.

1.1. Research Significance

Basson *et al.* (2007) stated that growth and activity have been reported in the South African ferroalloys industry despite a number of potentially threatening developments. These include new legislation affecting the

mining and minerals industry, a shortage of some types of suitable reductants and depletion of surplus electricity generation capacity with resultant threat of real escalation of electricity prices. There is also potential pressure resulting from cyclic strengthening of the South African Rand.

Against this background, the current research seeks to investigate a series of currently used conventional reductants and one unconventional reductant with a view to establishing which would provide the highest process optimization and which would be the most sustainable reductant for the ferrochrome industry. It is hoped that this would provide one factor at least, that could contribute to stabilizing this industry.

1.2. Problem Statements and Research Motivation

Reductants form a significant part of the increased input costs for ferrochrome processing and thus it is important to find alternative effective reductant sources.

Ideal reductants are expected to have a high reactivity and fixed carbon content with low ash content but their current availability is low. Innovation together with substitution has therefore become a necessity to ensure sustainability and competitiveness of processing operations.

1.3. Research Objectives

The main objective of this research is to study and compare the reactivity of commonly used conventional reductants, and that of readily available new and sustainable unconventional carbon materials for the reduction of natural chromite in the solid state.

The sub-objectives are as follows:

- I. To characterize a number of reductants to determine the merits and demerits of each in the current ferrochrome processes;

- II. To undertake reactivity tests in the solid state within the temperature range 1100-1400°C, and determine the effectivity of each reductant for ferrochrome processing;
- III. To establish the relevancy of the current reductant products used in ferrochrome processing and their future sustainable use in the South African ferrochrome industry; and
- IV. To establish whether selected new unconventional reductants can substitute for local conventional reductants, especially when the quality of the latter deteriorates to levels not economic for further processing, and the costs of importing such materials becomes too exorbitant to be economic for the ferrochrome industry, or new environmental legislation puts a constraint on their application in South Africa.

2. LITERATURE REVIEW

Previous studies in the characterization and reactivity of selected carbonaceous reductants are addressed in this chapter. The background is laid by examining important issues including South African ferroalloy production, typical smelting technologies, reduction process of chromite ores and reductants, reductant applications, reductant characterization and reactivity tests.

2.1. SA Ferroalloys Production

According to Cramer *et al.* (2007), South Africa had more than fifty ferrochrome furnaces in 2007 that utilized various technologies. These included conventional open submerged-arc furnaces (SAFs) for direct smelting of run-of-mine quality chromite ore. There are also expensive pelletizing and sintering plants producing pre-oxidised pellets which are fed preheated to closed SAFs as well as hollow-electrode direct fines feed to direct current (DC)-arc furnaces (Cramer *et al.*, 2007).

There are seven major ferrochromium producers in South Africa namely, Samancor Chrome, Mogale Alloys (producing FeCr and SiMn in campaigns), Xstrata Alloys/Merafe, Assmang Chrome, Herculon Ferrochrome, ASA Metals and International Ferro Metals. The major producers have plants in more than one location (Cramer *et al.*, 2007).

2.1.1. Typical Smelting Technologies

There are a number of technologies that are in existence for the production of ferroalloys ranging from use of sub-merged arc furnaces, surface or open arc furnaces and direct current furnaces.

2.1.1.1. Submerged (Conventional) and DC Arc Furnaces

Production of high carbon ferrochromium (HCFeCr) and Ferrosilicon Chrome (FeSiCr) alloys has conventionally been conducted in an open or semi-open SAF with medium/low carbon being produced in an open-arc tilting refractory furnace via the Perrin process (Curr, 1996). See Figure 2.1. The author further confirmed that submerged-arc process operational efficiency and safety aspects require that only lumpy feed material (>6 mm) is used to allow permeability for the movement of reduction gases, which also leads to good heat dissipation within the furnace raw materials feed mass or charge bed. The process also requires refractory chromite, high quality coke and electrical energy with a Low Carbon ferrochrome open-arc process instead of utilising fines raw material feed (<10 mm) Curr (1996).

Xiao *et al.* (2007) also demonstrated that SAF processes are generally used for the smelting of chromite ores, with the material fed to the furnace being essentially chromite ore, and reducing and fluxing agents. The reductant could be in the form of coke, anthracite or char whilst flux could be quartzite, dolomite or limestone. The main purpose of fluxing is to regulate slag properties *viz.* viscosity, electrical conductivity and the liquidus temperature all of which also impact upon operational efficiency. The feed material particle size is selected such that good permeability of the packed bed in the SAF is maintained (Xiao *et al.*, 2007).

Processes are available for the pre-reduction of ore external to the SAF. These usually operate at low temperatures (below 1300°C) as above that the ore blend can start to sinter and melt. Such processes have several advantages including lower operational cost, lower capital cost and increased life of refractory used in the 'pre-reduction' furnace (Xiao *et al.*, 2007).

The friable nature of South African chromite ore necessitates some form of agglomeration, e.g. pelletizing, briquetting or Xstrata's "block" process, which uses brick making techniques, followed by cold charging to the SAF together with lumpy reductants and fluxes (Naiker *et al.*, 2006).

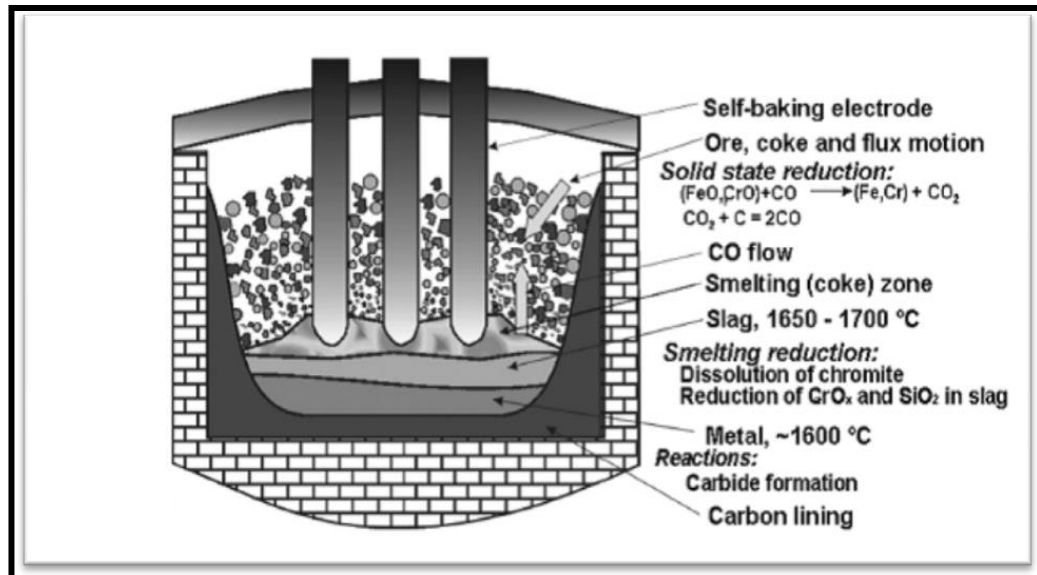


Figure 2.1: A Schematic Reaction Diagram in Submerged-Arc Furnace for Chromite Smelting (Source: Holappa and Xiao, 2004).

According to these authors, a widely used system is the patented Outokumpu process that incorporates steps of ore-milling, blending with coke fines and suitable binder, pelletizing and sintering. Preheating is done in a shaft furnace where gravity feeds the SAF. Fuelling the pre-heating shaft furnace and the sinter furnace is achieved by the capture of CO-rich furnace gas generated by a closed furnace.

The first solid state reduction of chromite for the production of charge chrome was installed in South Africa in 1975 (Basson *et al.*, 2007). This utilised a rotary kiln to pre-reduce composite pellets of milled chromite and coke fines to achieve as high as 70% Cr metallization. Pellets were then fed hot to a closed SAF. The SRC process was originally patented by Showa Denko. The Showa Denko process is implemented by Glencor as Premus technology.

2.1.1.2. DC Arc furnaces

Since 1983, the DC open-bath furnace (Figure 2.2) has been in use and this utilises 100% ore fines. The DC Arc furnace does not use lumpy coke or char, but operates best using fine coke and char that cannot be used in an AC furnace. Coal can be used but cracking of the volatiles increase electrical power consumption. It has the disadvantage of higher energy losses through the roof and upper side-walls, as well as lower availability due to the time lost to make electrode additions (Naiker *et al.*, 2006).

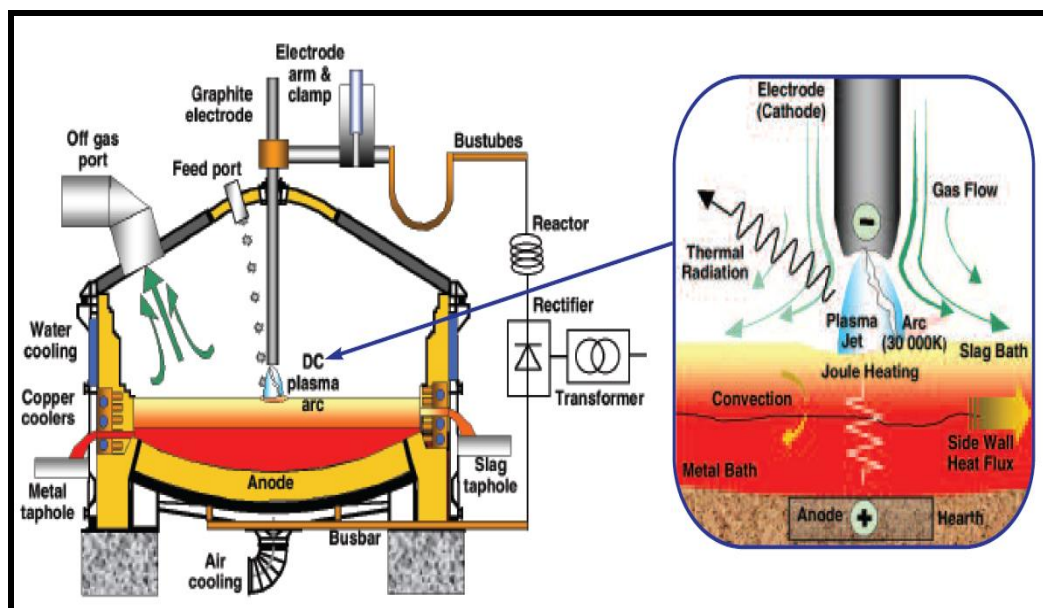


Figure 2.2: Typical DC- Arc Furnace (Source: www.bateman-dc.com)

The hollow graphite electrode is utilised to feed dried raw material through its centre gap, or material is fed through ports on furnace roof thereby allowing use of solid electrodes which greatly improves availability as it is simpler to operate plus more cost effective (Naiker *et al.*, 2006). Graphite electrode sections are now added on line without cutting power thus improving furnace availability.

2.1.2. Chromite Ore and Typical ferrochrome Reduction Process

2.1.2.1 Chromite ore

The general formula $(Fe, X)O(Cr, Y)_2O_3$ is associated with Chromite ores, which are known to have a spinel structure (Chakraborty *et al.*, 2007). X and Y are elements that will dissolve in the given cationic sub-lattices, with the latter representing the tetrahedral and octahedral sites in the spinel. The tetrahedral and octahedral sites are occupied by divalent (e.g. Mg) and trivalent (e.g. Al, Fe) cations, respectively.

Previously, studies have been conducted regarding pre-reduction and smelting characteristics of Upper Group 2 (UG2) on the Merensky reef chromium concentrate (Barnes *et al.*, 1983). This layer represents the top most of 13 chromite seams located in the Bushveld Complex. The following two important facts are highlighted by Barnes *et al.* (1983) as to why the UG2 layer is of great significance to South Africa:

1. It comprises about a fifth of South Africa's known chromite reserves; and
2. Existence of platinum group metals (PGM's) occurs with the ore.

Cramer *et al.* (2007), confirm that the UG2 chromite ore is essentially mined due to its co-existence with PGMs, despite having the lowest grade of the bushveld complex reefs. The latter are noted to have Cr/Fe ratios between 1.3 and 1.4, and are increasingly being used in South Africa for charge chrome smelting due to their availability as discard concentrates during PGMs beneficiation. Compared to the other reefs, mining of UG2 seams is accomplished by simple scrapper-winch and handheld drill rigs or mechanised drill rigs in cases of seam widths of more than 1.5m (Cramer *et al.*, 2007).

According to Cramer *et al.* (2007), seams LG6 (Lower Group 6) and MG1/2 (Middle Group 1/2) generate typically about 5-40% lumpy material, amenable to smelting in conventional submerged arc furnaces. Fines

produced can be beneficiated using gravity for chromite concentration upgrading followed by pelletizing as furnace feed. The authors highlight how in South Africa, the development and use of a cost effective pelletizing and sintering oxidative technology (Known as Outokumpu Technology) has resulted in favourable application of UG2 chromite for ferrochrome smelting.

2.1.2.2 Smelting Characteristics of UG2 Chromite Ore

Cramer *et al* (2007), compares the chemical composition of UG2 and typical MG2 and LG6 concentrates generated from their respective ores .

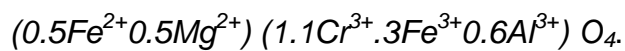
Table 2.1 : Typical UG2, MG2 and LG6 Chromite Ore Compositions in Mass %. (Adapted from Cramer *et al.*, 2007)

Composition	LG6 concentrate	MG2 concentrate	UG2 concentrate
Cr ₂ O ₃	44.2	43.6	41.6
FeO	24.1	25.1	-
Cr/Fe Ratio	1.6	1.5	1.36
V	0.2	0.2	0.21
Al ₂ O ₃	13.8	14.5	15.3
MgO	11.5	9.6	9.62
CaO	<0.30	0.3	<0.30
SiO ₂	2.5	3.0	2.88
Ni	0.1	0.1	0.13
TiO ₂	0.5	0.7	0.91
K ₂ O ppm	30.4	87.5	57.00
Na ₂ O ppm	155	400	247
Total C	0.0	0.0	0.05
Gain on ignition	1.0	1.8	-
Loss on ignition	-	-	1.6
H ₂ O	<0.1	<0.1	0.1
Fe ²⁺	<0.5	0.1	0.73
Total S	<0.01	<0.01	0.01
P ppm	27.0	<0.5	58
Cl ppm	<300	394	0

It is demonstrated that the components Cr₂O₃, FeO, TiO₂ and Cr/Fe ratio, occur with huge variances. The Cr grade of the ferrochrome is affected by the Cr/Fe ratio, with different product uses requiring different grades.

Charge chrome (CCr) grade acceptable is >48% and for other ferrochrome end uses elements like Titanium in the product is critical, thus controlled blending with conventional ore is important (Cramer *et al.*, 2007).

As concluded by Barnes *et al.* (1983), the potential to convert the chromite concentrate into a suitable ferrochromium grade presents a great opportunity to both ferrochromium and PGM producers. The molecular formula for the chromite is given as:



This has chromium to iron ratio as low as 1.35. It is further demonstrated by Barnes *et al.* (1983), Basson *et al.* (2007) and Cramer *et al.* (2007) that this ore can produce a high-carbon alloy with a chromium content of between 48 to 50 % (10 %carbon plus silicon) ferrochromium. The ore portrays an energy balance with relatively reduced energy input requirements, based on the resulting unit of ferrochromium as well as maximum chromium obtained (Barnes *et al.*, 1983).

The UG2 ore contains a lower chromium-to-iron ratio in comparison to some Transvaal chromite. Barnes *et al.* (1983) attribute this to be essentially as a result of increased iron content and not reduced chromium levels. The ore produces a ferrochromium alloy that gives chromium levels suitable for use as either an alloying component or during the processing of stainless steel. The most used ferro-alloy in the metallurgical industry is known to be high-carbon ferrochrome (referred to as charge chrome), with a chromium per cent between 50 to 55 % (Barnes *et al.*, 1983).

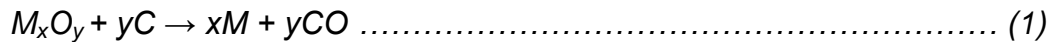
Another important characteristic of UG2 chromite is the requirement for agglomeration due to its fineness, which is reported to be 99percent of the particles less than 300µm (Barnes *et al.*, 1983). In the current study,

instead of agglomerating the ore and reductant, the latter has been milled to a suitable size for blending with the ore concentrate so as to increase and maximise the contact surface area.

2.1.2.3 Direct Reduction of Chromite

Several studies have been carried out on carbothermic solid state Chromite reduction viz. Barcza *et al.*, (1971); Otani and Ichikawa (1975); Barnes *et al.*, (1983); Soykan *et al.*, (1991); Neuschutz (1992), Barnes and Eric (1995); Weber and Eric (2006) and Chakraborty *et al.* (2007). These authors demonstrate that due to the spinel structure of the ore, carbon directly reduces the iron oxides in the presence of a reducing atmosphere to iron and chrome carbides

Chakraborty *et al.*, (2007) illustrated the direct reaction of carbon and iron oxide using expression (1):

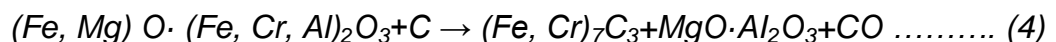


Nonetheless, the reaction takes place through a mechanism represented by:



Reaction (2), also known as the Boudouard reaction, controls the rate of reaction at temperatures below 1000°C (Chakraborty *et al.*, 2007).

The following overall reaction as given by Otani and Ichikawa (1975) summarises the spinel reduction:



2.1.2.4 Thermodynamics of Chrome Ore Reduction

The oxides considered to be undergoing reduction, used to calculate both the reduction and metallisation degree in this test work, are FeO and Cr₂O₃.

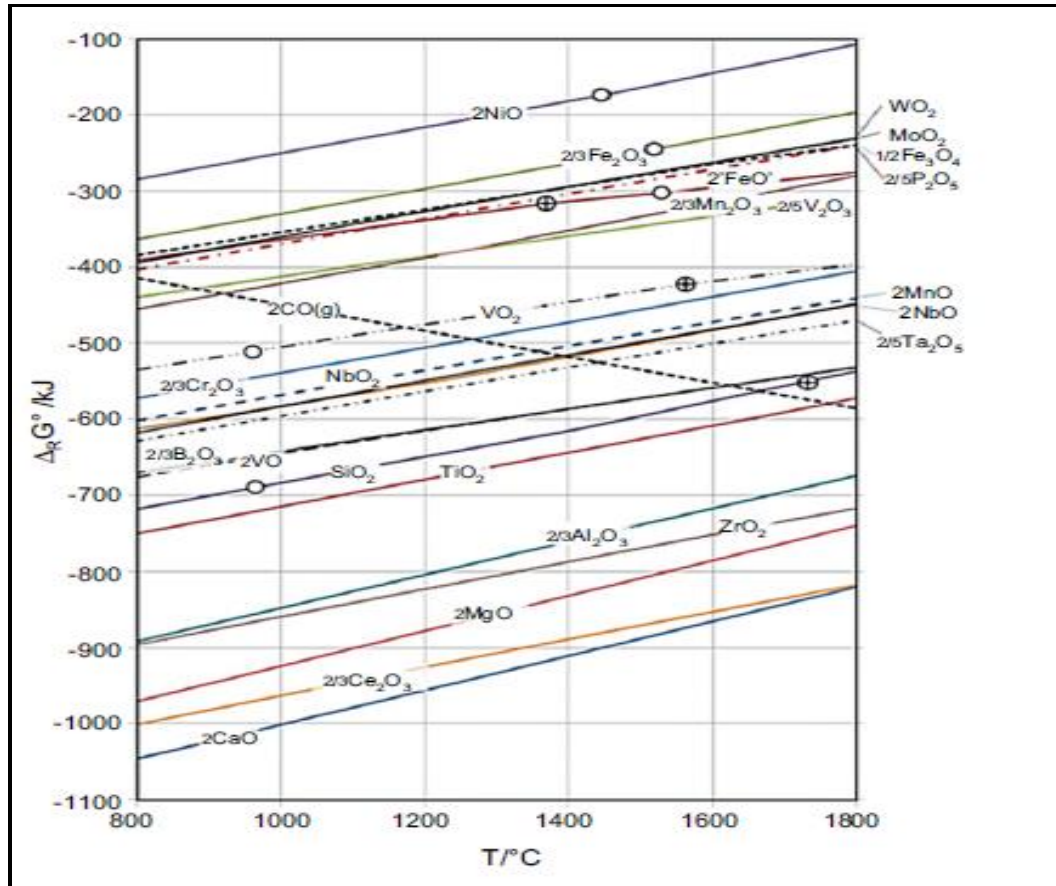


Figure 2.3 : The Ellingham diagram (ΔG^0) for some oxides corresponding to the reaction of type $2x/y \text{ Me} + \text{O}_2 (\text{g}) + \text{C} \rightarrow 2/y \text{ Me}_x + \text{O}_y$ (Calculated by HSC Chemistry 7 – (Source: Gasik M, 2013))

The Gibbs' (ΔG) free energy of formation, partial pressure of oxygen in equilibrium with the oxide and the ratio of carbon monoxide to carbon dioxide for the two oxides are illustrated in figure 2.3. ΔG gives a measure of the thermodynamic driving force which allows the reaction to take place. Spontaneous and non-spontaneous reactions have negative and positive ΔG , respectively.

At the chosen test work temperatures, ΔG for reduction of FeO is lower than that of Cr_2O_3 . This means that FeO is reduced first compared to Cr_2O_3 , with the latter also taking place with increased difficulty due to the chromite spinel structure. See Figure 2.3.

2.1.2.5 Kinetics and Mechanism of Chromite Reduction

Efforts have been reported elsewhere (e.g. Curr (1996), Xiao & Laplante (2004) and Basson *et al.* (2007)) with investigational work done on ways to influence and fully understand the reduction mechanisms during various ferroalloys production processes.

Xiao and Laplante (2004) carried-out tests to establish the reaction kinetics of solid state reduction of industrial and laboratory made chromite pellets in comparison with lumpy ore. They utilised the TGA technique, with carbon monoxide used as a reducing agent in the presence of graphite next to the chromite. In another investigation by Xiao *et al.* (2007) SEM/EPMA was utilised to confirm microstructural changes of solid-state reduction experienced by industrial chromite pellets and lumpy ore. SEM/EPMA helped to discern alterations in structure and composition of the chromite samples. The test work was done at 1500°C and to imitate what takes place in the SAF packed bed zone, CO was used as a reducing agent with graphite in propinquity to the chromite ore. They established that, chromite pellets reduction was faster than the lumpy ore, with the rate of reduction in all cases quicker on the external region compared to the internal region of the chromite ore.

Xiao *et al.* (2007) concluded that the energy consumption is comparably high in the SAF, with high carbon ferrochrome ranging from 2000 to 4000 kWh/t when there is pre-reduction and no pre-reduction coupled with preheating, respectively. They established that due to interaction of factors linked to electrical, thermal, chemical and feed characteristics, a significant temperature gradient is found in the SAF. The temperature at the top of

the feed material and the tip of electrodes changes from probably room temperature to more than 2000°C, resulting in several zones and consequently changing reaction mechanisms within the charge material.

According to Xiao *et al.* (2007), different chromite ore types have different reaction mechanisms. Transformations within the ore microstructure, when sintering and reduction takes place, are important to be correctly determined, as a component of furnace analysis as well as interpreting the reduction sequence in the furnace charge (Xiao *et al.*, 2007). In this study, the reaction mechanism of the carbon-containing chromite pellet is determined by use of the unreacted core model, with mathematical simulation of CO reduction of the pellets achieved by the use of a modified grain model.

Sundar Murti and Seshadri (1981) investigated synthetic chromite reduction from 1150°C to 1300°C, using varying quantities of carbon, and analyses of the reduced material consequently done by XRD. The main objective of their study was to illustrate kinetic aspects of chromite reduction and demonstrate factors in the theoretical aspects of mixed powder reactions which generally affect the rate of product growth. These are given as:

- Diffusion of reactants through product layer;
- Phase boundary reaction; and
- Growth of nuclei.

The following expressions are utilised to explain the aspects:

- a. Fractional reduction of spherical particles with time by Jander in Sundar Murti and Seshadri (1981) is expressed by;

$$1 - (1 - x)^{\frac{1}{3}} = Kt \dots\dots\dots (a)$$

Where;

x ÷ Fractional Reduction;

$K \div$ Rate Constant; and
 $t \div$ Time.

The following relation for a diffusion controlled process was obtained by Ginstling and Braunstein (Sundar Murti and Seshadri, 1981)

$$1 - \left(\frac{2}{3}\right)x - (1 - x)^{\frac{2}{3}} = Kt \dots\dots\dots (b)$$

When it is assumed that there is the same probability of nucleation occurring for all active sites and when the rate limiting step is from both nucleation of product at active sites and the rate of growth of nucleated product, this is utilized with the expression:

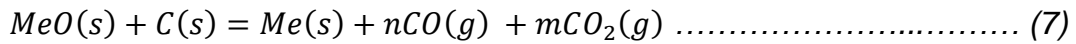
$$\text{Ln}\left(\frac{1}{1-x}\right) = Kt \dots\dots\dots (c)$$

Besides the above general factors and scenarios, Sundar Murti and Seshadri (1981) emphasised that specifically with regards chromite reduction, the effect of intermediate oxides, phases and the gasification reaction should also be considered. They proposed that metallic oxide reduction by carbon in a powder mixture is likely to occur as follows (I-V):

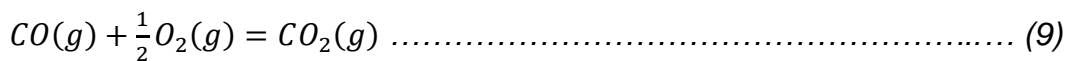
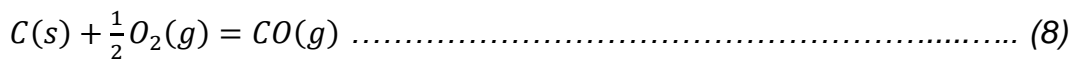
Direct reaction of oxide with carbon at the contact point to give CO, this then reacts with the oxide to form CO₂. The gasification reaction is noted to restore CO through equation (10), (Sundar Murti and Seshadri, 1981):



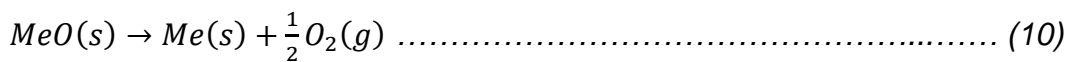
Metallic layer develops after the reaction of carbon and oxygen, followed by diffusion of carbon through the formed layer, to react more with the metal oxide to yield CO and CO₂.



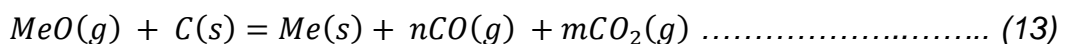
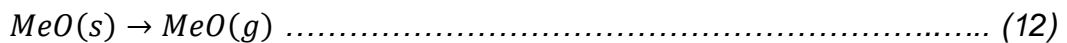
Metallisation then occurs within the oxide particles, resulting from oxygen penetrating the oxide layer and reacting with either carbon or carbon monoxide on the surface.



Metal and oxygen evolve after oxide dissociation with the oxygen further oxidising carbon.



Reaction of vaporised metal-oxide with solid-carbon,



In an attempt to gather more information with regards the mechanism and kinetics of Transvaal chromite ore reduction, Barcza *et al.* (1971), illustrated how the two processes depend on mineral constitution during

the production of high-carbon ferrochromium. Kadarmentov (1964) in Barcza *et al.* (1971) concluded that the quality of ferrochromium alloy in terms of silicon and carbon, mainly depends on chromite ore quantity and quality as well as quantity of reductant utilised during smelting in the SAF. The correct ore selection is highlighted and confirmed to be made difficult by variations within the following factors;

1. Chemical;
2. Mineralogical;
3. Particle-size; and
4. Nature of cementing gangue.

The author further confirmed that typical reduction of chromite actually starts at 1150°C to 1200°C and ends at 1400°C to 1500°C.

Following the discovery of significant reserves of quality chromite ore in the remote location of Northern Toronto, several efforts were directed at projects that could process the material economically. Barnes *et al.* (2015), in a study of alternative processing routes to produce ferrochromium, summarized some of the factors affecting the solid-state reduction of chromite ore as including:

- a. Particle size of ore;
- b. Particle size of reductant;
- c. Reactivity of solid reductant;
- d. Temperature; and
- e. Presence of catalyst or accelerators.

As a result of prevailing aggressive market conditions, Farjadi and Azari (2004) undertook a cost analysis of chrome ore reduction as one of the major issues affecting ferrochrome. The authors portrayed how chrome ore quality and composition affect electrical consumption and process efficiency during reduction. Poor grade or low quality chromite ore is

linked to higher energy consumption and low recoveries, compared to high grade chromite ore.

2.2. Reductants Application in Ferroalloys Production

Reductants for the production of ferroalloys in South Africa have been readily available for many years but in recent times it has become necessary to import market coke, mostly from China (mainly for chrome alloys) and Zimbabwe (mainly for manganese alloys).

Basson and co-workers (2007) summarised the reasons for this as:

- rapid increase in ferroalloy production capacity;
- no significant growth in coke production capacity; and
- increased coke requirements due to use of closed furnaces for environmental reasons.

Specific coke consumption for Charge Chrome (ChCr) production has been reported by Basson *et al.* (2007) to have increased from 0.31 tonnes to 0.33 tonnes coke per tonne of alloy while specific char consumption increased by 0.2 tonnes at the cost of coal. DC ChCr furnaces and smaller alternate current (AC) ChCr and manganese alloy furnaces mainly utilise anthracite. A number of carbonaceous materials exist, that can be utilized for ferroalloys production and these range from coal to charcoal as illustrated below.

2.2.1 Coal

The Environmental Protection Agency (EPA, 1998), defined coal as a mixture of organic and inorganic mineral matter obtained over time, from the accumulation of fallen vegetation. Coalification is a term that describes the maturation of plant tissues from peat through different stages from lignite/brown coal, sub-bituminous and bituminous coals to anthracites and meta-anthracites (Mitchell, 2003). A schematic representation of coalification is illustrated in Figure 2.4:

Classification of coal material is achieved by rank, which is linked to material changes experienced during the natural transition from lignite to anthracite (EPA, 1998). There are four major types of coal by classification, viz.

- lignite;
- subbituminous;
- bituminous; and
- anthracite.

Due to lack of clear cut transition between these groups, sub-groups exist such as semi-anthracite, semi-bituminous, and sub-bituminous (Speight 2013).

The EPA (1998) illustrated the difference amongst some of the groups as follows:

Sub-bituminous coals are characterized by higher moisture and volatile matter, with lower sulphur content than bituminous. Bituminous coals possess higher volatile matter and lower fixed carbon in comparison to anthracite. The main characteristics of bituminous coal that sets it apart are sulphur and relative volatile matter content plus its slagging and agglomerating characteristics.

UNEP (2015) differentiated between anthracite and lignite from a geological perspective. On the one hand, anthracite is the oldest compared to Lignite (youngest) and is confirmed to be hard, consisting mainly of carbon with little volatile matter and virtually no moisture content. On the other hand, lignite is given as a soft coal that contains mostly volatile matter and moisture but having low fixed carbon. Coals in general are grouped according to particular properties as defined by their rank (degree of metamorphism), type (constituent plant materials) and grade (degree of impurities and calorific value) (Mitchell, 2003). Of these, rank is

a fundamental concept that involves a qualitative expression of the coalification sequence and is universal to all classification schemes.

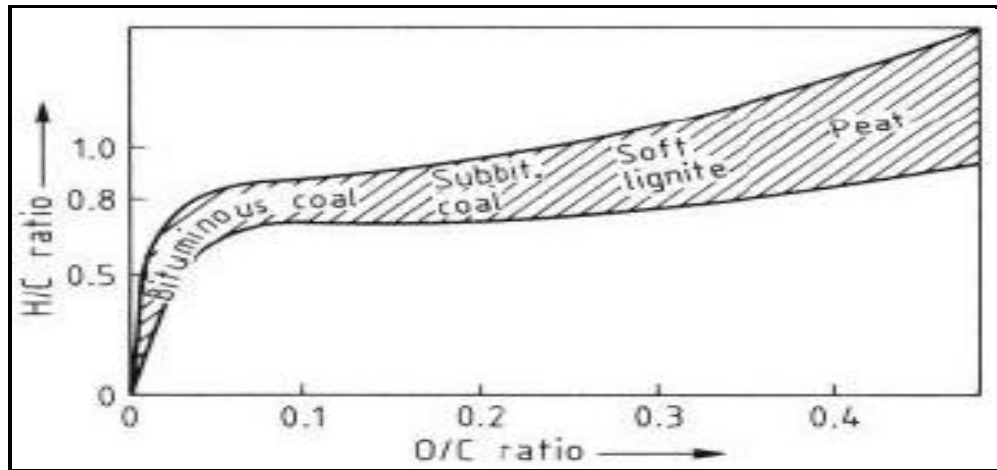


Figure 2.4: Coalification series: atomic ratios H/C vs. O/C (Source: Habashi, 1998)

2.2.1.1 Rank

Coal rank is a measure of coal maturity. As the rank increases, the vitrinite reflectance, carbon content, and C/H ratio of coal increase, while the coal volatile matter decreases. Under specific coking conditions, the rank and type of the feed coal determines the coke yield and coke quality (Diessel and Pickel, 2012).

According to EPA (1998), rank is based on a combination of several coal parameters that include:

- Volatile matter;
- Fixed carbon;
- Inherent moisture; and
- Oxygen.

The rank has an inverse relationship with the amount of volatile matter and moisture but instead, increases with increasing fixed carbon content (EPA, 1998).

Another very important rank parameter that is useful in the characterisation of coking coals is the measurement of mean maximum vitrinite reflectance. This analytical technique is sensitive, persistently changing throughout coalification and is particularly important for accurately measuring minor differences in those coals used for coke making, *i.e.* high volatile bituminous through low volatile bituminous. The technique measures the amount of incident light reflected from a polished surface of the main component of coal, vitrinite. Vitrinite is that component of coal principally derived from woody tissues (Mitchell, 2003). Rank is the most fundamental concept relating both coalification history and utilization potential of a coal.

Volatile matter and maximum vitrinite reflectance are important values used to determine the worth of coking coals. However, because volatile matter is dependent on both rank and composition, coals of different composition may be assigned to the same rank value even though their levels of maturity may differ. Kumar *et al.* (2008) observed that Volatile Matter (VM) is the most important parameter in deciding the blend for non-recovery type ovens. Low VM coals generate less gas and hence, the total thermal energy on its combustion may be insufficient for attaining the coking temperatures in the oven. On the other hand, high VM coal results in coke with high porosity and hence poor CRI (Coke Reactivity Index) and CSR (Coke Strength after Reaction) characteristics. According to Lu *et al.* (2013), high-volatile coals tend to give a low coke oven wall pressure, but produce coke that is too weak and reactive to be used in the blast furnace due to both the large volume of gas generated during carbonisation and subsequent shrinkage that affects the newly formed coke during cooling. Conversely, low-volatile coals tend to produce a dangerously high coke oven wall pressure and yield a coke product inferior to the quality required by the blast furnace, due to insufficient volatiles to initiate and sustain the fluidity required during coking. Medium-volatile coals tend to produce a high coke oven wall pressure, but also a high-quality coke product.

2.2.1.2 Coal Type (Macerals)

There are three main groups of materials that constitute coals and that are used to define coal type. These material groups identified under an optical microscope in reflected white light are referred to as vitrinite, liptinite and inertinite and are composed of individual constituents called macerals (Mitchell, 2014).

Diez *et al.* (2002) defined the vitrinite group macerals as derived from the humification of woody tissues and that it can possess remnant cell structures or may appear structureless. Typically, this material contains relatively more oxygen than the other macerals at any given rank level. The vitrinite group macerals are usually the most abundant macerals group occurring in higher rank coals. Liptinite group minerals are derived from plant resins, spores, cuticles and algal remains that are fairly resistant to bacterial and fungal decay. They are characterized as having higher hydrogen content than the other macerals, particularly at lower rank. However, at the boundary between sub-bituminous and bituminous coal there is a marked decrease in their volatile content and increase in carbon. By medium volatile rank a further decrease in hydrogen and volatile content occurs which makes them nearly indistinguishable from vitrinite.

Table 2.2 shows the key characteristics of coal macerals. Oxygen-containing functional groups and alkyl side chains of vitrinite are lost at different rates with an increase in coal rank. The extent of aromatization increases with the rank of coal. The inertinite group macerals are derived mostly from woody tissues, plant degradation products or fungal remains, and are characterized by a high carbon content resulting from thermal or biological oxidation. Inertinite group macerals are found in variable abundance in coals.

Table 2.2 : Comparison of key characteristics of coal macerals (*Source: Lu et al. 2013*).

Maceral	Liptinite	Vitrinite	Inertinite
Abundance	Minor	Major	Major, especially in Southern hemisphere coals
Appearance in hand specimen	Resinous	Bright, vitreous or glassy	Dull and dusty
Appearance under reflect light	Relatively low in reflectance	Low to moderate and consistent reflectance	Moderate–high and variable reflectance
Chemistry	Higher hydrogen content and volatile matter, more aliphatic	Intermediate hydrogen content and volatile matter	Lower hydrogen content and volatile matter, high carbon content
Reactivity during carbonisation	Highly reactive	Reactive, principal reactive component of coking coals	Inert

The following observations on vitrinite were made by Li *et al.* (2013):

- ✓ Vitrinite structure is characterized by the presence of short aliphatic chains and its high stability is due to a greater aromatic content in comparison to the aliphatic component.
- ✓ Vitrinite also has a larger aliphatic hydrocarbon proportion than raw coal, which makes vitrinite a major hydrocarbon-generating maceral.
- ✓ The higher carboxyl content and H-bonding are essential contributors to the stability of the macromolecular structure of vitrinite.

Volatile matter and maximum vitrinite reflectance are the most important rank parameters used to determine the value of a coking coal. The Mean random reflectance of vitrinite is restricted to the range of Vitrinite steps 6

to 18 (Diez *et al.*, 2002). Prime coking coals have a much narrower rank range of 1.1–1.45% vitrinite reflectance and 23–28% volatile matter (Diessel and Pickel, 2012). The major organic component used for carbonization in coal is made up of ‘reactive’ material, *i.e.* material which, on heating in the coke oven, reacts to the conditions in a definite pattern as the temperature rises. The vitrinite and liptinite of the coal undergo the softening stage in the 400-500°C and act as the binder for the ‘inert’ material. The ‘inert’ material does not soften, nor does it undergo subsequent contraction to the same extent as the ‘reactive’ components. It does, however, lose volatile matter and suffer internal structural chemical change. The role of the ‘inert’ material in the coking process is to reduce the overall swelling and contraction. If a good quality coke is to be produced, a balance in terms of the charge to the oven must be achieved. Table 2.3 shows a simplified petrographic classification of coal for coking technology (Gibson, 1979).

Table 2.3 : Petrographic classification of coal for coking technology
(Source: Gibson, 1979)

Coking characteristic	Petrographic constituents
Reactive	Vitrinite with reflectance between 0.5 and 2.0% Liptinite (ex Exinite)
Intermediate (partially reactive)	Semifusinite (reflectance <2.0%)
Inert	Fusinite, micrinite Vitrinite with reflectance >2.0% Mineral matter (shale, pyrite)

2.2.1.3 Coal Grade

Mitchell (2014) defines coal grade as a term used to indicate the value of coal material, as determined by the amount and nature of ash yield and the sulphur content following the complete oxidation of the organic fraction. Calorific value is one of the principal measures of a coal’s value as a fuel and is directly influenced by mineral impurities (Mitchell, 2014).

Calorific value is defined as the amount of heat evolved when a unit weight of coal is burnt completely and the combustion products cooled to a standard temperature of 25°C, this is termed gross calorific value (Majumder, *et al.*, 2008). Calorific value equation as determined by:

$$CV (MJ/kg) = -0.038A - 0.118M + 0.33VM + 0.35FC \{R^2 = 0.98\} \dots\dots\dots (d)$$

(From 250 coals) where A = ash, M = moisture, VM = volatile matter, FC = fixed carbon

$$CV (kJ/kg) = 328.4C + 1422H + 92.7S -138.0O + 636 \dots\dots\dots (e)$$

(From a set of 1004 coal samples (Given *et al.* 1986).

Coal mineralogy is not only important to combustion characteristics, but also as materials that can be passed on to secondary products such as metallurgical coke. Alkalis-containing compounds derived from coal minerals can contribute to excessive gasification of coke in the blast furnace and attack of blast furnace refractories, whereas phosphorus and sulphur from coal minerals can be passed on to the hot metal, thus reducing the quality for steelmaking.

During the coal to coke transformation, coal ash reports completely to coke while coal sulphur partially reports to coke. Mineral matter may occur finely dispersed or in discrete partings in coal. The majority inorganic matter is emplaced either during the initial stage of coalification (being introduced by wind or water to the peat swamp) or during the second stage of coalification, after consolidation of the coal by movement of solutions in cracks, fissures and cavities. The primary mineral components incorporated during plant deposition tend to be layered and intimately intergrown with the organic fraction, whereas the secondary mineral matter tends to be coarsely intergrown and associated with cleat, fractures and cavities. The secondary minerals may be more readily

separated (cleaned and washed) from the organic matrix to improve the value of the material.

2.2.1.4 Typical Characteristics of Coal Used as a Reductant

Coke of high stability can be produced from coal blends which have an optimum ratio of reactive components to inert components. The reactive components contribute fluidity to the coal and act as binders, while the inert components (either organic or inorganic) act as fillers in the formation of the coke structure. As the coal rank increases, the coal molecular structure becomes more ordered with the aliphatic carbon structures decreasing and the aromatic carbon structures increasing. Table 2.4 and Table 2.5 summarise desired coking coals properties.

Table 2.4 : Desirable properties of coking coals (*Source: Mitchell 1999a*)

Key utilisation parameters	Desirable properties
Coal rank	High volatile through low volatile bituminous $\approx 0.7\text{--}1.8\%$ vitrinite reflectance $\approx 45\text{--}15\%$ volatile matter (dry mineral matter free basis)
Coal type	Balance of reactive and inert components
Thermoplastic properties	Caking ability and thermoplasticity

Table 2.5 : Coal quality parameters for coke making (Sanders et al., 2010)

Coal characterisation tests	Key parameters	Typical range	Coke making related issues
Proximate analysis: moisture, volatile matter, fixed carbon, and ash	Total moisture	<10% (ar)	High moisture, creates handling difficulties at the coke ovens, lowers the bulk density of the charge and impacts on oven productivity and coke strength. Consumes energy to evaporate in the coking process.
	Volatile matter	16-36% (ad)	Coke yield is inversely related to volatile content. High volatile content is associated with reduced coke strength and of excessive shrinkage during the final stages of the coking process. Low volatile coals are associated with the formation of strong cokes but at the expense of excessive oven wall pressure.
	Ash	<12% (ad)	High ash contributes to slag formation
Ultimate analysis: C, H ₂ , N ₂ , S and O ₂	Sulphur Oxygen	<0.8% (ad)	Most sulphur in coal reports to coke. Higher oxygen content leads to lower coke yields. Also, during coking, the oxygen reacts with hydrogen endothermically, increasing the energy requirements of the coking process.
Ash analysis	Phosphorus Alkalis, K ₂ O and Na ₂ O	<0.1% (ad) <3% Total	All phosphorus in coal reports to coke. Alkalis (K ₂ O and Na ₂ O) in coal ash report to the coke ash. Alkalis cause a range of problems among which are a reduction in coke hot strength and subsequently coke breakdown.

Table 2.5: Continued...

Coal characterisation tests	Key parameters	Typical range	Coke making related issues
Crucible Swelling Index	CSN	>3	Those coals which exhibit little or no caking may not produce good coke in their own right but this does not disqualify them for inclusion in a blend since they can be blended with other coals which have superior caking properties.
Gieseler Plastometer	Maximum fluidity	>100 ddpm	Fluidity of Japanese blends is about 100–1000 ddpm.
Maceral analysis	R _{o, max} or R _{v, max}	0.7–1.5%	Mean R _{o, max} of Japanese blends is about 1.1–1.2%.
Hardgrove Grindability Index	HGI	50 - 52	High values indicate a coal is easy to grind and low values indicate a coal is hard to grind. HGI tends to increase with rank for bituminous coal types, although high rank anthracites tend to have low HGI values.

2.2.2 Graphite and Semi-graphite

Kwiecińska and Petersen (2004) reviewed the 'ICCP' (International coal and coking programme) classification of carbonaceous material that covers graphite, semi-graphite, natural coke and natural char. The four materials are shown to be basically secluded from the macerals of the ICCP system 1994, as they were found to be nonconforming to any of the definitions for the vitrinite, inertinite and liptinite maceral groups.

Graphite and Semi-graphite are mainly obtained by graphitization and, basically, represent the final product or a high metamorphic grade in the coalification process (continuous transformation of organic matter), which starts from peat through bituminous coals and anthracite to graphite (Kwiecińska and Petersen, 2004). Werner (1789) in Kwiecińska and Petersen (2004) is confirmed to have coined the term graphite. Kwiecińska and Petersen (2004) defined graphite as a crystalline polymorphic type of elementary carbon.

2.2.3 Natural Coke and Natural Char

Natural coke is also known as geological coke, burnt coke, cinder, Jhama and thermally metamorphosed coal (Taylor *et al.*, (1998) in Kwiecińska and Petersen (2004)). In comparison to graphite, Kwiecińska and Petersen (2004) described natural coke as being formed from increased flow of heat from an intrusive body. This means that it can be seen in all forms of coalification stages. Stach (1952) in Kwiecińska and Petersen (2004) described natural coke as normally dull, compact and hard as well as containing pores that are either empty or full of mineral matter, mostly calcite. These pores have varying features that include size, shape, distribution and orientation.

Natural char is also found in all coalification stages but mainly resulting from the effect of heat from fire on coal or jellified organic matter in peat (Kwiecińska and Petersen, 2004). ICCP (2001) in Kwiecińska and

Petersen (2004), illustrated that char could not be grouped together with the rest of the inertinite group macerals due to its morphology. This is characterized by a random distribution of pores and varying porosity. The distribution of pores plays a major role in differentiation from other macerals which could be confused with natural char, as in charcoal (fusinite), semifusinite and funginite. A combustion char classification system based on the morphological similarities to chars obtained from low-temperature coal pyrolysis, is confirmed to make it possible to classify the natural chars (Kwiecińska and Petersen, 2004). Several systems were noted by the authors including systems from Bailey *et al.* (1990), Rosenberg *et al.* (1996), and the ICCP Combustion Working Group in Kwiecińska and Petersen (2004).

2.2.4 Coke (Metallurgical and Market)

Jordan and Falcon (2010) defined coke as a macro-porous, low mineral content, carbon material. It is processed from coals that transform into fluid at a given temperature but will re-solidify at a higher temperature. This is attributed to the specific range in coal rank, with the coke basically produced over 16 to 65 hours at temperatures starting from 950°C to 1200°C, according to the coking technique utilised (Jordan and Falcon, 2010).

The authors confirmed that the major application for coke is found in the blast furnace production of iron where it plays the role of a fuel, chemical reducing agent and permeable support for both the liquid and gas phases. This type of coke in South Africa is known as metallurgical coke which is mainly used in iron making as stated above. Market coke is the reductant mainly used in the Ferrochrome industry and this has relatively lower physical strength/properties compared to metallurgical coke (Jordan and Falcon, 2010).

2.2.5 Typical Carbon Reductant Characteristics for the Metallurgical Industry (Quality, Reactivity, Strength, CRI, CSR)

The following are some of the critical characteristics required or desired in the metallurgical industry. The most important properties of the carbonaceous materials in ferroalloys production include:

- high reactivity;
- high conversion;
- physical strength;
- low amount of impurities.

Porosity of the char/coke is a function of the coal composition as well as the carbonisation condition. Information on the coal characterisation, procedures and analyses of the char/coke is important. For example, pore size distribution of the material affects the effective diffusivity and thus determines the reactivity and conversion (Basson *et al.*, 2007).

2.2.5.1 Coke Quality

A high quality metallurgical coke should be able to support smooth descent of the burden in a blast furnace with as little degradation as possible, while providing the lowest amount of impurities, highest thermal energy, highest metal reduction, and optimum permeability for flowage of gaseous and molten products (Valia, 2010).

2.2.5.2 Reactivity

Reactivity is a term that characterizes the velocity of generation of reducing gas according to the reaction:



The NSC test determines the Coke Reactivity Index (CRI) which is expressed by the mass loss (%) of the specimen (d = 20 mm, τ = 120 min,

t = 1100 ± 5°C, CO₂ = 5 l/min) (American Society for Testing and Materials, 1993).

$$CRI = \frac{\text{Original weight} - \text{Weight of residue}}{\text{Original weight}} \times 100 \dots\dots\dots (f)$$

2.2.5.3 Cold strength

The cold strength of a coke refers to its resistance to breakage or friability in ambient temperature. The tests used are the Micum test, IRSID test or ASTM test, all using rotating drum indices as indicated below:

- Micum Test: drum indexes M₄₀, M₁₀: grain sizes of +40 mm (breakage) and - 10 mm (abrasion) in % (drum: 1 × 1 m, 100 revolutions, 25 rev.min⁻¹) (Jones and Kruse, 1982).
- IRSID test: drum indexes I₄₀, I₁₀: grain sizes of +40 and -10 mm in % (drum: 1 × 1 m, 500 revolutions, 25 rev.min⁻¹) (Jones and Kruse, 1982).
- ASTM test: grain sizes of +1 " (25 mm) and - ¼" (6 mm) in % (drum: 0.46 × 0.91 m, 1400 revolutions, 24 rev.min⁻¹) (Jones and Kruse, 1982).

2.2.5.4 Hot strength

The NSC test determines the Coke Strength after Reaction (CSR). The CSR value is measured in one test procedure with CRI under gasification of the coke sample with carbon dioxide and expressed by the grain size portion (in %) +10 mm after 600 revolutions at 20 rev.min⁻¹ (American Society for Testing and Materials, 1993; Menéndez *et al.*, 1999).

$$CSR = \frac{\text{Weight of +10 mm coke after tumbling}}{\text{Initial weight of coke}} \times 100 \dots\dots\dots (g)$$

Stankevich *et al.* (2001) have observed that Mechanical strength (M₄₀ & M₂₅) of coke increases and its abrasability (M₁₀) decreases with increasing

vitrinite reflectance index of the coal blend up to 1.25-1.3%. It is important to note that besides these standard tests to evaluate coke quality, there are also methods to simulate specific conditions. Examples of these tests are:

1. Global Coke Quality Index (Bonte *et al.*, 2005),
2. Deadman Cleanliness Index (DCI) (Nightingale *et al.*, 2002),
3. Coke dissolution investigation (Gudenau *et al.*, 1990),
4. Investigation of coke behaviour under simulated changing BF conditions using a Tammann furnace experimental set (Babich *et al.* (2006); Babich *et al.* (2009)),
5. Optical particle analyser to measure the shape of the coke particles and grain size distribution of blast furnace coke (Peters *et al.*, 2011).

As these tests will not be used in the current research programme, they are not described any further.

2.3. Ferrochrome Reductant Characterization and Reactivity Tests

Characterization of the various reductants is important as this helps to link their properties to performance in the furnace. This is demonstrated by Sahajwalla *et al.* (2004), who proved that reductant performance is greatly linked to its properties which include:

- physical properties;
- structural order;
- amount of mineral matter; and
- composition.

2.3.1 Reductant Characterization

Sahajwalla *et al.* (2004) described typical characterization techniques with regards to reductant selection for use in the ferroalloys production. These can be summarised as follows:

- **Chemical Analysis** – this includes basic characterization by establishing the amount of moisture, ash, volatile matter, fixed carbon (proximate analysis) together with chemical elemental analysis of the carbonaceous material (ultimate analysis, *i.e.* C, H, O, N and S). Other techniques for quantitative determining elemental/chemical composition include the Atomic Absorption Spectroscopy (AAS) and X-Ray Fluorescence analysis (XRF).
- **Physical Parameters** – This includes mechanical and physical tests e.g. grindability, free-swelling index, specific gravity, fusion temperature, coke strength after reaction (CSR – mainly critical for blast furnace processes), coke reactivity index (CRI).
- **Structural Characterization** – Techniques that provide structural molecular data include XRD (X-ray Diffraction), TEM (Transmission Electron Microscope), Tomography, NMR (Nuclear Magnetic Resonance), SEM (Scanning electron Microscope) and Raman Spectroscopy. Combined with computer simulations, these techniques are used to improve the appreciation or understanding of material structure at atomic level, and after transformation following heat treatment and oxidation.
- **Optical characterization** - Other authors (e.g. Steyn and Smith, 1977) also used coal and coke petrography to establish the nature of coal used to produce the reductant and the resultant product to be used in the metallurgical process.

More techniques are applied to coke as adopted from tests described in the Speight (2013) for coal that cover mechanical, thermal and electrical properties as summarised in Table 2.6. A brief review of some of the techniques applied in this study is given below.

Table 2.6: Electrical, Mechanical and Thermal Properties (Source: Speight, 2013)

Test	Results/Comment
<i>Mechanical properties</i>	
Strength	Specification of compressibility strength
Hardness/abrasiveness	Specification of scratch and indentation hardness; also abrasive action of coke
Friability	Ability to withstand degradation in size on handling, tendency toward breakage
Grindability	Relative amount of work needed to pulverize coal
Dustiness index	Amount of dust produced when coal is handled
<i>Thermal Properties</i>	
Calorific value	Indication of energy content
Heat capacity	Measurement of the heat required to raise the temperature of a unit amount of coal 1°
Thermal conductivity	Time rate of heat transfer through unit area, unit thickness, unit temperature difference
Plastic/agglutinating	Changes in a coal upon heating; caking properties of coal
Agglomerating index	Grading on nature of residue from 1-g sample when heated at 950 °C (1550 °F)
Free swelling index	Measure of the increase in volume when a coal is heated without restriction
<i>Electrical Properties</i>	
Electrical resistivity	Electrical resistivity of coal measured in ohm-centimetres
Dielectric constant	Measure of electrostatic polarizability

2.3.1.1 XRD (X-ray Diffraction Analysis)

According to Brugemann *et al.* (2004), X-ray photons find use in several significant analytical techniques like X-ray diffraction or scattering (XRD) and X-ray fluorescence analysis (XRF). In XRF, the material under

investigation emits X-ray radiation following excitation, and this radiation has unique energy levels for each material constituent or element(s). Prediction of the material's elemental composition is consequently achieved by quantifying the discharged photons' energy levels. The XRD instead, works by scattering of the radiated beam whose wavelength is of the same size to inter-atomic distances of the material probed (Brugemann *et al.*, 2004).

This is also described by Munson (2001) as single-crystal XRD that is used to establish the molecular arrangement of material, since the wavelength of the X-rays diffracted is related to the space between the molecules within the material, thereby representing a diffraction matrix or grid. The correlation between the angle of diffraction and distance between the molecules is given by the Bragg equation:

$$n \lambda = 2d \sin \theta \dots\dots\dots(h)$$

- Where;
- λ represents the X-rays' wavelength;
 - d represents the distance between reflection planes; and
 - θ represents the angle between the incident and diffracted beam.

This technique is applied to differentiate the crystal phases occurring under two dimensional matrix points linked to the crystal lattice planes of the material under investigation. The same information can then be used to derive the three-dimensional orientation of atoms (Munson, 2001).

2.3.1.2 SEM (Scanning Electron Microscope)

The SEM is mainly used during micro analysis of mineral phases. In a review of characterization and recovery of platinum group metals, Xiao and Laplante (2004) summarised the strengths and weaknesses of the various analysis techniques available to the minerals industry. The SEM is confirmed as being amongst the flexible and extensively utilised present

day techniques, which is basically attributed to its capabilities for investigating both the material's morphology and structure.

The SEM achieves this by essentially scanning an electron beam over a specimen at either very low or very high resolution to generate morphological or topographical images of the specimen. The authors describe the SEM as significantly different from the other optical instruments as it utilizes a focused beam of electrons and not of light to produce a visible impression of the specimen. This electron beam is generated under high vacuum by a gun mounted above the SEM column and is narrowed and concentrated or intensified through the use of slits and magnetic lenses. An outer layer film is used to cover the sample and help avoid surface charging. The electron beam acts on the sample resulting in signals like backscattered electrons (BSE), secondary electrons (SE), and X-rays being generated. These signals are detected by the corresponding detectors on the SEM.

Petruk (2000) in Xiao and Laplante (2004) further illustrated the use in process mineralogy of SEM coupled with an energy dispersive analyser (EDX) to analyse polished and/or narrow segments of a sample as well as unmounted material components. This means the following can be achieved with regards to most minerals being investigated:

- Identities of minerals;
- Size and relationship of mineral grains; and
- X-ray spectra, displaying the various elements dispersal (Xiao and Laplante, 2004).

Steyn and Smith (1977) reiterated that South Africa is endowed with considerable reserves of coals of a relatively low quality and quantities for making metallurgical coke. In their review of South African coals, they emphasized the importance of taking advantage of all technological means available that can assist with competent characterization, manufacture and application of coking coals. In support of this approach,

documentation is noted of several techniques existing on the assessment of coke quality using petrographic data. The link in coal petrographic properties to the produced coke is shown to have been given more focus from the time when a Russian scientist, Ammosov, successfully established a way of interpreting petrographic information in numerical terms, with a correlation to the coke strength (Steyn and Smith, 1977).

Optical methods were further expanded by Shapiro and co-workers in Steyn and Smith (1977), where this method was found to be applicable for the evaluation of the coking coal potential of some American and high vitrinite coals but not to Australian, Indian and South African coals. Steyn and Smith (1977) pointed to the insufficient classification of macerals found in the method by Shapiro and co-workers and illustrated their own method which was found to be more successful in translating coal petrographic data into coke quality parameters for South African coals. The authors demonstrated their understanding in terms of fusible or reactive macerals and in particular the part semifusinite and micrinite play in the carbonization process, as outlined in the next section.

2.3.2 South African Coal Properties Affecting Coking and Coke Properties

Coal properties with regards to coal in general have been summarised earlier. This section presents data pertaining in particular to South African coals.

2.3.2.1 Vitrinite

Vitrinite was earlier defined as the main reactive component of coking coals that turns to plastic, exudes volatiles, swells, and re-solidifies (ref). In the process, this maceral bonds all the inert components that stay unchanged during carbonization (Steyn and Smith, 1977). The potential of vitrinite to bond the inerts is related to its rank as indicated by vitrinite

reflectance. The capacity bond is established as rising with a rise in reflectance of 1.2-1.3% but this falls with further increase in rank.

Steyn and Smith (1977) demonstrated that the bonding capacity greatly falls when vitrinite reflectance for the South African coals goes beyond 1.49 and when above 1.89, the vitrinite is considered to be inert. Shapiro *et al.* in Steyn and Smith (1977), in their classification, instead gave all vitrinite with a reflectance up to 2.19 as reactive. Oxidation and the negative effect of dolerite intrusions renders the vitrinite inert. The extent of inertness is directly related to the level of oxidation and alteration (Steyn and Smith, 1977).

2.3.2.2 Liptinite (ex Exinite) Group

In evaluating the coking properties of local coals, the possibility of exinites (now known as liptinites) to take part in the coking process, were assumed to be at the same level as vitrinite and thus mistakes can occur in coals rich in liptinite (Steyn and Smith, 1977). It is however confirmed that South African coals contain less than 5% liptinite, with sporinite as the major component. Also, liptinites are characterized (e.g. Snyman, 1961) in Steyn and Smith (1977) as the corresponding vitrinite or micrinite when the reflectance is the same as the vitrinite or micrinite.

2.3.2.3 Reactive Semifusinite and Micrinite

According to Steyn and Smith (1977), opposing views concerning the behavior of semifusinite and micrinite during carbonization are noted in literature as follows:

- Shapiro *et al.* (1961 and 1960) and Ammosov *et al.* (1957) in Steyn and Smith (1977), classified a third of the semifusinite as reactive and two thirds plus all micrinite as inert.
- Taylor *et al.* (1957) in Steyn and Smith (1977), initially stated that all semifusinite and micrinite looked inert when undergoing carbonization but later noticed an intermediate substance linking vitrinite and semifusinite.

The substance was observed to change consistency on carbonization and the authors grouped this material with vitrinite in order to keep away from applying the phrase semi-vitrinite.

- Thompson *et al.* (1968) in Steyn and Smith (1977), grouped the substantial, but with inferior reflectance, micrinite together with semifusinite to make a semi-inert class that had a fixed proportion assigned to the reactives.

These disparities, however, do not have any significance for the coking process with regards to coals occurring in the USA and Europe as they are comprised of significantly lower amounts of these partially reactive maceral components (Steyn and Smith, 1977). In comparison, South African coals with the exclusion of Northern Transvaal, are confirmed to be similar to the majority of Gondwana coals that have significantly low vitrinite contents and an extremely high semifusinite and micrinite content. The coals are known to be rich in micrinite that is similar to semifusinite with regards to hardness and reflectivity. For these reasons it is imperative to know the action of semifusinite and micrinite under carbonization conditions in order to be able to link the coals petrographic composition with the corresponding coke's physical properties (Steyn and Smith, 1977).

Studies by Steyn and Smith (1977) on coke and semi-coke concluded that both semifusinite (structured or slightly structured) and micrinite (granular and massive) with inferior reflectance notably participate in coke making and consequently these are categorized as reactive components in coal that contribute to the coke-making structure. Following several petrographic analyses on South African coals at different vitrinite levels ranging from 40% to plus 90%, the authors also deduced that semifusinite and semi-micrinite must be taken as a separate group of reactives that make up to 60% of total semifusinite plus micrinite than be taken on a discretionary base.

Another important conclusion made by Steyn and Smith (1977) was that the South African coals having a substantial amount of micrinite similar in *hardness* and *reactivity* to semifusinite. Differentiating the structure-less semifusinite from micrinite is almost impossible when dealing with milled coal despite use of up to 50 times magnification lens during micrometric analyses (Steyn and Smith, 1977). Consequently, the macerals are known as inert 'semifusinite' and reactive 'semifusinite'. This categorization of semifusinite and micrinite helps justifying how some coals with low proportions of vitrinite and very high proportions of 'semifusinite' produce relatively superior coke. In so doing, this process also enables the linking of petrographic information (coals with vitrinite from 40 to plus 90 percent) with the physical properties of coke (volatile matter content, Roga-index and Micum indices). This methodology has now been in practice in the South African iron and steel industry for more than a quarter of a century.

2.3.3 Reactivity Tests

The reactions of carbonaceous materials in processes including gasification, carbon dissolution into molten metal and reduction of slag by solid carbon are illustrated by Sahajwalla *et al.* (2004). Several tests have been reported on reactivity and reduction tests with chromite ore and various reductants e.g. charcoal, coal, coke plus graphite under fluxing and non-fluxing conditions by authors including Soykan *et al.* (1991), Neuschutz (1992), Barnes and Eric (1995) and Weber and Eric (2006), . The tests concluded that thermogravimetric analyses (TGA) coupled with metallisation and microscopic data, give all the information required to predict, model and simulate the process kinetics during reduction. As indicated in Barnes and Eric (1995), a pre-weighed sample of reductant and chromite ore is subjected to a fixed temperature for a set period of time using TGA. This offers a simpler test of assessing reactivity. The TGA data is compared to metallisation data to verify the reactivity of studied reductants.

For the reactivity measurements, Pistorius (2002) further explained how CSR and CRI are inversely linked, with percentage mass loss through the Boudouard reaction representing the CRI, whilst the CSR gives a measure of the deterioration in terms of size as given by amount of coke remaining after tumbling, *i.e.* providing the proportions of coke particles that are greater than 10 mm, expressed as a percentage.

Reactivity tests done by Barnes *et al.* (2015) revealed that, during solid state reduction of UG2 chromite ore, about 85% reduction can be achieved in 50 minutes when using the patented Winter process (Figure 2.5).

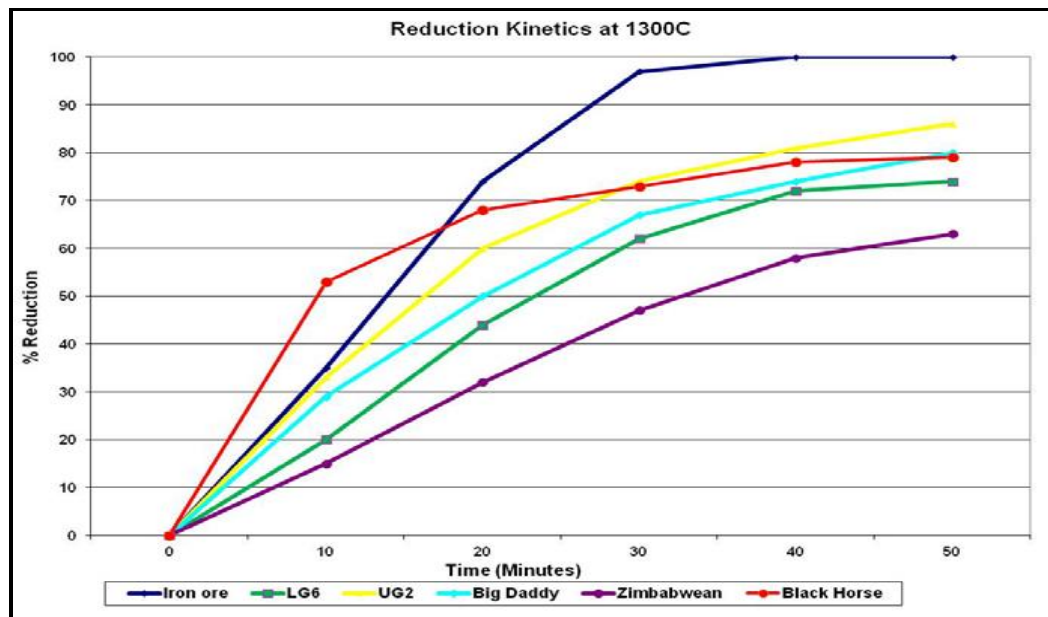


Figure 2.5 : Chrome Ore Reactivity at 1300°C (Source: Barnes *et al.*, 2015)

Barnes *et al.* (2015) emphasized that due to the tendency of re-oxidation of highly metallised products, as a guide 80% metallisation is thus taken as a norm in solid-state reduction.

Wilkinson (1984) concluded that coal properties of rank and chemistry exercise considerable influence on coke reactivity. Influence of coal rank on reactivity is demonstrated by the inclusion of the volatile matter term in

the relationship. Of the coke structural properties considered, porosity and feature count correlate more closely with reactivity than others examined. The more reactive a coke is, the higher its consumption (Hermann, 2002).

2.3.3.1 Quality and Nature of Reductant

Nurmukhanbhetov *et al.* (2013), in a comparative study demonstrated how important quality factors of reducing agents, *viz.* electrical resistance and reactivity, in ferroalloy production depended on the nature of coal and processing conditions. They illustrated the kinetic behaviour of chromite reduction by different types of carbonaceous materials during HC FeCr production.

Reactivity tests were carried-out at laboratory scale by Nurmukhanbhetov *et al.* (2013) using thermogravimetric method under temperatures ranging from 1200°C to 1600°C, with the following reductants;

- ✓ China Coke;
- ✓ Russian Coke;
- ✓ Char; and
- ✓ Special Coke.

The special coke under investigation represents a non-coking coal charred under flash heat conditions and oxidising environments. The 0.315-1.000 mm ore analysing 50% Cr₂O₃ and 3.000-6.000 mm sized reductants, with the proximate analysis in Table 2.7, were mixed in stoichiometric quantities.

Table 2.7: Reductant Proximate Analysis (*Source: Nurmukhanbhetov et al., 2013*)

Reductant	Ash	Moisture	Volatiles	Sulfur	Phosphorus
Russian Coke	13.5	1.8	1.5	0.50	0.045
China Coke	14.0	3.5	2.7	0.27	0.015
Char	10.0	4.1	20.0	0.51	0.040
Special Coke	7.1	3.2	7.5	0.27	0.020

The evolution of CO was assumed to represent the conversion of Fe and Cr and thus determined from the resultant mass loss (Nurmukhanbhetov *et al.*, 2013).

It is established that both the conversion and reduction rates of chromite at all temperatures are relatively high for special coke, and that both rates of reaction also increased with rising temperature. In summary, much has been achieved in understanding the coals of the world in terms of their capacity to form reductants. Few, however, compare South African coals and non-conventional carbon forms in ferrochrome reduction.

3. METHODOLOGY

This section outlines the materials used (reductants and chromite ore) and experimental techniques used during the test work. The solid-state reduction methodology and apparatus described in Soykan *et al.* (1991), also used by Barnes and Eric (1995), were applied to determine reactivity of the selected reductants.

3.1. Equipment

Thermogravimetric Analysis (TGA) was identified as a suitable technique to investigate the reactivity of various reductants during solid -state reduction of chromite. Schematic and photographic images of the TGA setup that was used in the test work are shown in Figure 3.1 and Figure 3.2, respectively. The TGA setup is constructed of a vertical tube furnace heated with MoSi₂ elements.

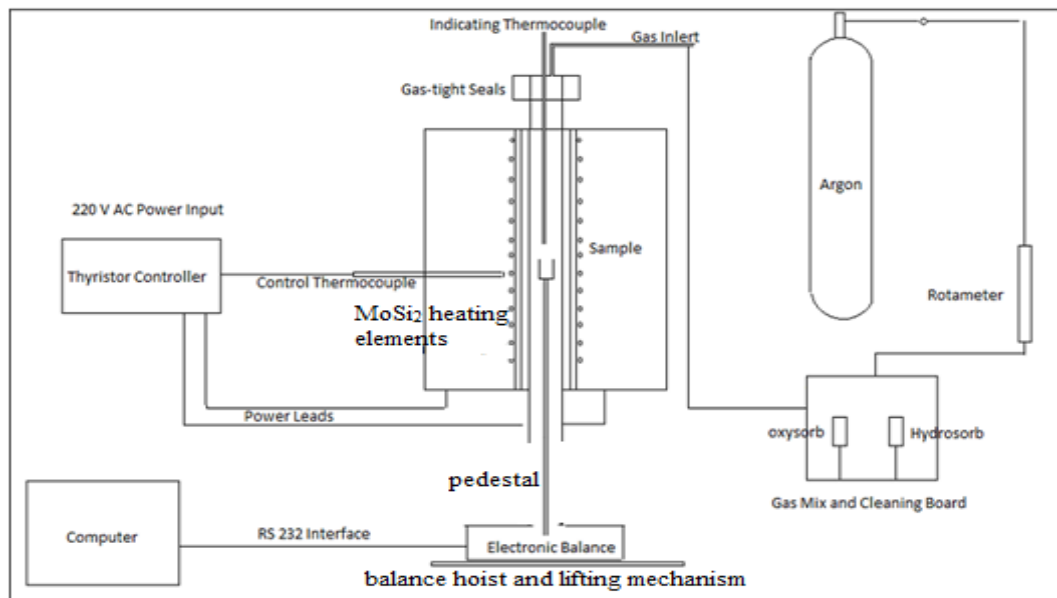


Figure 3.1: Schematic Thermogravimetric analysis setup (Source: Barnes and Eric, 1995)

Typically, a TGA test involves taking a sample and loading it into a high purity alumina crucible which is placed on a thermo balance and inserted

into the TG furnace tube reactor (high purity alumina tube) by means of a mechanical lifting mechanism. The sample mass change is continually measured as a function of temperature and time throughout the experiment. For thermal profiling, the sample is introduced to a cold TG furnace tube reactor and slowly heated up to the test temperature. However, for isothermal testing, the crucible is pre-heated in the lower temperature zone of the tube, to avoid crucible thermal shocking, before rapid lifting to the hot zone of the already hot furnace.

As it appears in the setup, the test gas, *i.e.* Ar, is first subjected to a gas mixing and cleaning stage where the residual moisture and oxygen are removed by means of hydrosorb and oxysorb systems, respectively. The operating gas atmosphere of the TGA is introduced from the top of the sealed alumina reactor (Figure 3.2). The inlet gas strategy allows for a gas flow of known composition to occupy the reactor, *i.e.* reaction zone, with limited air ingress. The (limited) gas flow is allowed to continuously vent from the bottom of the reactor without disturbing the balance.

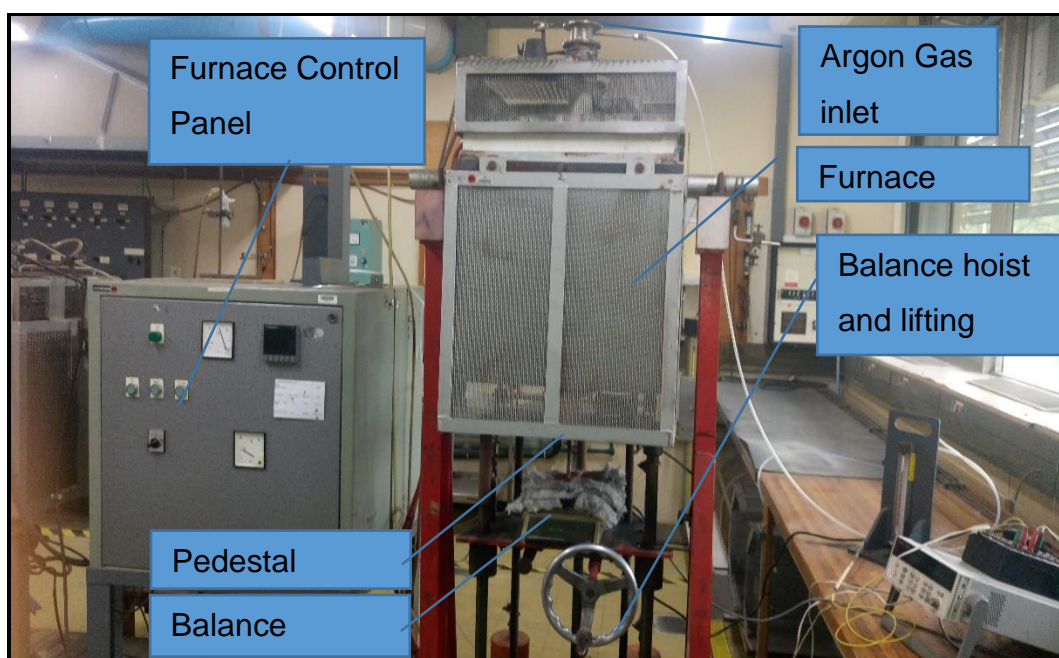


Figure 3.2: Photographic image of the thermogravimetric setup (Mintek, 2016)

The configuration of the envisaged TGA setup is limited to the processing of one sample at a time. The analyzer allowed for a sizeable amount of sample material per test, *i.e.* 20-50 grams, which guaranteed that enough material will be available for product characterization.

3.2. Materials

Feed material for the TGA reduction tests comprised of chromite ore and a range of reductants that include the unconventional reductant (Charcoal from Eucalyptus hardwood) and a selection of conventional reductants made from different types of coal (coking, semi-soft non-coking and a blend of the two). The reductants chemical analysis determined by ICP-OES, including bulk chemical composition of ashes from the respective reductants was also done. All the reductants were initially pulverized in a ring-mill and dried before mixing with the chromite concentrate in stoichiometric quantities. Both reductant and chromite ore's particle size distribution (PSD) was determined at Mintek, using the Malvern apparatus. These are described further below.

3.2.1 Chromite ore

The chromite concentrate used was a typical UG2 chromite ore, provided by Siyanda Mine. It is a flotation by-product obtained during beneficiation of platinum ore.

3.2.2 Reductants

The reductants tested included two types of conventional reductants comprising (1) Typical Market Coke (A) used in the ferrochrome industry, (2) Trial Market Cokes produced from varying proportions of coking and non-coking coals (B, B1) and (3) Industrial Char (C). 25 kg of each sample was obtained from a Ferrochrome industrial source. Preparation and analyses done are listed below.

The conventional cokes were tested against an unconventional reductant, i.e. charcoal made from Eucalyptus hardwood, sample labeled (D). The reductants used during the test work are summarised as follows:

- i. Conventional reductant A –Standard Market Coke (Control)
- ii. Conventional reductants B and B1 – Trial Market Coke (different coal blends)
- iii. Conventional reductant C – Industrial Char
- iv. Unconventional reductant D – Charcoal from Hardwood

The selection of conventional reductants was such as to cover the whole spectrum of reductants made from coal sources available in South Africa, from coking to non-coking coal and a blend of the two.

3.3. Sample Preparation

The sample size for both the reductant and chromite was chosen to be fine, as demonstrated in Weber and Eric (2006), as this afforded the highest possible contact area between the two reactants. Significant quantities of feed material (Master sample) were prepared to ensure enough material would be available for unforeseen repeats during characterization of feed material and the reactivity tests. Sample crushing, sizing and weighing were undertaken according to available test equipment requirements, e.g.

1. A -250 μm particle size sample for all the tests was required except for petrography sample (-1 mm),
2. Respective masses of 30g of the sample blends were weighed and processed in the TGA test work.

The chromite ore concentrate size distribution (Figure 9.1 in Appendix A), dictated that the reductant be milled to enable thorough blending. The process summarised in Figure 3.3, shows typical stages undertaken during reductant feed material preparation before mixing with the ore.

Drying of the feed materials was carried-out in an oven, at 105°C for 3 hours.

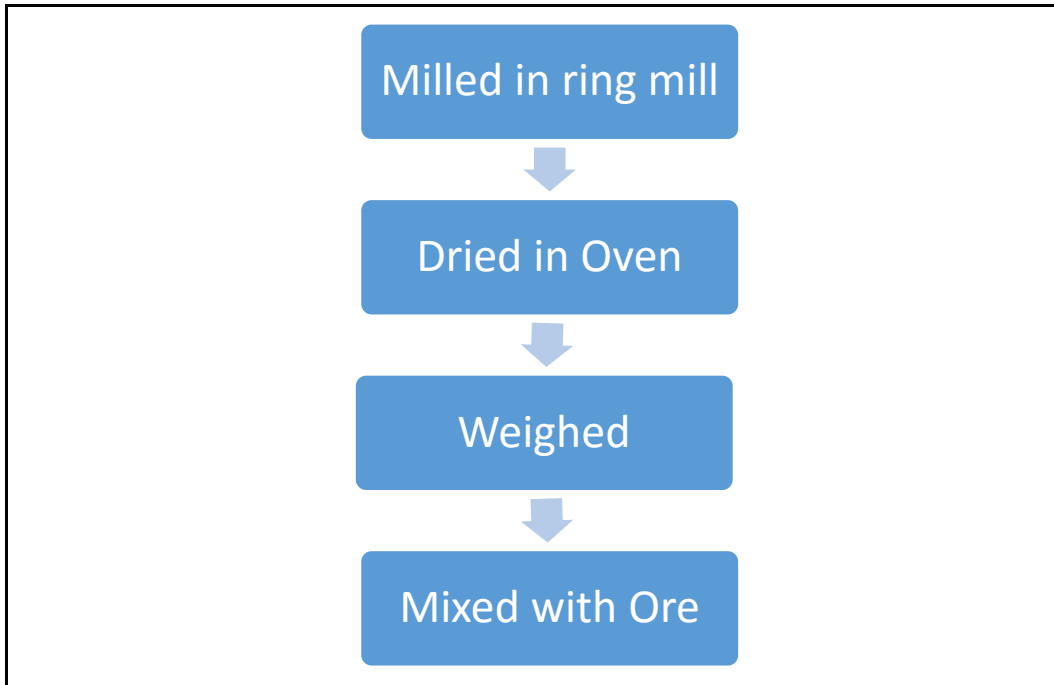


Figure 3.3: Reductant Feed Material Preparation

Respective test sample blends of reductant and chromite, weighing a total 30g, was prepared from the dried materials for completing the test matrix in the TGA furnace.

The reductant additions for reactivity tests were calculated at 40% excess of the stoichiometric requirements (see Table 3.1).

Table 3.1: Typical Reaction Mix of Reductant and Chromite Ore

Reductant Type	Fixed Carbon Mass (%)	Reductant Mass (g)	Chromite Ore Mass (g)
A	87.1	115.22	500
B	83.0	120.91	500
B1	73.0	137.47	500
C	76.4	131.36	500
D	65.0	154.39	500

Nb. Calculations based on ore and reductant oven-dried to 0 % moisture.

This was done in order to ensure that there was no carbon dioxide generated by immediately converting any carbon dioxide to carbon monoxide (ensure presence of a reducing atmosphere).

3.4. Reductant Reactivity Tests

The reductant reactivity tests were conducted using TGA. Well-mixed milled and pre-dried samples of the selected reductant and UG2 chromite concentrate were introduced to a vertical alumina reactor of the resistance tube furnace, which had been pre-heated to the required test temperature. The furnace temperature was controlled and monitored by the use of a B-type (Pt-6%Rh/Pt-30%Rh) thermocouple, and a Eurotherm thyristor coupled controller unit utilized as a control linked to the TG furnace. There were some inherent limitations with the experimental configuration of the TGA setup. This included that only one sample at a time could be processed and also the lack of an opportunity to quench the sample at the end of the 4 hour holding period, to instantly preserve the actual reaction stage and state of the reaction mix. However, at the end of the holding period, further reactions were limited by cutting-off the furnace power and continued argon purging.

The sample was weighed into a high-purity alumina crucible with the mass of both the sample and crucible recorded. The weight taken for each sample was captured in the TGA operating program. The crucible was placed on the pedestal of a balance that is part of the TGA system (Figure 3.2). The sample was lifted up to the hot/ reaction zone from the bottom by means of a mechanical lifting mechanism when the furnace was already at required isothermal test temperature. The lifting rate was slow in order to avoid thermal shock on the ceramic crucibles.

The reactivity tests were carried-out at 1100 °C, 1200 °C, 1300 °C, and 1400 °C for 4 hours (Table 3.2) under an inert argon (Ar) atmosphere, before the reactants were allowed to cool down to room temperature

inside the furnace, under the same argon atmosphere. A maximum holding time of 4 hours at each temperature was chosen to determine the effect of time on the solid state reaction. Duplicate tests were conducted for each reductant to evaluate the reproducibility of the test procedure, with further repeats performed whenever the TGA results appeared inconsistent. The equipment was also used by other clients both from academia and the industry, which negatively affected availability and turnaround times as well as the number of repeat tests done (Table 3.2).

The Argon gas used was supplied by Afrox. Gas purging was done at 400 cm³ per min during the holding period. The mass loss was determined immediately after the sample was introduced to the hot zone, by zeroing the weight on the balance. The measurements were captured and recorded on a computer linked to the balance. The data captured continuously per second, was averaged over one-minute intervals and used to plot TGA mass loss profiles. The mass loss measurements stored on the computer were then processed to determine the degree of reduction and degree of metallisation, on the basis that the mass loss incurred was mainly due to the generation of carbon monoxide.

Table 3.2: Final Test Work Matrix (Solid State Chromite Reduction)

Reductant	1100 °C	1200 °C	1300 °C	1400 °C
A	1	1	1	2
B	1	1	1	2
B1	1	1	1	2
C	1	1	1	2
D	1	1	1	2
Total	5	5	5	10

3.5. Reactivity mechanism and characterization

The temperatures and holding times utilized were selected based on the reactivity tests performed by previously mentioned authors, including the

adopted sample preparation procedures. A fixed amount of chromite ore was used as a basis to calculate the stoichiometric reductant required. As the fixed carbon in the selected reductant changed, the reductant mass was also adjusted to match the 500g chromite ore sample. The mass loss of each sample was measured continuously and recorded with a personal computer (Figure 3.1). The data was further processed and utilized for determining essential parameters including but not limited to:

- Isothermal profiles of the chromite and reductant reactions;
- Calculating the reactivity or degree of reduction (R (%)); and
- Calculating the degree of metallisation (M (%)),
- Saturation point of each test.

The degree of reduction is generally determined by applying equation (i) below, as the mass of CO evolved is assumed to be equal to the mass loss recorded by the TGA. This is also assumed to be mainly resulting from chromium and iron oxides reduction by carbon.

Barnes *et al.* (1983) clarified that the terms *degree of reduction* and *metallisation* depended on the experimental technique applied by researchers. The terms are understood to be more clearly demonstrated for iron ore reduction compared to chromite reduction. The following two expressions of reduction, *i.e.* (i) and (j) are given to illustrate this view based on the TGA mass loss taking place.

$$R(\%) = \left(\frac{\text{Mass of CO evolved}}{\frac{28}{16} * \text{Original Removable Oxygen}} \right) * 100 \dots\dots\dots (i)$$

$$R(\%) = \left(\frac{\text{Mass of O}_2 \text{ evolved}}{\text{Original Removable Oxygen}} \right) * 100 \dots\dots\dots (j)$$

Expression (i) is applied when solid carbon is the reducing agent, with carbon monoxide generated according to Boudouard reaction whereas

expression (j) is used when reduction is specifically accompanied by the loss of oxygen.

The original removable oxygen in both (i) and (j) was assumed to be mainly derived from Fe₂O₃, FeO and Cr₂O₃ oxides analyses of the chromite ore (Barnes *et al.*, 1983).

Eric and Burucu (1992), in a typical study of metal oxides reduction by carbon also confirmed that it is widely acknowledged that when a mixture of the metal oxide and carbon is heated under inert conditions, reduction takes place through the gaseous species carbon monoxide. The presence of solid carbon is thus emphasised as being critical for the regeneration of carbon monoxide from carbon dioxide.

According to Barnes *et al.* (1983), Metallisation (M) is given by the following relationship:

$$M(\%) = \left(\frac{Cr+Fe}{Cr_{tot}+Fe_{tot}} \right) * 100 \dots\dots\dots (k)$$

Where;

Cr = metallic chromium

Fe = metallic iron

Cr_{tot} = total chromium

Fe_{tot} = total iron

The two mechanisms, metallisation and reduction, have a non-linear relationship due to the characteristic stages that take place during reduction, listed below:

- Initial stages of reduction are accompanied by the reduction of Fe₂O₃ to FeO, that occurs without any metallization



- Metallisation of Fe from FeO follows, generating 1 mol. of CO with each mole Fe obtained ($M = R + k_1$):



- Metallisation of Cr₂O₃ to Cr, generating 1.5 mol. of CO with each mole Cr metal obtained ($M = 2/3R + k_2$):



Constants K_1 and K_2 above are consecutively linked to the generated iron and chromium metal. From the stages listed above, full metallization is accompanied by full oxygen removal, thus complete reduction is equal to complete metallisation (Barnes *et al.*, 1983).

3.6. Analytical Techniques

Characterization tests for both the chromite ore and reductants were carried-out, followed by analyses of the reduction products. Various techniques were applied on the reduced products, *viz.*

- ✓ Chemical speciation followed by analytical instrument technique to quantify the various elemental species present;
- ✓ X-Ray Diffraction to identify the different phases
- ✓ Scanning electron microscopy for microanalysis of the phases; and
- ✓ Total Carbon to quantify the fixed carbon contents of reductants.

3.6.1 Reductant Characterization Tests

Proximate (moisture, volatile matter, ash and fixed carbon (by difference)) and ultimate (carbon, hydrogen, nitrogen, sulphur and oxygen) analyses of all reductant samples were undertaken. Reductant ash composition was determined by chemical analysis. Petrographic analyses of the reductants were achieved by microscopic assessment so that the carbon forms, reductant porosity, rank and macerals (vitrinite, liptinite and inertinite) were established. Further analytical details are given below.

3.6.1.1 Petrography

The main objective of reductant petrographic analysis was to establish the nature and texture of the carbon material. The following parameters were used to determine the different carbon forms:

- i. reflectance;
- ii. anisotropy;
- iii. morphology;
- iv. particle and pore size.

Representative portions of each reductant sample were selected and a petrographic block of each sample was prepared in accordance with the ISO Standard 7404 – 2 (1985) and then examined using reflected light microscopy and oil immersion objectives (50x magnification objective). Reductant constituent analysis (petrographic composition and binder phase forms) was carried out on each sample according to the ASTM Standard D 5061 – 92 using a Leica DM2500P microscope. An average was calculated from the results obtained for four individual portions.

Reflectance measurements were carried out on each sample using a microscope with an S&M – PMT – Photometry System. Random reflectance measurements (250) were determined in accordance with ISO Standard 7404 – 5 (1994).

3.6.1.2 Image Analysis

Optical image analysis was carried out in order to determine the porosity and cell wall width and size distribution. The latter analysis is of particular significance as it can be used to provide an indication of the strength and reactivity of the reductant. Four representative portions of each reductant sample were selected and prepared for optical microscopy by impregnating the sample with epoxy resin. Each block was then analysed using a Zeiss Axioscope A1 microscope (fitted with an automated stage). The Zeiss image analysis software, *i.e.* Mosaic, was used to measure and

calculate macro-porosity and cell wall thickness (20x magnification objective). An average was calculated from the results obtained for the four individual portions.

3.6.2 Chromite Ore and Reactivity Test Products

The UG-2 concentrate chemical and physical analysis plus the solid state reduction products chemical and XRD were performed at Mintek. The bulk chemical compositions of the chromite and reactivity test products were carried-out by the Vista Varian PRO CCD Simultaneous Inductive Coupled Plasma Optical Emission Spectrometer (ICPOES). Other procedures applied include Wet Chemical Analysis (Speciation Analysis), powder X-Ray Diffractometer (XRD), Scanning Electron Microscopy (SEM), and Total Carbon by combustion.

3.6.2.1 Chemical Speciation (Wet Chemical Analysis)

This essentially involves the selective leaching of the reduction product followed by determination of elemental/atomic composition using ICPOES. In this way, the contents of metallic Fe, Fe²⁺, Fe³⁺, metallic Cr and Cr³⁺ in the unprocessed and processed samples could be determined. These are then converted into the corresponding oxide. In the process, selective leaching of the metallic ions is undertaken by use of different acid concentrations. Initially mild acid leaching is used followed by a strong acid leach to target for example the Fe⁰ and Fe²⁺, respectively. The total iron in the sample is determined by the complete dissolution of the (un)processed sample followed by reading in the ICPOES spectrometer. In this way, the Fe³⁺ content of the sample was determined by difference [total Fe – (Fe⁰ + Fe²⁺)].

3.6.2.2 SEM and XRD

The SEM analysis was carried-out using Zeiss MA15 Scanning Electron Microscopy equipment that is equipped with a Bruker Energy Dispersive Spectrometer (EDS). This determined the way phases are associated (morphology) after reduction.

X-ray diffraction (XRD) analysis was performed on a pulverised sub-sample of each sample, to identify the crystalline phases present and determine their relative proportions. No amorphous phases can be identified using this method. A Bruker D8 Advance diffractometer with a LynxEye detector and Fe-filtered CoK α radiation was used. Samples were analysed over a range of 3 - 80° 2 θ , with a step size of 0.02° and a counting time of 3 seconds per step. The data were quantified using Rietveld refinement to provide phase proportions in mass percent. The detection limit for this technique is approximately 1 mass percent, and is dependent on the diffraction behaviour of the individual phases.

4. RESULTS

This chapter summarises results obtained from the experiments done. All results from analyses carried-out during the test work on feed materials and products, as well as data from the TGA reactivity tests (4 hour solid state chromite reduction at 1100°C, 1200°C, 1300°C and 1400°C) are presented in this chapter. Raw data of the recorded mass readings captured per second during the TGA isothermal tests were condensed into 10 minute intervals for the 4 hour holding period. This data is given in Appendix E.

4.1. Physico-Chemical Characterization of Raw Materials

The UG2 chromite concentrate and five reductants were subjected to chemical analysis to determine their respective bulk chemical compositions. The chromite concentrate was analysed by Inductively Coupled Plasma Optical Emission Spectrometry (ICP-OES, Varian Vista-PRO CCD simultaneous instrument) to obtain the chemical composition thereof, which was required for the chromite reducing test recipe calculations (Appendix C). The chromite ore didn't contain any Cr (VI), as it was a flotation concentrate obtained from UG2 platinum ore processing. The results of the different analytical and tests procedures follow below.

4.1.1 Chromite Ore Chemical and Physical Analyses

4.1.1.1 *Chemical Composition*

The bulk chemical composition of chromite concentrate used during the testwork is given in Table 4.1. The concentrate is predominantly composed of chromium oxide at 41.94% and iron oxide at 26.42%. This composition translates to a chrome to iron ratio of 1.4. These two oxide species are specifically targeted for as mainly participating in the chromite ore carbothermic reduction.

Table 4.1: Bulk chemical composition of UG2 Chromite (mass %).

Component	Mass (%)
Cr ₂ O ₃	41.94
FeO	26.42
MgO	11.01
Al ₂ O ₃	15.13
SiO ₂	2.37
CaO	0.22
V ₂ O ₅	0.25
MnO	0.23
NiO	0.23
TiO ₂	0.88
S	0.01
H ₂ O	1.60

4.1.1.2 Chemical Speciation Tests

The chromite ore was further taken for wet chemical analysis by selective leaching, in order to determine the iron and chromium oxide(s) related species, available before reduction. Results obtained are summarised in Table 4.2.

Table 4.2 : UG2 Concentrate Fe and Cr Speciation Analysis (mass %)

Species	Fe ⁰	Fe ²⁺	Fe ³⁺	Fe total	Cr ⁰	Cr ³⁺	Cr Total
Mass %	0.0	20.6	0.0	20.6	0.0	28.7	28.7

The following iron and chromium species, namely Fe⁰, Fe²⁺, Fe³⁺ and Cr⁰, Cr³⁺ were analysed for, no metallic forms were found.

4.1.1.3 Particle Size Distribution

[Appendix A, Figure 9.1](#) shows the typical size distribution of the chromite concentrate. Particle size distribution was done using screen sizes: 3.25 mm, 2 mm, 1 mm, 0.71 mm, 0.5 mm, 0.524 mm, 0.3 mm, 0.212 mm, 0.18 mm, 0.15 mm, 0.106 mm. The particle size distribution (PSD) shows more than 80% of the particles as reporting below 75 µm.

4.1.2 Reductants Chemical and Physical Analyses

4.1.2.1 Proximate, Ultimate and Ash Analysis

Air-dried proximate analysis (inherent moisture, ash, volatiles, calculated fixed carbon), Ultimate elemental analysis (C, H, O_{calculated}, N, total S) and ash composition was carried-out for the reductants. The proximate analysis is given in Table 4.3.

Table 4.3: Reductants Proximate Analysis (air dried – Mass %)

Reductant	Fixed C	Ash	Moisture	Volatiles
A	87.10	8.66	<0.05	2.29
B	83.00	16.00	0.10	0.81
B1	73.10	18.20	0.10	0.70
C	76.40	15.65	2.94	7.93
D	65.00	14.64	0.83	19.55

<0.05: the analyte content is below the 0.05% detection limit of the analytical method for the specific analyte

The highest fixed carbon content (87.10%) is in Reductant A, followed by Reductants B (83.00%), C (76.40%) and B1 (73.10%), respectively. Unconventional reductant D has the lowest at 65%. Reductant A correspondingly has the lowest ash content (8.66%). The moisture content was of no significance as all the reductants were dried at 100°C to 0°C moisture content before use.

Results for ultimate analysis of the reductant material are illustrated in Table 4.4.

Table 4.4: Reductants Ultimate Analysis (air dried - mass %)

Reductant	C	H	N	O	S	CV(MJ/Kg)
A	81.44	0.07	1.59	0.51	0.71	24.89
B	82.87	0.02	0.66	0.45	0.79	26.41
B1	71.14	0.05	0.62	0.89	0.87	28.41
C	74.82	0.09	0.62	0.78	0.85	32.05
D	63.21	0.11	0.62	0.91	0.93	34.92

<0.05: the analyte content is below the 0.05% detection limit of the analytical method for the specific analyte

The results indicate important parameters like the caloric value, sulphur and carbon content. Sulphur which is one of the undesired components known to transfer directly to the reduced chromite alloy and consequently to the steel product, was found to be more in unconventional Reductant D (0.93%) followed in decreasing order by conventional reductants B1, C, B and A, with 0.87%, 0.85%, 0.79% and 0.71%, respectively. Unconventional Reductant D has the highest caloric value (34.92 MJ/Kg). This is accompanied by the lowest carbon content (63.21%). Reductant C has the highest caloric value (32.05 MJ/Kg), followed by Reductants B1 (28.41MJ/Kg), B (26.41MJ/Kg) and A (24.89MJ/kg), respectively.

Table 4.5 gives the reductant ash composition. The ash's oxide components that were likely to react with the reductant thereby reducing the carbon available for chromite reduction were found in minute quantities compared to the excess carbon available. The latter was calculated at 40% excess of stoichiometric requirements for the FeO and Cr₂O₃ in the chromite ore.

Table 4.5: Reductant Ash Chemical Composition (mass %)

Component	A	B	B1	C	D
Al ₂ O ₃	1.21	19.4	24.3	39.68	5.07
CaO	3.12	1.26	1.94	1.39	22.79
Cr ₂ O ₃	0.10	0.17	0.16	<0.05	0.11
FeO	88.72	5.96	7.33	0.41	7.61
MgO	0.60	0.70	0.91	1.10	2.98
MnO	0.63	0.18	0.17	<0.05	0.57
SiO ₂	2.90	69.99	61.73	54.4	59.93
TiO ₂	0.14	1.70	2.67	2.06	0.46

<0.05: the analyte content is below the 0.05% detection limit of the analytical method for the specific analyte

The highest ash content was found in Reductant B1 (18.20%), followed by B (16.00%), C (15.65%), D (14.60), with A (8.66%) having the least amount. The highest ash constituents are the oxides SiO₂ (54.4% – 69.99%) and FeO (88.72%) for Reductant A. Although Reductant A has

the highest FeO content, this is of not much significance as it was found in an ash content of only 8.66% of the total reductant mass.

4.1.2.2 Particle Size Distribution

Reductants particle size distribution was done using screen sizes: 3.25mm, 2.0mm, 1.0mm, 0.71mm, 0.5mm, 0.524mm, 0.3mm, 0.212mm, 0.18mm, 0.15mm, 0.106mm. The particle size distribution for the reductants is summarized in [Appendix B, figure 9.3](#). The most friable of the reductants was Reductant D, with the highest number of particles (+65%) reporting as less than 100 microns. The rest of the reductants were ranging between 42-50%, with the least amount found in Reductant A (42%).

4.1.3 Reductants Petrography

Analysis of the selected reductants (A, B, B1 and D) was mainly done by the Coke Petrographic procedure (Ref: ASTM Standard D 5061 – 92). The primary objective was meant to establish the nature of the texture of carbon in reductant binder phase. Reductant A was chosen as the control as it is widely used in the metallurgical industry, with Reductants B and B1 being selected specifically for comparison with the unconventional Reductant D.

4.1.3.1 Conventional Reductants (A, B and B1)

Petrographic analysis of three selected reductant samples was undertaken. The different carbon forms were distinguished on the basis of their reflectance, anisotropy, morphology and size.

Analysis of reductant A showed that it consisted predominantly of binder phase material, although it contained higher quantities of organic inerts (remnants of other inertinite macerals), as well as miscellaneous inerts (pyrolytic carbon and “burnt” coke) when compared to the Reductants B and B1. The high binder phase content is indicative of a high vitrinite coal, with a high percentage of reactives. The most significant difference

between the samples was highlighted upon analysis of the forms of carbon: Reductants B and B1 mostly consisted of isotropic carbon (indicating that a high volatile coal of low rank was used as feed material). Reductant A displayed a wide range in forms of carbon (from isotropic to medium ribbon anisotropic carbon), which may suggest that a blend of coals was used to form this reductant. The wide range in reflectances displayed by Reductant A further emphasized this. Reductants B and B1, on the other hand, display a more restricted range in reflectances, indicating that they were not well-graphitized.

Reductants B and B1 contained considerable quantities of both organic and inorganic inerts, as well as miscellaneous inerts (in the form of non-coking vitrinite), although the latter was restricted to the finer fraction. Some miscellaneous material (both depositional carbons, such as spherulitic and pyrolytic carbon, and other carbons in the form of “burnt” material) occur in the coarser fractions, with these carbons of particular significance in the finer fraction. Instances of green coke were also identified.

4.1.3.2 Unconventional Reductant (D)

Due to the nature of the material, typical analyses (including organic composition), could not be carried out, as no coal macerals were present to be identified. The degree of maturation (rank) was determined based on the ISO standard on the available organic matter (see Table 4.6).

Thus, no compositional information is available, but rank determination and multiple images to provide an indication of the nature of the material are provided. Table 4.6 has the 100 random reflectance measurements classified as per ISO 11769-2005 of the as-received reductants A, B (both conventional) and D (unconventional) samples. Multiple particles were analysed to determine the rank. The degree of maturation varies between particles (Micrographs in Appendix D), ranging from meta-bituminous (medium-rank B) to meta-anthracite (high-rank A).

Some particles display a higher degree of maturation, approaching the appearance of carbon similar to Reductants A and B.

Table 4.6: Reductant Random Reflectance Data

RANK DESIGNATION	A	B	D
<i>Mean Rr%</i>	7.23	6.95	2.48
<i>Standard. Deviation</i>			0.80
V-Class	Relative Frequency		
BINDER PHASE			
Isotropic (from V7 or lower)	33.2	90.7	0
Incipient Anisotropic (from V8)	4.7	4.1	0
Sub-Total	37.9	94.8	0
Circular Anisotropic (Granular)			
Fine (From V9) 0.5 - 1.0 µm	11.1	2.0	1
Medium (from V10) 1.0 - 1.5 µm	16.9	1.2	2
Coarse (From V11) 1.5 - 2.0 µm	16.1	0.4	6
Sub-Total	44.1	3.3	9
Lenticular (Leaflet) Anisotropic			
Fine (From V12) width 1.0 - 3.0 µm	6.7	0.5	2
Medium (from V13) width 3.0 - 8.0 µm	8.1	1.0	2
Coarse(From V14) width 8.0 - 12.0 µm	0.9	0.1	8
Sub-Total	15.7	1.6	12
Ribbon (Flow) Anisotropic			
Fine (From V15) length 2.0 - 12.0 µm	2.1	0.0	1
Medium(from V16) length 12.0 - 36.0 µm	0.2	0.0	4
Coarse (From V17) length >25.0 µm	0.0	0.0	73
Sub-Total	2.3	0.0	78
TOTAL %	100	100	100

Rank Determination (Ref: ISO 7404 – 5, 1994); R_{r%} - Random Reflectance using oil immersion objectives; σ - standard deviation; Inertinite includes fusinite, semifusinite, secretinite, macrinite, inertodetrinite and micrinite; Mineral Matter refers to minerals visible microscopically.

Particles that generally appear lower in rank include Particle 3, while the remainder will be higher in rank. An example of Particle 4 (unconventional reductant) is given below (Figure 4.1), with the rest of the particles appended. Although highly porous, these textures appear solid, more isotropic in nature. In comparison, a significant number of particles appear to contain remnants of plant material where the heating process was not completed. Though the majority of the particles retain some form of plant-

like features, these remnants are most evident in Particle 3 and to a lesser extent in Particle 1.

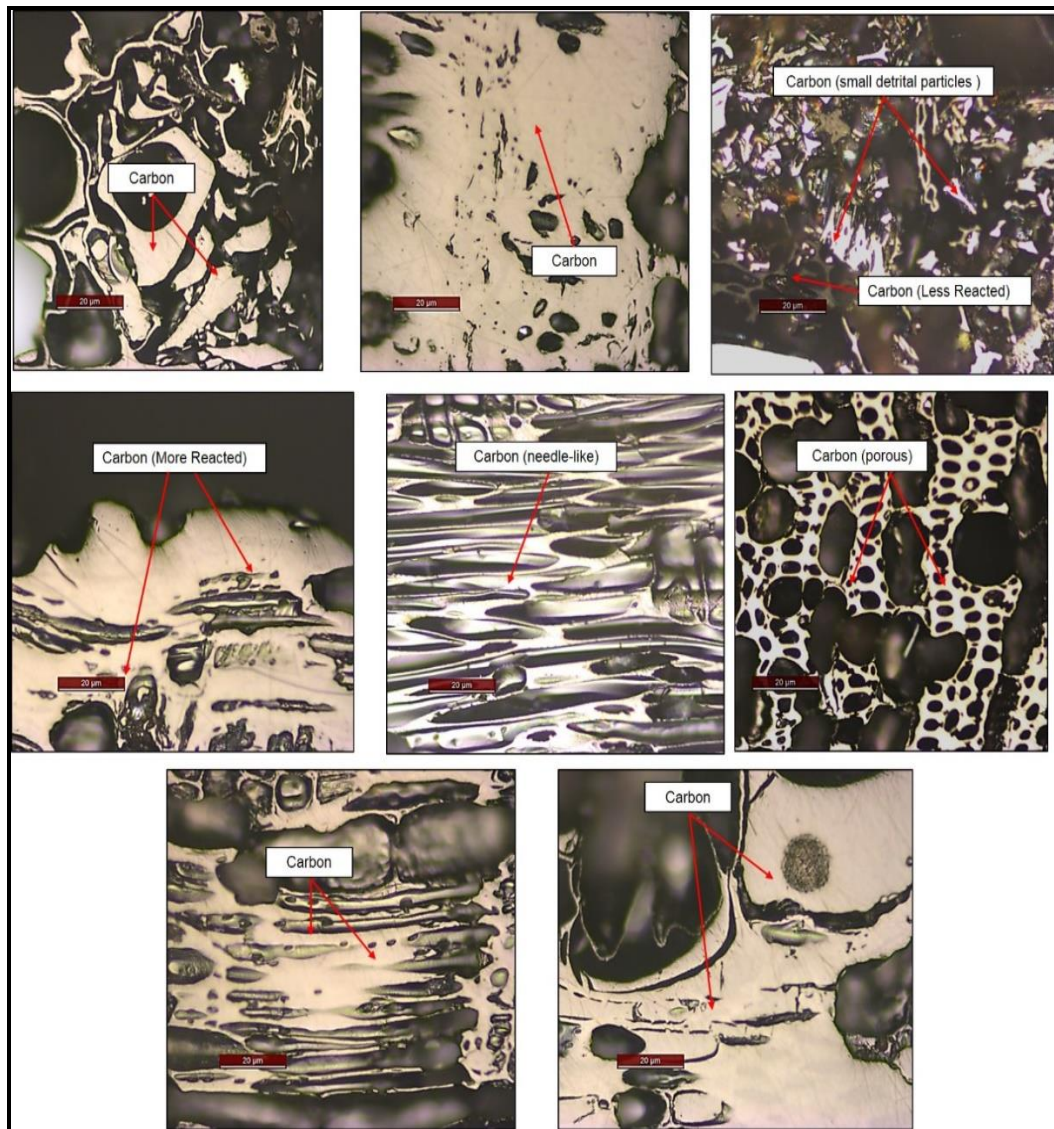


Figure 4.1: Unconventional Reductant D Particle-4 Photo micro-graphs (500x magnification objective).

Certain particles appear to contain mineral inclusions, particularly in Particles 2 (A, D), where some of the pores may have been in-filled by mineral matter. Despite the fact that detailed analysis of binder/filler content and carbon forms could not be carried out for the charcoal, it could be established that the majority of the carbon occurs as binder-like (more reactive) material, with minor filler (inert material) in the form of the plant-like remnants and mineral inclusions.

4.1.4 Optical Light Microscopy

Three selected conventional reductants (A, B and C) were analysed to illustrate typical cell-wall width and macro-porosity. However, in this instance, image analysis could not be applied to determine macro-porosity of the unconventional reductant D, due to its friable nature.

4.1.4.1 Conventional Reductants - Cell-Wall Width and Macro-porosity

Optical image analysis of the samples shows that reductant B has a higher macro-porosity and slightly greater cell wall width than reductants A and C (Table 4.7). The results indicate that ~65% of the cell walls for A are less than 100 microns in width, whilst ~90% are less than 200 microns. Thus, the majority of the cell walls are less than 200 microns in size. The widest cell walls measured for the sample are between 10 000 and 20 000 microns (10-20 mm).

Table 4.7: Macro-porosity and Compactness (Reductants A, B & C).

Physical Characteristics	A	B	C
Macro-pores (%)	51.18	67.78	61.80
Cell Walls (%)	48.80	32.22	38.20
Index of Compactness	0.95	0.48	0.62

The results indicate that ~58% of the cell walls in Reductant B are less than 100 microns in width, with ~90% are less than 300 microns. Therefore, generally, the cell walls of Reductant B are slightly wider than those in Reductant A. The widest cell walls measured in this sample are between 10 000 and 15 000 microns (10-15 mm). It should be noted that the measurement of cell widths was determined automatically by the computer software program. Thus, cell wall widths are measured both horizontally and vertically.

Typical macro-porosity of the selected conventional Reductant B (Figure 4.2) is relatively high at ~68%, resulting in a low index of compactness at ~0.48.

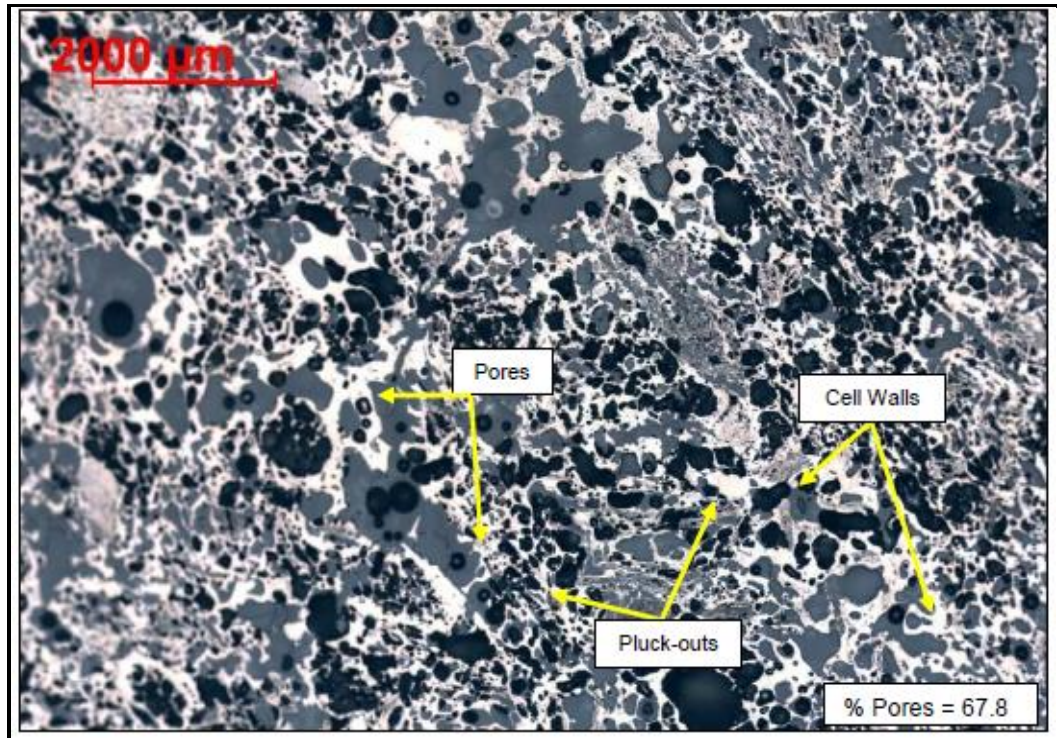


Figure 4.2: Cell Wall and Macro-pores Distribution in a Section of Reductant B (*20x magnification objective*).

4.1.4.2 Unconventional Reductant D Cell-Wall Width and Macro-porosity

Although an attempt was made to determine the macro-porosity through image analysis, the friable nature of the material did not allow for accurate macro-porosity measurements to be taken. Photomicrographs illustrating the main features occurring in the sample are attached in Appendix D. Images were taken at 500x magnification, using oil immersion and under plane polarised light.

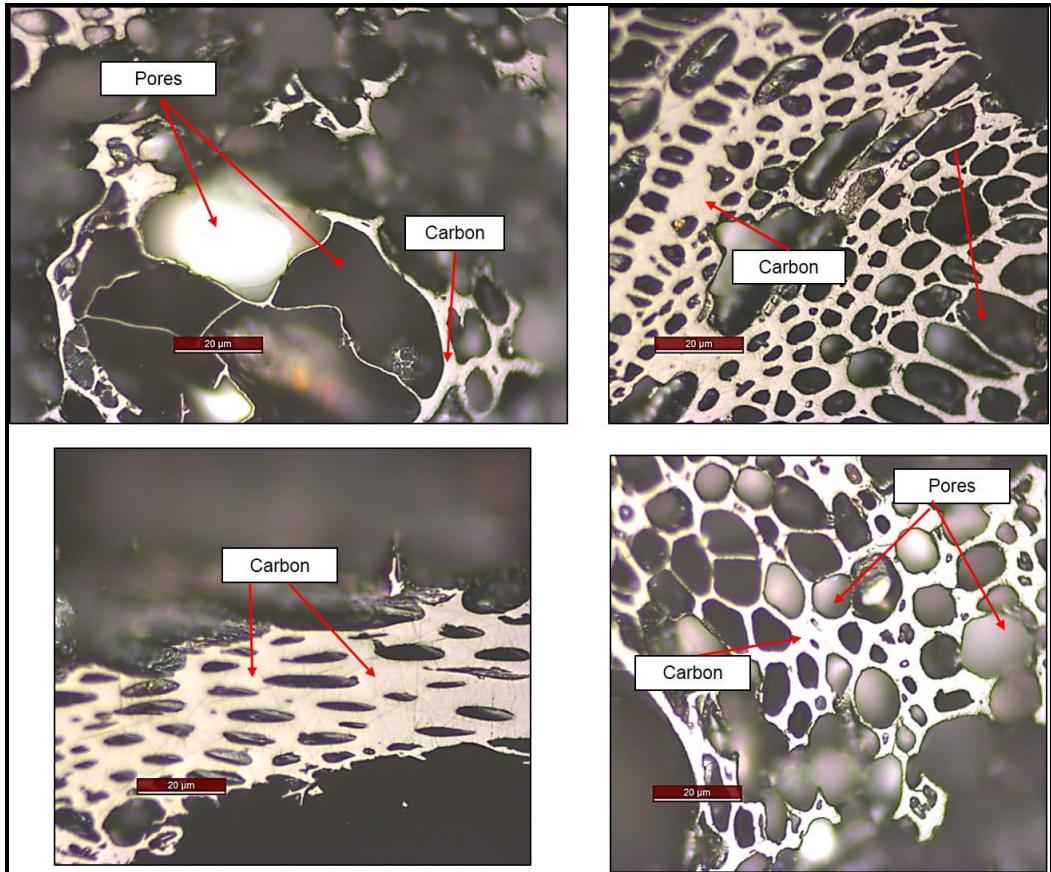


Figure 4.3: Cell Wall and Macro-pores Distribution in a Section of Reductant D at 20 μm (500x magnification objective).

The charcoal sample is highly porous in general (Figure 4.3), with the size of pores varying greatly between and within the particles themselves.

4.2. Isothermal Thermogravimetric Analysis - Reactivity Tests

Solid state chromite reduction reactivity tests were carried-out at Mintek's Pyrometallurgy Division. TGA mass losses for the reductants were plotted as a function of reaction time for tests conducted at 1100°C, 1200°C, 1300°C and 1400°C. Typical mass losses for each reductant at the test temperatures are summarised in Appendix E.

4.2.1 TGA Feed Material and Furnace Preparation

4.2.1.1 Feed Material – Chrome ore and Reductant

Following successful milling and drying of the reductants, batches of mixed chromite ore and carbon reductant were prepared according to reductant requirements for 500 grams of UG2 concentrate as summarised in Table 3.1 Feed material preparation was done according to stoichiometric requirements at 40% excess carbon and the calculations carried-out are given in Appendix C. Finely milled, dried reductant samples were weighed-out and mixed with the dried chrome concentrate to ensure increased contact area as demonstrated in Weber and Eric (2006). The samples were kept dry in tightly sealed plastic bags kept in an oven maintained at ambient temperature, from which 28-30 grams was weighed-out into the alumina crucible for the tests.

4.2.1.2 TGA Furnace profiling

Thermal profiling was conducted to determine the temperature gradient in the reaction tube prior to conducting the high temperature testwork. The aim of temperature profiling was to determine the position and length of the hot zone of the furnace. To complete the temperature profiling at 1000°C, the furnace was heated up at a rate of 10°C/minute to a temperature of 1000°C and allowing it to remain at temperature for the duration of the thermal profiling or temperature verification test. The temperature gradient along the tube of the furnace was measured using a K type thermocouple. The position and length of the hot zone was determined by lowering the thermocouple inside the furnace while recording the length of the thermocouple inside the furnace. Temperature readings were taken by moving the thermocouple by 1 cm into the tube furnace. The thermocouple temperature was allowed to stabilise at a specific position over a period of 10 minutes.

The hot zone of the furnace was found to be around the centre of the furnace where the heating elements are situated. The hot zone with a maximum temperature of 1005°C was found to be 9 cm long as shown in Figure 4.4.

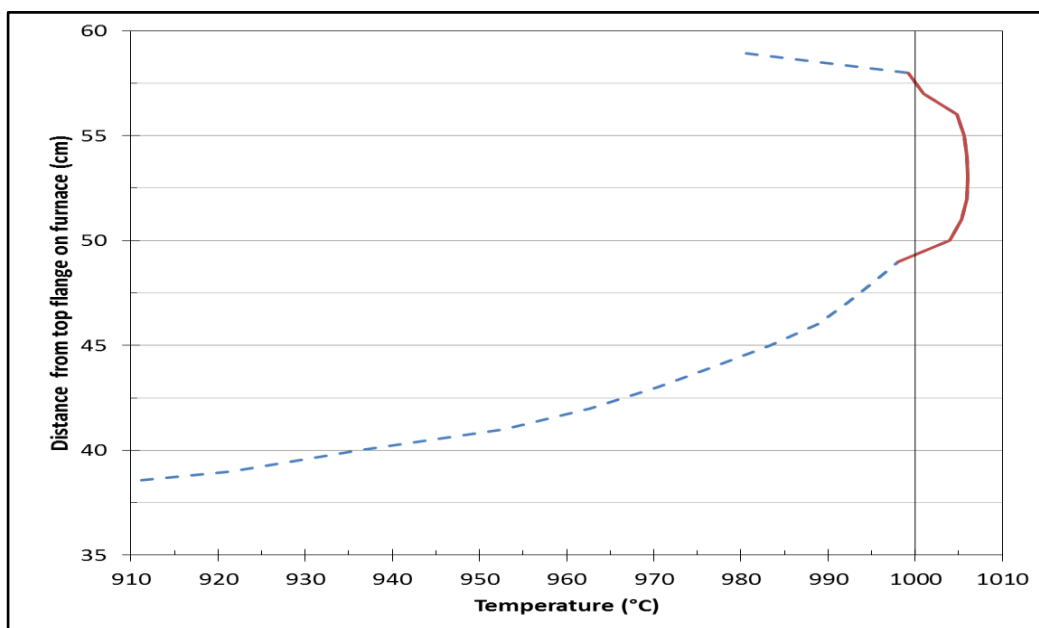


Figure 4.4: Temperature Profile of the TGA Furnace (hot zone is shown by the solid red line)

Overheating of the furnace was experienced and this was attributed to incorrect positioning of the furnace control thermocouple. The hot zone was long enough to ensure a consistent sample temperature, since the test crucible was only 5 cm long. The temperature measurement uncertainty was therefore within $\pm 5^\circ\text{C}$.

4.2.2 Reductant A – TGA Reactivity Curves

Reactivity curves obtained during the tests for Reductant A are shown in Figure 4.5. Reductant A portrays an incremental trend in reactivity with increasing test temperature.

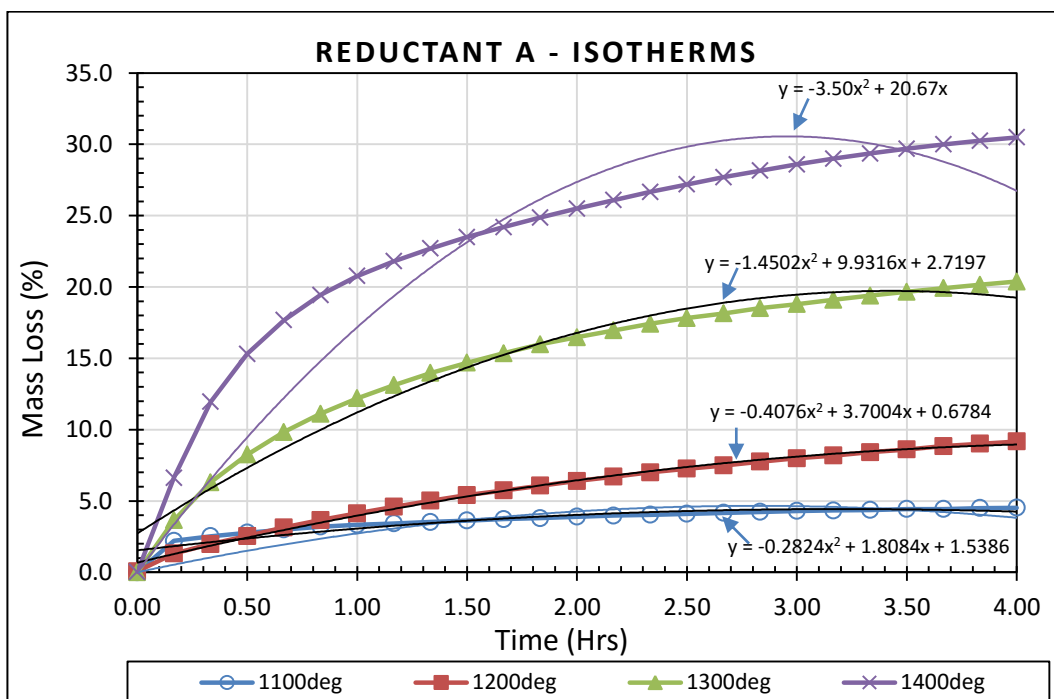


Figure 4.5: TGA Curves for Reductant A at 1100°C to 1400°C

The test at 1100°C initially starts at a slightly higher rate compared to the 1200°C test. It (1100°C test) recorded a mass loss of 2.53% and 2.77% within 20 and 30 minutes, respectively compared to the 1200°C test that lost 1.98% and 2.54% at the same time. However, the reactivity rate for the 1100°C test starts slowing down as if approaching saturation, whereas the 1200°C test steadily continues to react at a rate such that it surpasses the 1100°C test after 45 minutes and finishes with a mass loss of 9.17% compared to 4.53% for the 1100°C test. Both the 1300°C and 1400°C tests start off with almost similar mass losses within the first 3-4 minutes, with the latter gradually getting more superior and only begins to slow down after an hour (Mass loss: 20.63%), to end with a total 30.45% mass lost within 4 hours. The 1300°C test follows the same trend but at a slower rate, losing only 12.20%. Mass loss at 1300°C and 1400°C, is respectively, plus 5 and 7 times more than the loss attained at 1100°C. The steepest isotherm representing the highest reactivity for the reductant is illustrated by the trend line at 1400°C, with an equation $y = -3.50x^2 + 20.67x$. The slope obtained by differentiating the trendline equation (dy/dx

= $-7x + 20.67$) in comparison to the least reactive test at 1100°C , with equation $y = -0.2824x^2 + 1.8084x$ with a gradient obtained from $dy/dx = 0.5648x + 1.8084$ demonstrates that it is almost 12 times more reactive for the holding period.

The isothermal curves at 1200°C , 1300°C and 1400°C show that saturation was still not attained within 4 hours, although the reactions were relatively slowing down. The test at 1100°C had significantly started to slow down after 2.5 hours, with signs of nearing saturation. In the end, all the four tests portray an increasing rate with rising test temperature.

4.2.2.1 Differential Time Analysis

Figure 4.6, illustrates the typical changes in mass loss experienced with time for Reductant A, during the tests.

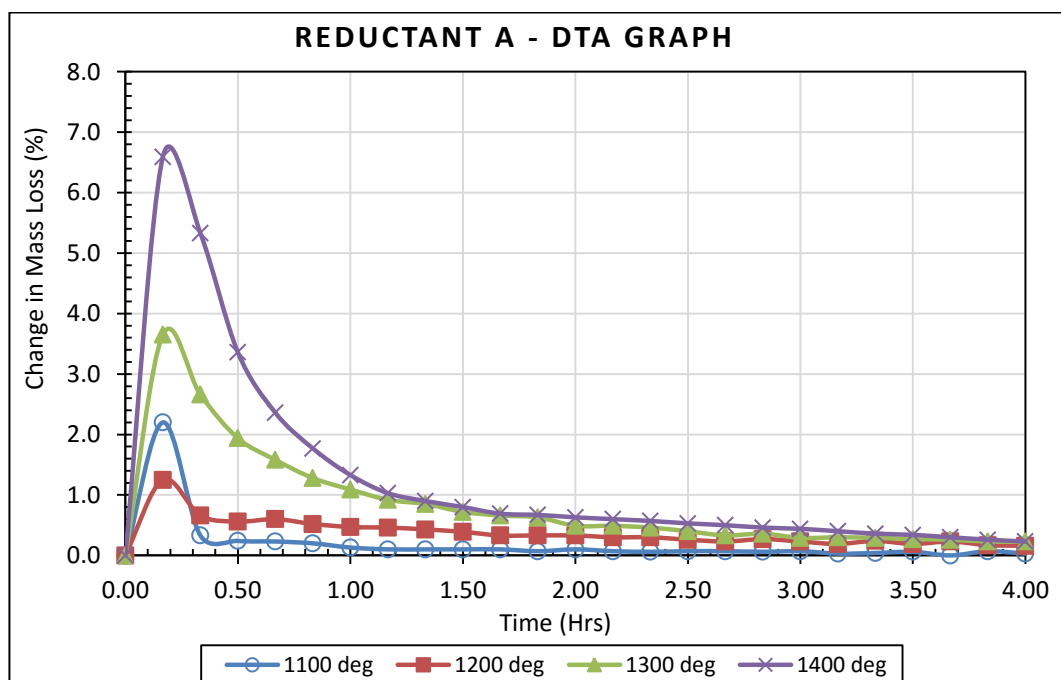


Figure 4.6 : Differential Time Analysis Graph - Reductant A (1100°C to 1400°C).

The graph depicts an almost similar trend for all the tests due to the effect of temperature, as seen by the attainment of an increased maximum change in mass loss within the first stages. This is evident within the first

0.33 hours for both the 1100°C and 1200°C tests, and 1.17 hours for the 1300°C and 1400°C tests. The maximum change in mass loss for all the tests occurred within the first 0.17 hours of reaction time. The highest change in mass is 6.6%, recorded for the 1400°C test. This is followed by 3.7% change at 1300°C, 2.2% at 1100°C and lastly 1.3% at 1200°C. Despite the 1100°C tests having more mass change in the first stage compared to the 1200°C test, the latter experienced continuous mass change until the end. The 1200°C test is seen to peak and drop to 0.7% compared to 0.3% for the 1100°C, within 0.33 hours. The 1100°C test displays no more mass change from 3.17 hours, with the rest of the tests still experiencing minute mass changes up to the 4th hour.

4.2.3 Reductant B – TGA Reactivity Curves

The obtained reactivity tests graph is given in Figure 4.7. Reductant B had a gradual increase in reactivity rate with increasing test temperature.

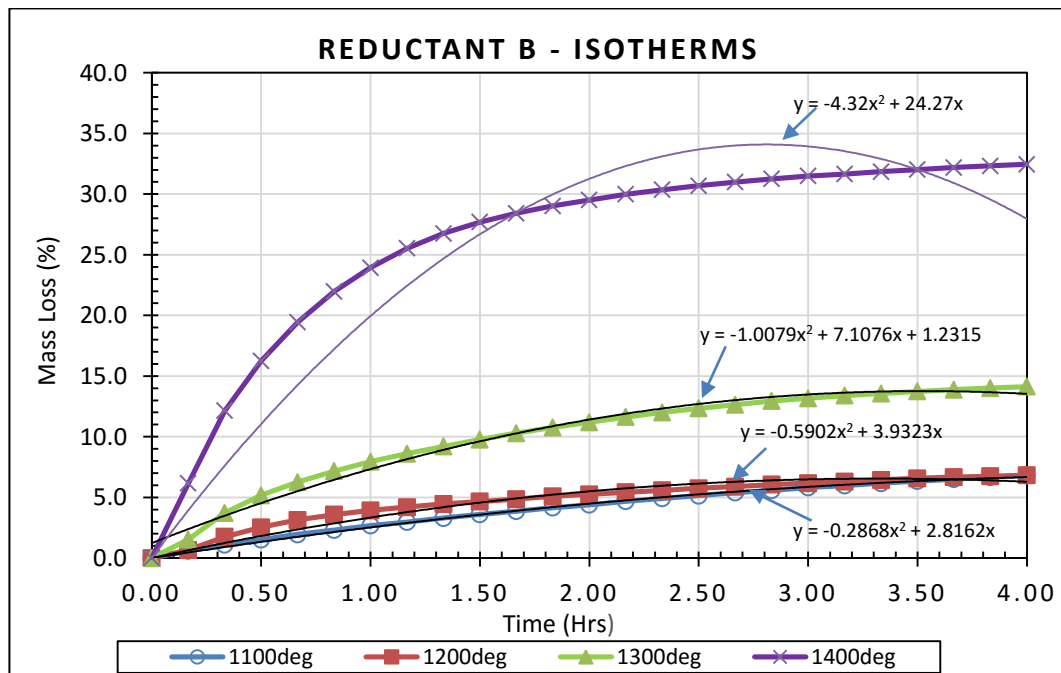


Figure 4.7: TGA Curves for Reductant B from 1100°C to 1400°C.

The 1100°C test starts off at the slowest rate followed by 1200°C, 1300°C and 1400°C, in increasing order. After 30 minutes, all respectively recorded the following mass losses; 1100°C (1.52%), 1200°C (2.54%), 1300°C (5.17%) and 1400°C (13.12%). However, the 1100°C test eventually finished almost at the same rate as the 1200°C at 6.81% and 6.84%, respectively. Both tests at 1300°C and 1400°C show significant increase with temperature, and at the end of the 4 hour holding period had lost 14.13% and 28.65%, respectively.

The most reactive test was at 1400°C and is represented by the trend line which has a slope of 8.64 compared to 0.57 at 1100°C. They all were showing signs of slowing down and about to reach saturation at the end of 4 hours.

4.2.3.1 Differential Time Analysis

Change in mass loss experienced with Reductant B is shown in Figure 4.8. The highest change in mass loss recorded was 6.1%, at 1400°C that occurred within 0.17 hours.

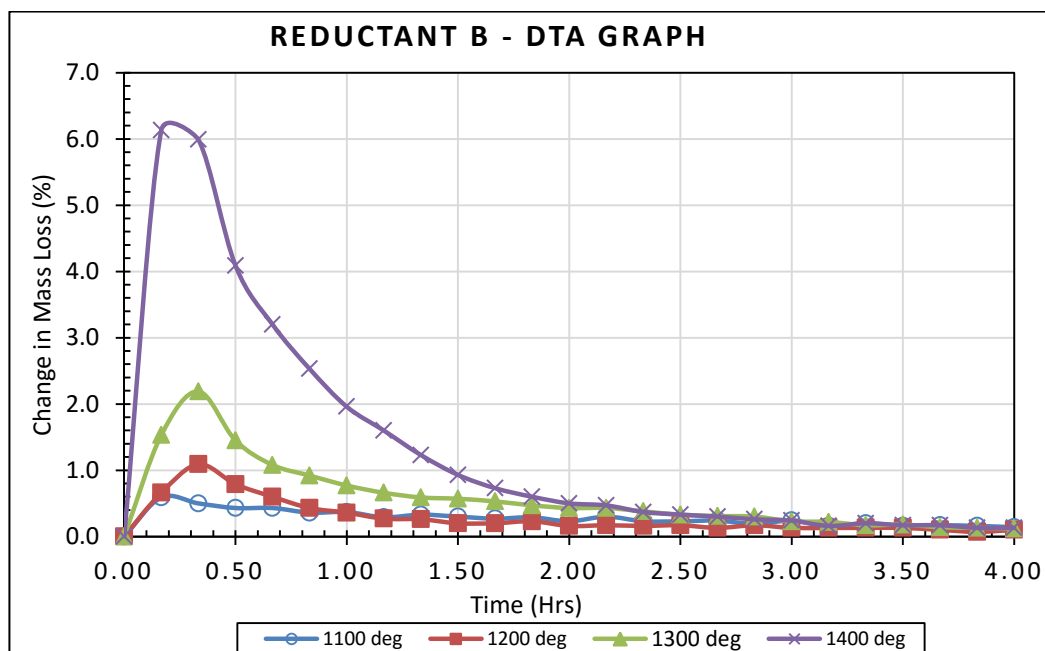


Figure 4.8: Differential Time Analysis Graph - Reductant B (1100°C to 1400°C).

A change of more than 6% was maintained for this temperature until 0.33 hours, which then suddenly decreased to 1% within 1.5 hours and 0.5% within about 2 hours. This progressed and eventually concluded the test at 0.1% change in mass loss. The test performed at 1300°C had the second highest change in mass loss of 2.2% in 0.33 hours, with only 1.5% change experienced in 0.17 hours (Nb. This was when the 1400°C had the highest change of 6.1%). The change in mass for 1300°C test concluded at 0.1% after decreasing to 0.6% within 1.5 hours. The 1200°C tests also peaked at 0.33 hours with only 1.1% change in mass loss. The least change was seen with the 1100°C test's graph that had the highest change in mass of 0.7% after 0.17 hours. It further drops to 0.4% within 1 hour and performed slightly better than the 1200°C test to 3.17 hours. All tests finished with change in mass loss less than 0.1%, which also confirmed that they were all approaching saturation point.

4.2.4 Reductant B1 – TGA Reactivity Curves

Figure 4.9 shows the reactivity curves derived for Reductant B1.

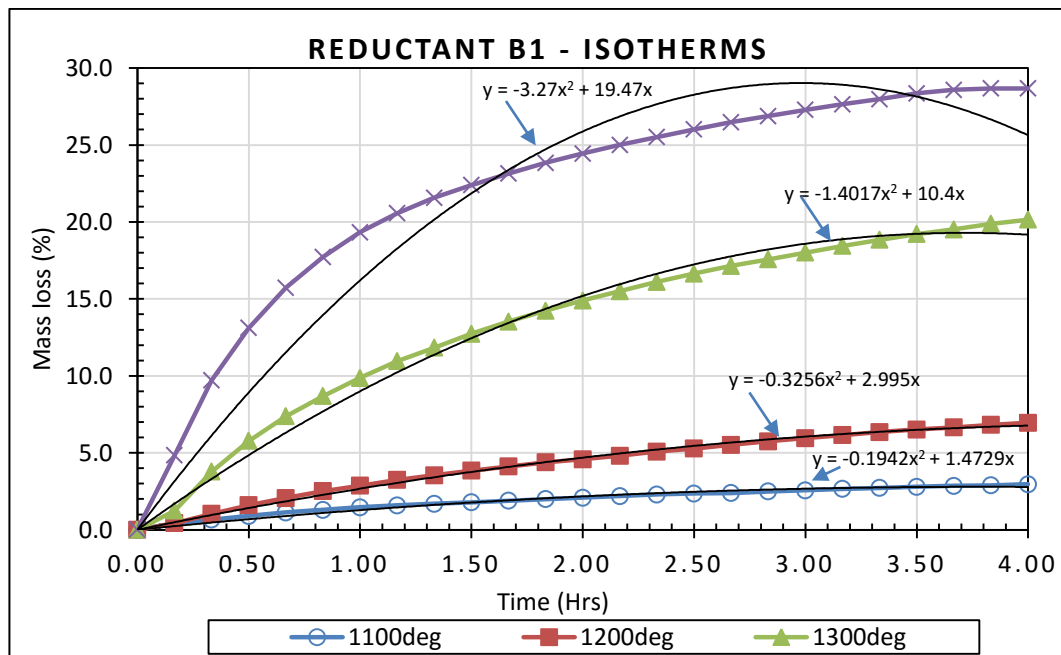


Figure 4.9 : TGA Curves for Reductant B1 from 1100°C to 1400°C

At 1100°C, 1200°C, 1300°C and 1400°C recorded mass losses were 3%, 7%, 20% and 29% respectively. This clearly illustrated the effect of rising temperature on apparent reactivity. The trend line of the highest temperature isotherm (1400°C) also reflects the increase in reactivity with temperature as it had a slope of 6.54 compared to 0.39 at 1100°C (Figure 4.9).

After the 4 hour holding period, the total mass loss and rate of reaction for each test temperature significantly increased with temperature. Towards the end all the tests were noted to slacken in reactivity with a corresponding flattening gradient.

4.2.4.1 Differential Time Analysis

The effect of temperature on change in mass loss for Reductant B1 is given in Figure 4.10. The graph clearly demonstrated the effect of increasing temperature, especially within the first 1.5 hrs for all the tests.

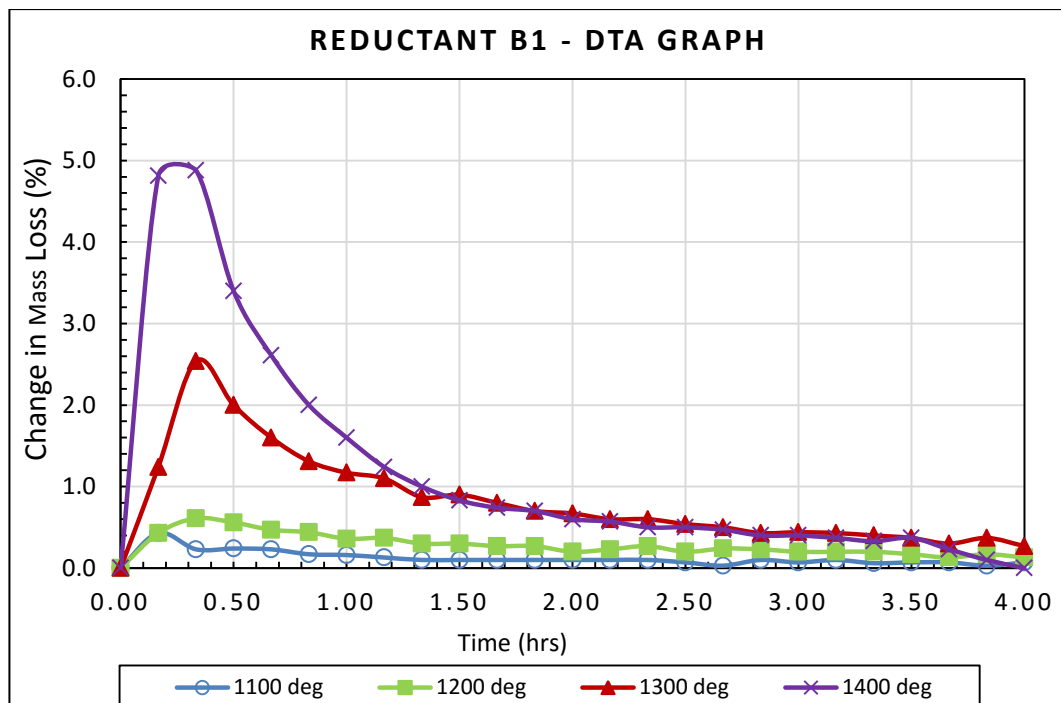


Figure 4.10: Differential Time Analysis Graph - Reductant B1 (1100°C to 1400°C).

The tests performed at 1300°C and 1400°C had the highest change in mass loss of 2.5% and 4.9% respectively, after 0.33 hours. The highest change in mass loss for the 1200°C was 0.6% within 0.33 hours. However, the 1100°C test had its highest change in mass loss of 0.4% within 0.17 hours, which was almost what the 1200°C test experienced at 0.17 hours, before peaking at 0.33 hours.

All the tests had a relatively reduced change in mass loss from 1.5 hours to complete the tests with 0% change in mass loss.

4.2.5 Reductant C – TGA Reactivity Curves

The reactivity curves for Reductant C are given in **Figure 4.11**. This portrayed a rather inverted trend in reactivity with temperature, compared to the other conventional reductants.

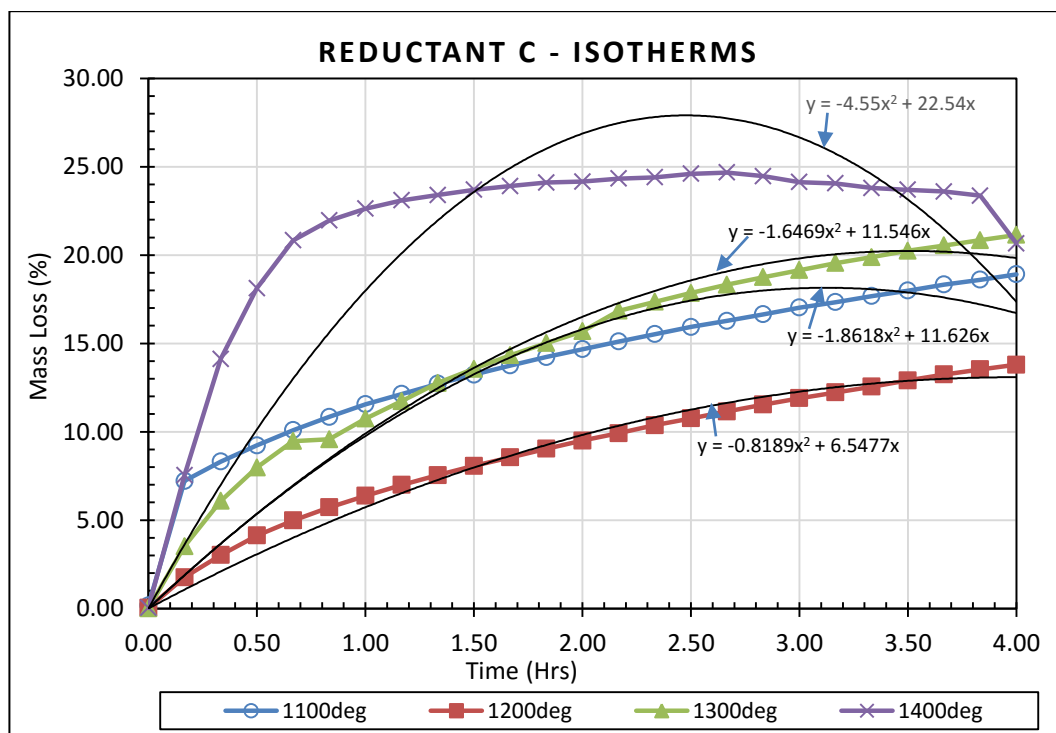


Figure 4.11: TGA Curves for Reductant C at 1100°C to 1400°C.

This in particular, was seen with the 1200°C in comparison to the 1100°C curve. The latter had a sharp rise in activity rate at the beginning (almost

7% mass loss within the first 10 minutes), which gradually reduced to eventually finish at a total 18.91% at the end of test. This is opposite to what the 1200°C curve portrayed, as it only decreased less than 2% within the first 10 minutes and a total 13.79% after 4 hours.

A gradual increase in reactivity with temperature there after takes place, as seen with the 1300°C test that decreased 21.17% within 4 hours. The reactivity rate for the 1300°C test was also lower than the 1100°C test, with only 3.80 % lost within the first 10 minutes. Another anomaly was found at the end of the 1400°C test which started at a higher rate almost similar but slightly more than that seen with the 1100°C test. A total 4.70% was lost within the first 10 minutes and this progressed at the same rate for the first 45 minutes, losing a total 21.45%. Mass loss continued past 2.5 hours at a reduced rate to 24.50% and thereafter to 23.00% at 3.96 hours, followed by a rapid decrease to finish at 21.66% within 4 hours.

The 1400°C isotherm has a trend-line that shows an average reactivity with a slope 9.10 compared to the lowest temperature slope of 3.72. Although it had the highest rate in the first hour, it did gain mass from about 3 hours. This was followed by a sudden gain at the end of the test, thus reversing most of the mass loss initially experienced. Instead, the 1100°C test was steadily losing more mass with time. Except for the 1400°C test that slackened with time, the rest of the tests show increased potential to continue reacting past the 4 hours.

4.2.5.1 Differential Time Analysis

The DTA graph for Reductant C is presented in Figure 4.12. This revealed some anomalies related to the four tests throughout the holding period. The highest change in mass loss occurred at the same initial stage of 0.17 hours for all the tests, but all are accompanied by significantly varying times taken to reduce below 1% change in mass loss.

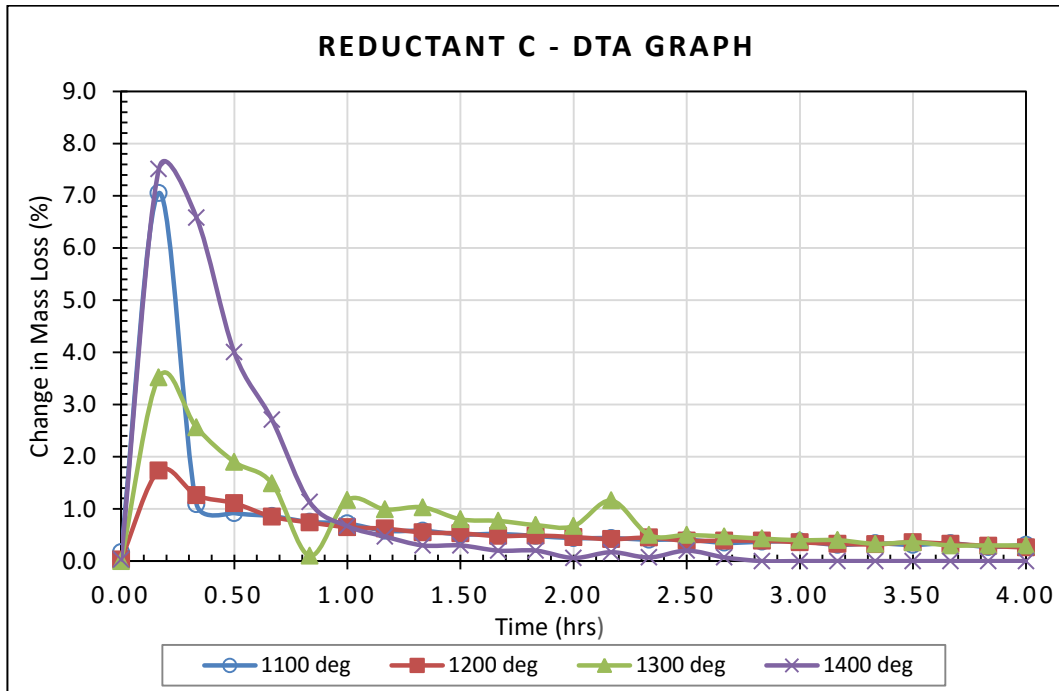


Figure 4.12: Differential Time Analysis Graph - Reductant C (1100°C to 1400°C).

The most change in mass loss was seen with the 1400°C test (7.51% change in mass) with the 1100°C test closely below at 7.05%. Both the 1300°C and 1200°C tests had significantly reduced changes in mass of 3.52% and 1.73%, respectively.

However the 1100°C test was the first one to decrease to a change in mass below 1% within 0.33 hours, followed by the 1200°C test in about 0.63 hours, 1300°C test in 0.67 hours and finally the 1400°C tests within 0.83 hrs. However, the 1300°C tests decreased further to 0% and immediately increased to plus 1%, before again decreasing below 1% within 1.40 hours. The same fluctuating trend was again seen within 2.17 hours to eventually decrease at 2.33 hours and finally finished with 0.30% mass change at the end of the holding period. After reducing below 1%, the 1400°C test continued further to 0% change in mass within 2.00 hours, with no other changes incurred until the end of the test.

The rest of the tests (1100°C and 1200°C) continued losing mass to complete the holding period, with 0.26% and 0.31% change in mass loss recorded, respectively. This confirmed that the tests at 1100°C, 1200°C and 1300°C continued losing mass (reacting) until the end, whereas the 1400°C test despite having had the highest mass loss, was saturated in almost half the holding period.

4.2.6 Reductant D – TGA Reactivity Curves

Main features of the solid state reduction tests performed with the unconventional reductant D are illustrated in Figure 4.13. The 1100°C test performed at a faster rate compared to the 1200°C test. Within the first 20 minutes, 1100°C test mass decreased by 7.48% compared to 5.51% for the 1200°C test. At the end of the 4 hour holding period, again the 1100°C test decreased with 17.46% compared to 12.39%.for the 1200°C test.

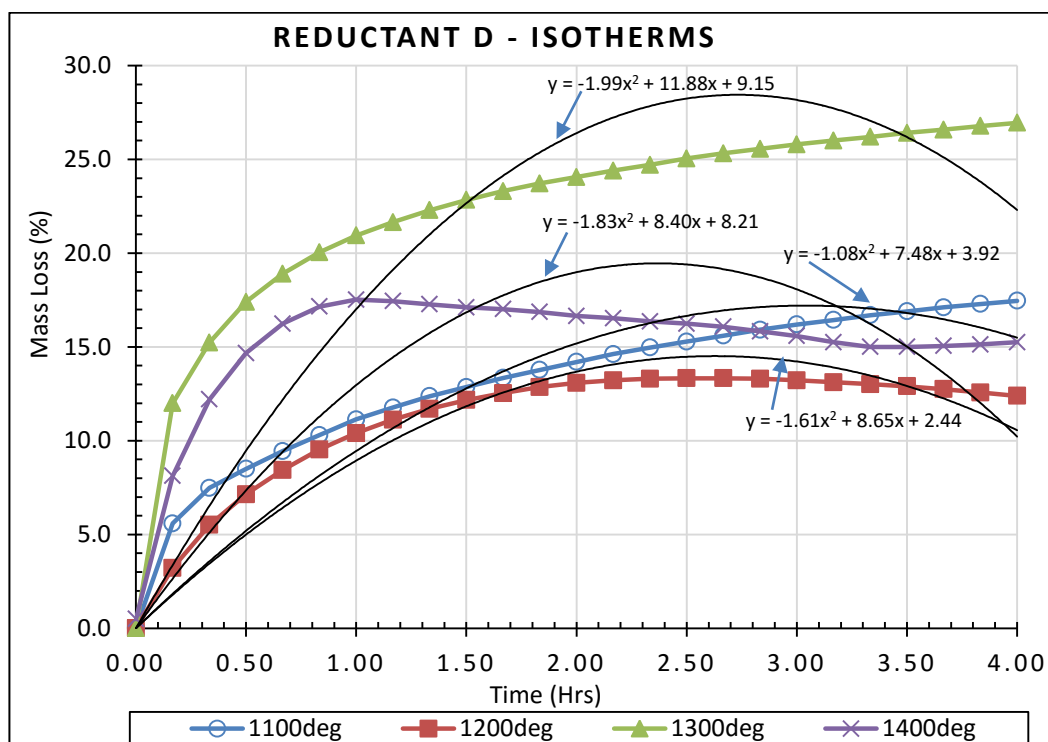


Figure 4.13 : TGA Curves for Reductant D from 1100°C to 1400°C.

The 1300°C test had a faster rate demonstrated by a 15.23% mass loss within the first 20 minutes and a total 26.95% in 4 hours. The 1400°C test started at a relatively slower rate than the 1300°C and lost only 12.24% within the first 20 minutes. This peaked to 17.52% within 60 minutes and started to decline until the end of the test, finishing at 15.25%. Both the 1100°C and 1300°C tests had not reached saturation at the end of 4 hours.

The best fit for the trend-lines for both the most and least reactive reductant have a slope of 3.98 (1300°C) and 2.16 (1100°C), respectively. However, the most reactive reductant was still progressively losing mass at the end compared to the least one that had started to slowly gain mass. Also a slight gain in mass is noted for the 1200°C test.

4.2.6.1 Differential Time Analysis:

Figure 4.14 depicts the consequences of increasing temperature on change in mass loss for Reductant D. The effect is more pronounced within the first 0.33 hours, although an anomaly is experienced at higher temperatures of 1300°C and 1400°C.

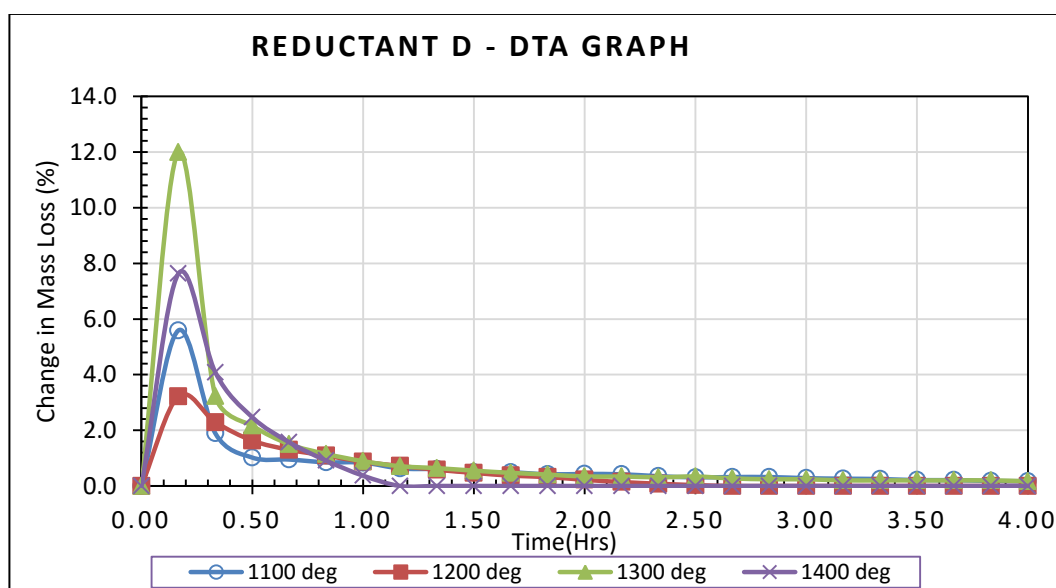


Figure 4.14: Differential Time Analysis Graph - Reductant D (1100°C to 1400°C).

The highest change in mass was 12% at 0.17 hours for the 1300°C test instead of the 1400°C, which had 7.63% at 0.17 hours. This is followed by a change of 5.59% for the 1100°C test and lastly by 3.22% for the 1200°C, within the same 0.17 hours.

4.3. TGA Test Product Analyses – (Chemical, XRD and SEM)

Various analyses were performed on the solid state reduction products. Products were selected for the different analyses not only to enable a general comparison between all reductants, but to specifically compare conventional reductant B and unconventional reductant D. All 5 products were analysed by chemical speciation method, to confirm species remaining after the 4 hour reduction. Further analysis was done on selected products to assist with the comparison as follows:

1. XRD analysis - 3 products from Conventional (A, B, C) and the unconventional reductant (D), all chosen from the 1400°C reactivity tests.
2. SEM analysis – 1 product from conventional reductants (B) and the unconventional reductant (D), both from 1400°C tests.

4.3.1 Reductant A Product – (Chemical, XRD)

4.3.1.1 Chemical

The solid state reduction product was analysed for bulk chemical composition as well as chemical species by selective leaching, with the results obtained given in Table 4.8.

Table 4.8 : Reduced Material Metallic Content –Reductant A (mass %)

Reductant	(°C)	Al	Cr	Fe	Ni
A	1100	6.31	0.20	0.68	<0.05
	1200	8.25	0.39	9.48	0.08
	1300	3.53	2.06	11.36	0.08
	1400	8.68	1.49	11.70	0.08

<0.05: the analyte content is below the 0.05% detection limit of the analytical method
(Analyte - Mn, Zn, Cu)

In terms of the oxide species taking part in the solid state reduction (FeO and Cr₂O₃), there was significant increase in metallic Fe product (0.68% to 9.48%) from the 1100°C to 1200°C test. This gradually increased with rising temperature to 11.36% and 11.70% at 1300°C and 1400°C, respectively. Relatively low chromium metal levels were obtained at 1100°C, which also started rising with increasing temperature. Chromium metal content in the product also showed a generally increasing trend with temperature, from 0.20% at 1100°C and 0.39% at 1200°C, to 2.06% at 1300°C, but then dropped to 1.49% at 1400°C.

4.3.1.2 XRD

The XRD pattern (Figure 4.15) obtained for reductant A, revealed that only the following minerals were identified *viz*, chromite, iron, chromium, Mullite, Wüstite, graphite, olivine and spinel. However, there was no chromium metal identified as with the chemical speciation results.

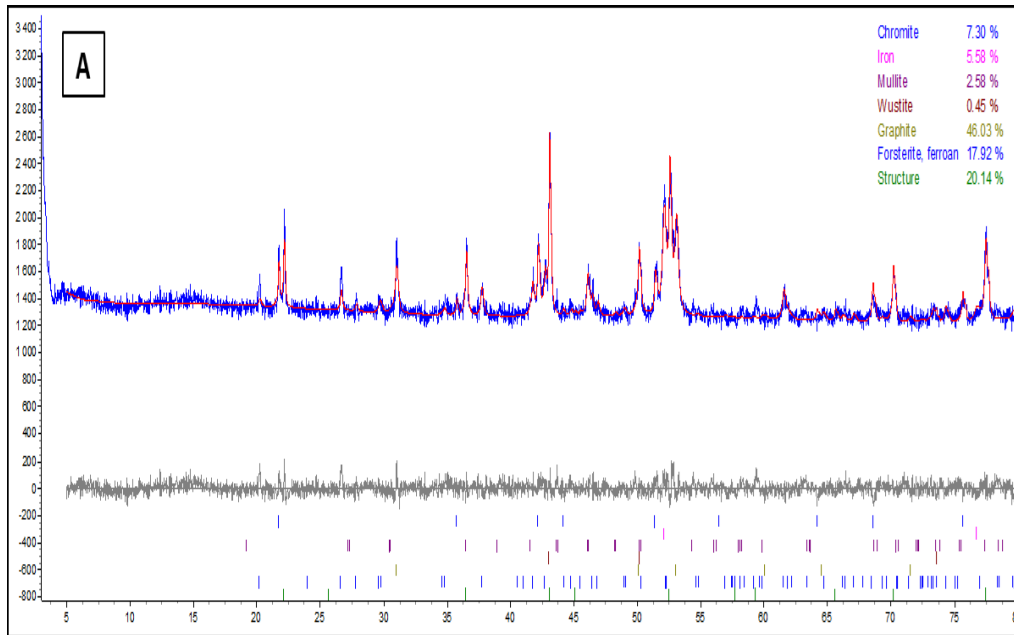


Figure 4.15: XRD Pattern for Reductant-A 1400°C Test Product

Further analysis was done to confirm the identified phases corresponding proportions, as summarised in table 4.10.

Table 4.9: Product Phases Relative Abundance - Reductant A.

Phase	Ideal Chemical Formula	Rel. Abundance (mass %)
Chromite	FeCr_2O_4	7.3
Iron	Fe	5.6
Chromium	Cr	-
Mullite	$3\text{Al}_2\text{O}_3 \cdot 2\text{SiO}_2$ / $2\text{Al}_2\text{O}_3 \cdot \text{SiO}_2$	2.6
Wüstite	FeO	0.5
Graphite	C	46
Olivine	$(\text{Fe, Mg})_2\text{SiO}_4$	17.9
Spinel	MgAl_2O_4	20.1
Hematite	Fe_2O_3	-
Cristobalite	SiO_2	-
Tridymite	SiO_2	-
Quartz	SiO_2	-
Total		100

Of the 7 phases, the highest in abundance was carbon (46%), followed by spinel (20.1%), olivine (17.9%), chromite (7.3%), iron (5.6%) and the least detectable was wüstite at 0.5%.

4.3.2 Reductant B Product – (Chemical, XRD, SEM)

The product for Reductant B at 1400°C was chosen as the main source for comparison to the unconventional Reductant D.

4.3.2.1 Chemical

The solid state reduction product with Reductant B was analysed for chemical species composition. Results of the metallic content after reduction are given in Table 4.10. The metallic content of Fe and Cr was quite low at 1100°C (0.75% and 0.20%, respectively) and this gradually increased with increasing test temperature.

Table 4.10: Reduced Material Metallic Content – Reductant B (mass %)

Reductant	(°C)	Al	Cr	Fe	Ni
B	1100	5.74	0.2	0.75	<0.05
	1200	4.74	0.36	8.33	0.07
	1300	4.40	1.28	9.67	0.08
	1400	13.79	0.80	9.81	0.07

<0.05: the analyte content is below the 0.05% detection limit of the analytical method (Analyte - Mn, Zn, Cu).

A significant increase in Fe content was noted at 1200°C (from 0.75% to 8.33%), which gradually peaked to 9.81% at 1400°C. This relationship was not gradual with regards to metallic Cr as it peaked at 1300°C to 1.28% but then instead decreased at 1400°C to 0.8%.

4.3.2.2 XRD

XRD was used to further analyse the selected 1400°C test product for Reductant B. This was done to enable evaluation of phase relations within the obtained pattern, in Figure 4.16. Only 5 mineral phases were identified, with the highest in abundance phases being Graphite/carbon

(91.92%), followed by Mullite (4.08%) then Quartz (3.07%) and in minute quantities Chromium (0.59%), Hematite (0.19%) and Tridymite (0.04%).

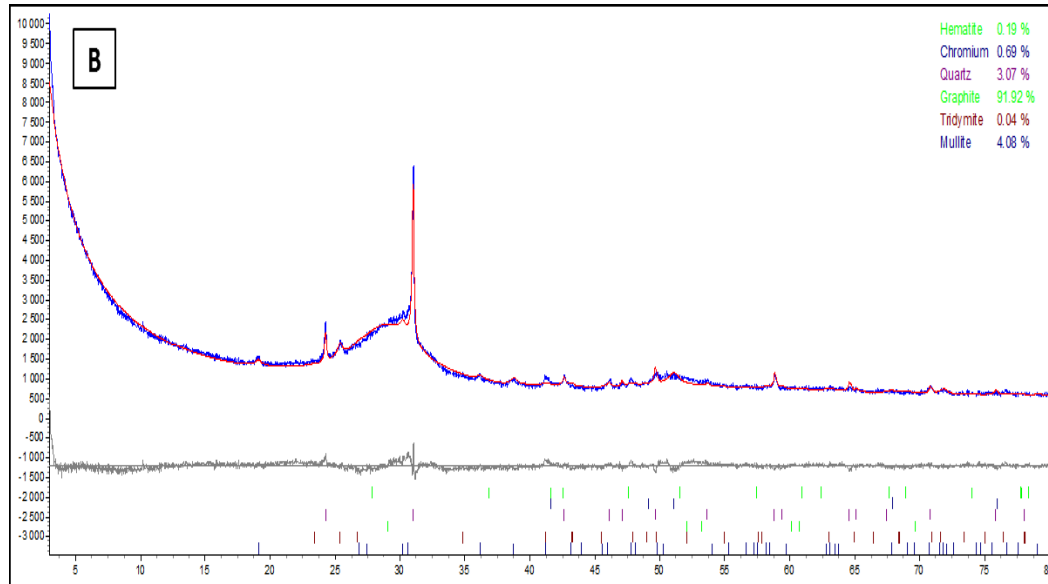


Figure 4.16: XRD Pattern for Solid-State Reduction of Chromite with Reductant B at 1400°C

There was no metallic iron identified, but only as the hematite Fe_2O_3 . The crystalline phases identified are summarised in Table 4.12.

Table 4.11: Product Crystalline Phases Relative Abundance - Reductant B.

Phase	Ideal Chemical Formula	Rel. Abundance (mass %)
Chromite	FeCr_2O_4	-
Iron	Fe	-
Chromium	Cr	0.7
Mullite	$3\text{Al}_2\text{O}_3 \cdot 2\text{SiO}_2$ / $2\text{Al}_2\text{O}_3 \cdot \text{SiO}_2$	4.1
Wüstite	FeO	-
Graphite	C	91.9
Olivine	$(\text{Fe}, \text{Mg})_2\text{SiO}_4$	-
Spinel	MgAl_2O_4	-
Hematite	Fe_2O_3	0.2
Cristobalite	SiO_2	-
Tridymite	SiO_2	<0.1
Quartz	SiO_2	3.1
Total		100

4.3.2.3 SEM-EDS

SEM-EDS technique was utilised on the product and six phases were identified in the sample. These phases include spinel, chromite, iron-chrome, chrome-iron, olivine and glass.

Two modes of iron-chrome occurrence were observed. iFlakes of Fe-Cr that are embedded in the spinel phase and discrete Fe-Cr phase that occur along the margins of the spinel phase. Chrome-iron phase occurred as regular blebs scattered in the glass phase. Olivine phase was sporadically scattered throughout the glass phase. Figure 4.17 shows the general appearance and nature of the phases.

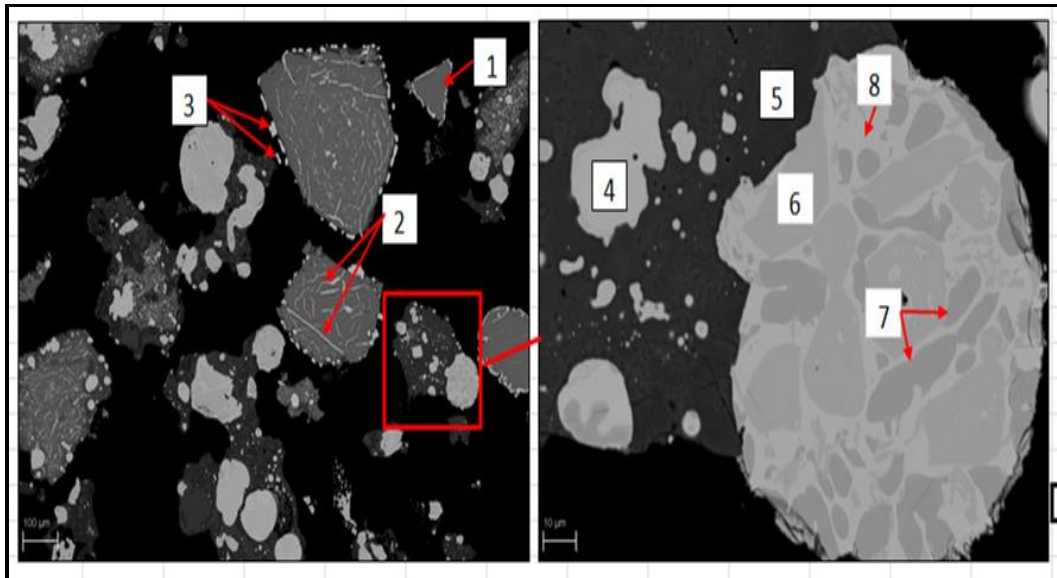


Figure 4.17: Backscattered Electron Image of Reduced Chromite with Reductant B at 1400°C (1-8 are the phases identified) .

A complete analysis of the phases present is summarised in Appendix- F.

4.3.3 Reductant B1 Product Analysis – (Chemical)

4.3.3.1 Chemical

Table 4.12 gives a summary of the elements analysed (Cr, Fe and C) with Al, Mn, Zn, Ni and Cu being undetectable. An increasing trend was

observed in the metallic Chromium and Iron contents, with increasing temperature.

Table 4.12: Reduced Material Metallic Content – Reductant B1 (mass %).

Reductant	Test (°C)	Cr	Fe
B1	1100	0.20	0.50
	1200	0.60	4.51
	1300	0.52	5.36
	1400	1.80	10.60

<0.05: the analyte content is below the 0.05% detection limit of the analytical method (Analyte – Al, Mn, Zn, Ni and Cu are not detectable).

There was a relatively large increase in Fe content from 1100°C to 1200°C and 1300°C to 1400°C of 0.5% to 4.51% and 5.36% to 10.60%, respectively. A similar change at the same rise in temperatures was also seen with regards Chromium that increased from 0.2% to 0.60% and 0.52% to 1.80%, respectively. However, there was a slight decrease in chromium from 0.60% to 0.52% from 1200°C to 1300°C.

4.3.4 Reductant C Product – (Chemical, XRD)

4.3.4.1 Chemical

Table 4.13 gives the metallic Fe and Cr content of products from the four tests. An increase in both metals content with temperature was evident from 1100°C to 1300°C but this was followed by a significant reduction at 1400°C. From 1100°C to 1300°C, chromium increased from 0.20% to 2.90% and iron from 1.37% to 11.60%.

Table 4.13: Reduced Material Metallic Content – Reductant C (mass %)

Reductant	Test (°C)	Cr	Fe	Ni
C	1100	0.2	1.37	<0.05
	1200	0.48	10.07	0.08
	1300	2.90	11.60	0.53
	1400	0.64	4.12	<0.05

<0.05: the analyte content is below the 0.05% detection limit of the analytical method (Analyte - Mn, Zn, and Cu not detectable)

At 1400°C, chromium and iron content dropped to 0.64% and 4.12%, respectively. The total iron (27.16%) from all the tests was almost 6.8 times the chromium (4.04%) content.

4.3.4.2 XRD

Figure 4.18 gives the XRD patterns for Reductant C product at 1400°C. A total of 8 phases were identified. The highest in abundance was the spinel structure (43.28%), followed by Chromite (24.16%), Hematite (16.38%), Cristobalite (10.45%), Graphite (4.12%), Iron (0.39%) and Wüstite (0.04%). There was no chromium identified.

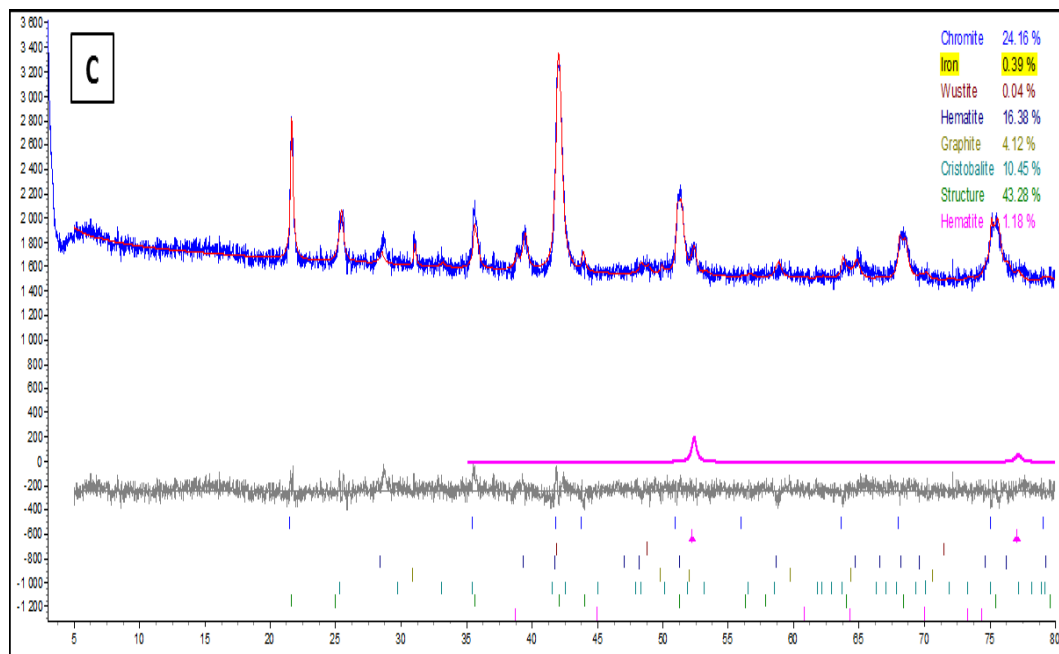


Figure 4.18: XRD Pattern for Solid-State Reduction of Chromite with Reductant C at 1400°C.

4.3.5 Unconventional Reductant D Product – (Chemical, XRD, SEM)

4.3.5.1 Product Analysis (Chemical) - Reductant D

Metallic iron and chromium from the reduction tests with unconventional Reductant D are summarised in Table 4.14. Despite the 1100°C test having a faster and more mass loss in the 4 hour holding period than the

1200°C tests, both tests resulted in the same iron and chromium metal content of 0.5% and 0.2%, respectively.

Table 4.14 : Reduced Material Metallic Content – Reductant D (mass %)

Reductant	Test (°C)	Cr	Fe	Ni
D	1100	0.20	0.50	<0.05
	1200	0.20	0.50	<0.05
	1300	1.87	11.46	0.07
	1400	8.24	14.56	0.05

<0.05: the analyte content is below the 0.05% detection limit of the analytical method (Analyte - Mn, Zn and Cu not detectable).

There was a marked increase in Iron content at 1300°C to 11.46%, with 1400°C test ending with 14.56%. Chromium content increased to 1.87% at 1300°C and significantly peaks to 8.24% at 1400°C. The total chromium and iron for all the tests were 10.15% and 26.12%, which represented about 2.57 times more metallic iron to chromium.

4.3.5.2 XRD Analysis

The 1400°C test product was selected for XRD analysis to confirm the crystalline phases and their abundance. According to Figure 4.19 and Table 4.15, only 7 phases were identified.

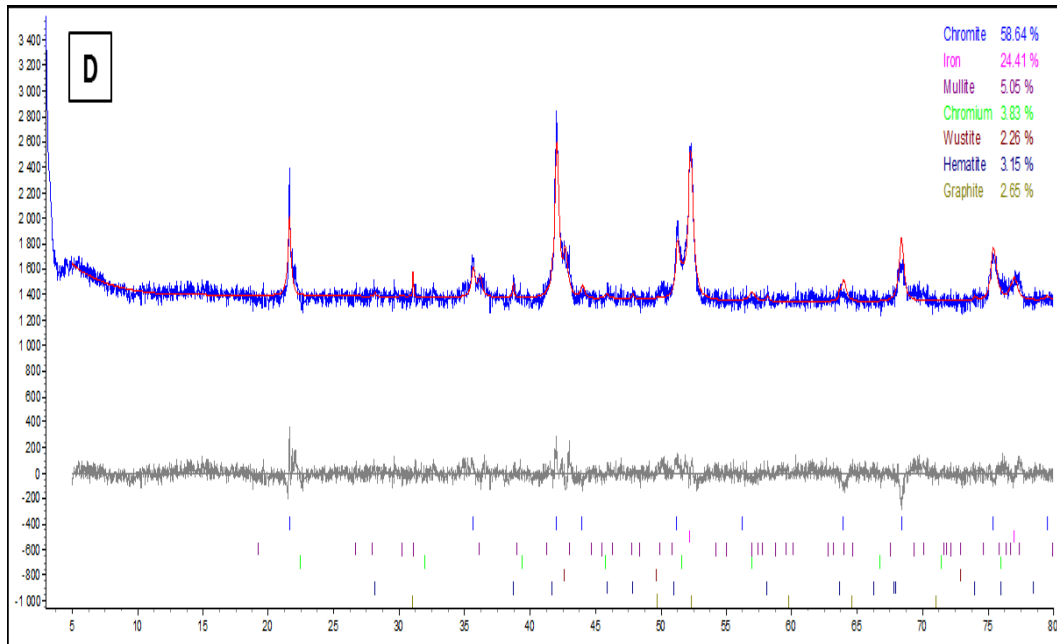


Figure 4.19: XRD pattern for solid state reduction of chromite using Reductant D at 1400°C

These include Chromite (58.64%), Iron (24.41%), Mullite (5.05%), Chromium (3.83%), Hematite (3.15%), Graphite (2.65%) and Wüstite (2.26%).

Table 4.15: Product Crystalline Phases Relative Abundance -Reductant D

Phase	Ideal Chemical Formula	Abundance (mass %)
Chromite	FeCr_2O_4	58.3
Iron	Fe	24.3
chromium	Cr	3.8
Mullite	$3\text{Al}_2\text{O}_3 \cdot 2\text{SiO}_2$ / $2\text{Al}_2\text{O}_3 \cdot \text{SiO}_2$	5.1
Wüstite	FeO	2.2
Graphite	C	2.6
Olivine	$(\text{Fe, Mg})_2\text{SiO}_4$	-
Spinel	MgAl_2O_4	-
Hematite	Fe_2O_3	3.1
cristobalite	SiO_2	-
Tridymite	SiO_2	-
Quartz	SiO_2	-
Total		100

4.3.5.3 SEM-EDS

A SEM-EDS analysis was performed on the 1400°C test product to identify and show the phase relations. The phases identified included spinel, chromite, iron-chrome, chrome-iron, olivine and glass. This was similar to phases identified for Reductant B (Table 4.16) product's results at 1400°C that had modes of iron-chrome occurrence observed *i.e.* flakes of Fe-Cr that were embedded in the spinel phase and discrete Fe-Cr phase that occurred along the margins of the spinel phase. Chrome-iron phase occurred as regular blebs scattered in the glass phase. Olivine phase was sporadically scattered throughout the glass phase. Figure 4.20 showed the general appearance and nature of the phases.

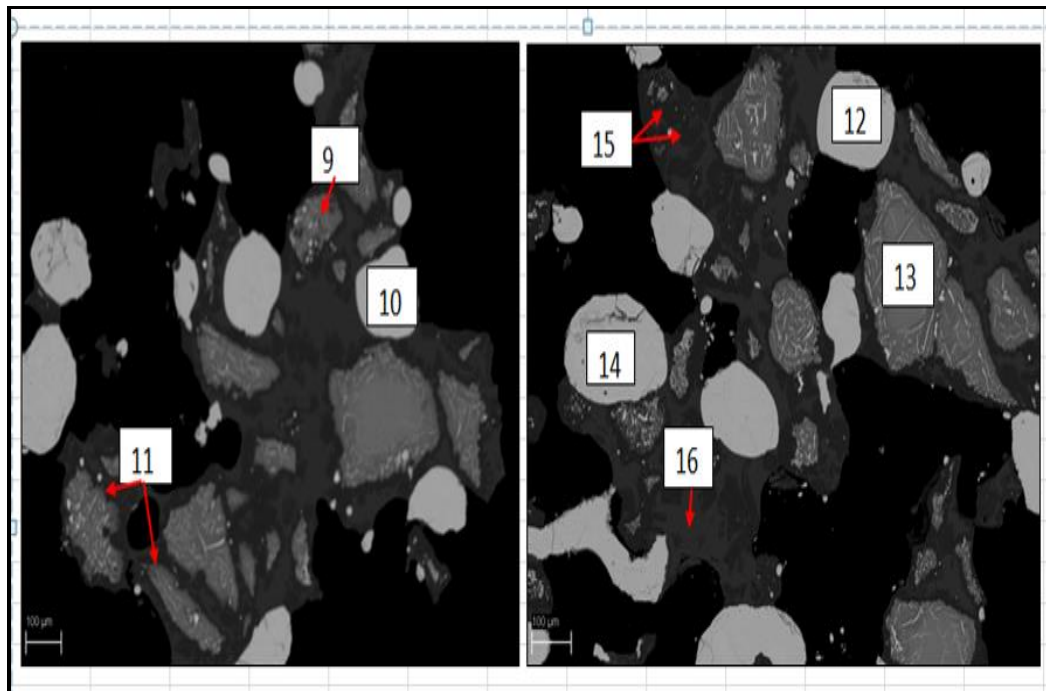


Figure 4.20: Backscattered electron image of reduced chromite with Reductant D at 1400°C (9-16 are the phases identified).

Chemical analysis carried out on the phases is given in Table 4.18. The SEM results showed that the dominant phases present in both samples were the Iron-chrome and chrome iron phases.

This means that these samples were substantially reduced, as the dominant phases were metallic.

Table 4.16: The SEM Phases Chemical analysis

Phase	O	Cr	Fe	Al	Si	Mg	Ti	Ca	
9	30.7	35.3	23.9	9.1	-	0.1	0.9	-	chromite
10	0.5	58.3	39.5		1.6	0.1		-	chrome-iron
11	49.0	8.9	0.4	39.9	-	0.2	1.7	-	spinel
12	-	75.3	24.7	-	-	-	-	-	chrome-iron
13	31.0	35.1	23.3	9.7	-	0.1	0.9	-	chromite
14	-	71.0	27.3	-	1.0	-	0.7	-	chrome-iron
15	60.2	3.0	5.3	1.4	30.4	0.1	-	-	silicate
16	46.3	-	-	15.7	25.8	01	-	12.1	glass

¹-Analyte was not detected.

5. DISCUSSION

This chapter interprets, highlights the significance of test work results obtained and the outcomes. Reductant performance and suitability for solid-state chromite reduction was determined by interpreting the corresponding isotherms and quantifying reactivity in terms of attained reduction and metallisation levels. An evaluation of the various reductants was performed by determining some of the critical parameters known to have an impact on reductant performance, *viz.* process temperature and time, reductant rank, porosity, friability, volatiles and fixed carbon content. Finally, an attempt to link displayed reactivity with reductant quality, factors that affect TGA solid-state chromite reduction and the obtained product analyses results demonstrated.

The tests undertaken on the reductants included the following:

- Characterization of selected conventional and unconventional reductants undertaken by various chemical and physical analyses including PSD, proximate, ultimate, optical light microscopy and petrography, to assist confirm suitability of each reductant for use during solid state chromite reduction.
- Isothermal reactivity tests carried-out in a TGA furnace within the temperature range 1100°C -1400°C, under inert atmosphere and a 4 hour holding period.
- Establishing the a) relevancy of the current reductant products and potential for sustainable utilisation in ferrochrome processing in South Africa; and b) likelihood of whether selected reductant can substitute conventional reductants, when the quality of the latter deteriorates to

levels not economic for further processing or new environmental legislation put a constraint to their application in South Africa.

The main significance of reductant characterization is that it plays a critical role of revealing quality parameters (chemical and physical including structural), required for successful chromite pre-reduction. For instance, conventional Reductants such as B and B1 were shown to generally display characteristics similar to those of Reductant A, a standard metallurgical reductant, in terms of macro-porosity, petrographic composition and forms of carbon, and reactivity to chromite. However, despite these reductants showing a presence of spherulitic and pyrolytic carbon that may serve to increase the strength of the cokes, this may also result in decreased reactivity. This was evident as both of them reported high fixed carbon content, compared to the unconventional Reductant D, but displayed low reactivity compared to the latter. In general, this suggested that these reductants (B and B1) may be successfully utilised in metallurgical or smelting operations, in which Reductant A is already widely used. Whilst for unconventional Reductant D, its characterization demonstrated the presence of both lower ranking and more mature carbon, with the consequence that certain fragments of the material reacted faster than others during the heating process. These differences were most likely due to the nature of the original plant material. This and its highly friable nature could possibly explain why some of the isotherms for Reductant D, are in some instances not continuously linear but rather irregular in pattern.

Macro-porosity and cell wall width tests were not successfully obtained for the unconventional reductant, as its friable nature hindered success in proper sample preparation. The micrographs showed its highly porous nature and this suggested that the charcoal should allow for better diffusion between the gases and reductant-chromite mixture. This is important for the Boudouard

reaction and enhances reduction as it improves contact between the evolved gases, carbon and chromite (diffusion controlled stage). Coupled with the high volatiles content, it serves to greatly enhance the unconventional reductants reactivity. This was visible during the early stages in most of the tests, before the volatiles had been expended and subsequently reactivity quickly diminished.

On the other hand, the low volatiles and well-structured or isotropic nature of the conventional reductants were seen to contribute to a lower, consistent but rather controlled reactivity throughout the tests. Their reactivity greatly improved with increasing temperature. Both reductant types pointed more to the effect of chemical control within the first stages of the test, as emphasised by the response to rise in temperature on reactivity. The second stage was apparently more prone to diffusion control.

Repeats and anomalies experienced during the testwork confirmed the potential negative results linked to equipment like TGA instability and leakages. This was caused by factors like inconsistency in placing sample into the furnace reactor, effect of argon (inert gas) purging on friable and/or fine material. The repeats and anomalies were also noted to be a result of inherent features typically found with sensitivity of different analytical methods or techniques utilised.

5.1. Chromite Reduction and Metallisation

Overall reduction efficiency of the different reductants was studied through quantification of both the degree of reduction and metallisation. This was done for both Fe and Cr in the UG2 chromite concentrate. A quantitative approach in determining efficiency in terms of the selectivity of each reductant to metalize iron and chromium was adopted. This was mainly due to

experienced highly inconsistent blank reductant TGA tests that were necessary for mass loss correction.

A number of solid state reduction studies have been carried-out and different expressions used to determine the degree of reduction. It was also generally accepted that TGA mass loss was assumed to be equal to the CO evolved from the oxygen in the reducible oxides. Notable examples include an investigation of solid state chromite pellet reduction with CO by Xiao *et al.* (2007). In this study, expression (l) was used to define the degree of reduction. This was given as the percentage of oxygen removed from the total removable oxygen in chromite, with mass loss correction to volatiles done.

$$R(\%) = \frac{W_0 + W_t - W_{volatiles}}{W_{oreducible}} * 100 \dots\dots\dots (l)$$

Where:

W_0 is the initial dried sample weight before reduction

W_t is the sample weight during reduction

$W_{volatiles}$ is the weight loss resulting from volatiles

$W_{oreducible}$ is the total chromite oxygen content from the iron and chromium oxides

Lintumaa *et al.* (2007) utilised expression (m) to determine reduction degree through the degree of metallisation, given as the ratio of chromium and iron metal after reduction to the total chromium and iron before reduction:

$$M(\%) = \frac{Cr_{met} + Fe_{met}}{Cr_{tot} + Fe_{tot}} * 100 \dots\dots\dots (m)$$

Oxygen removal was taken as the corrected mass loss in the TGA compared to the total oxygen in the initial chromium and iron oxides. Mass loss

correction was done by accounting for both the decompositions in ore and reaction of coke carbon with coke ash (Lintumaa *et al.*, 2007).

5.1.1 Degrees of Reduction and Metallisation by Speciation

During the pre-reduction of chromite, Fe^{3+} and Fe^{2+} ions were reduced to Fe^{2+} and Fe^0 , respectively, whereas Cr^{3+} species was reduced to Cr^0 . In these reactions, fractions of oxygen associated with the iron and chromium species were removed. In theory, the degree of reduction is expressed as the total oxygen removed from the sample divided by the total removable oxygen in the starting sample. The calculation of oxygen in the sample before and after reduction should theoretically be an easy task. However, experience suggested that the oxygen measurements are generally inconsistent and thus unreliable.

In practice, the degree of reduction is measured by TGA technique as used in the current study; however, successful quantification of the degree of reduction relied on the TGA furnace stability of the. This also meant that the procedure of introducing and removing the sample from the hot zone of the furnace should be consistent throughout. In most cases, consistent procedures during processing of pre-reduction recipes in the TGA instruments are somewhat difficult to attain due to the required high sensitivity of the balance to mass changes. Hence, a much more reliable approach to measure the degree of reduction, as was generally used in the Mintek laboratory, was adopted in the current study.

The procedure entailed the determination of iron and chromium chemical species, *i.e.* Fe^{3+} , Fe^{2+} , Fe^0 and Cr^{3+} , Cr^0 respectively, followed by the calculation of associated oxygen content in the sample before and after reduction. This calculation was based on the oxygen mass balance. Through this method, the degree of reduction in the isothermal tests was determined in relation to the oxygen associated with Fe^{3+} , Fe^{2+} , and Cr^{3+} .

However, the oxygen associated with other sample components was not considered. To calculate the overall degree of reduction, Equation (n) was used:

$$\text{Degree of Reduction} = \frac{(\text{Sum of } O_2 \text{ on Fe \& Cr in Feed} - \text{Sum of } O_2 \text{ on Fe \& Cr in Product})}{\text{Sum of } O_2 \text{ on Fe \& Cr in Feed}} \times 100 \dots\dots\dots (n)$$

The portion of the sum of Fe⁰ and Cr⁰ relative to the sum of iron and chromium in the sample signifies the degree of metallisation. To calculate the overall degree of metallisation, Equation (o) was used. The degree of reduction should always be higher than or equal to the degree of metallisation at any point:

$$\text{Degree of Metallisation} = \frac{\text{Sum of metallic Fe \& Cr in Product}}{\text{Sum of total Fe \& Cr in Feed}} \times 100 \dots\dots\dots (o)$$

A significant advantage of this method was in that; it was not necessary to do any mass loss correction due to loss of the volatiles in reductant feed or carbon reacting with ash as well as decrepitating ore.

5.1.1.1 Degree of reduction for iron in chromite

For simplicity, the degree of reduction of iron in chromite was calculated using the principles described above. Table 5.1 gives the speciation results, calculated percentage degree of reduction (%DOR) and percentage degree of metallisation (%DOM) of iron.

Table 5.1 : Iron Speciation (mass% Fe^x) and %DOR and %DOM.

Test (°C)	Fe ⁰	Fe ²⁺	Fe ³⁺	Fe total	%DOR	%DOM
A/1100	0.68	1.34	15.36	17.38	3.51	0.45
A/1200	9.48	1.89	7.15	18.52	53.14	47.94
A/1300	11.36	5.58	3.37	20.31	63.97	52.97
A/1400	11.70	9.51	1.77	22.98	63.57	48.29
B/1100	0.75	0.45	15.52	16.72	2.40	0.92
B/1200	8.33	1.45	7.68	17.46	48.91	44.28
B/1300	9.67	6.96	2.91	19.53	60.14	46.42
B/1400	9.81	9.23	1.52	20.56	61.51	44.81
<i>B1/1100</i>	<i><0.50</i>	<i>0.19</i>	<i>18.17</i>	<i>18.36</i>	<i><0.50</i>	<i><0.50</i>
B1/1200	4.51	1.37	13.03	18.91	23.93	20.68
B1/1300	5.36	9.98	4.04	19.38	43.08	24.57
B1/1400	10.60	6.91	0.62	18.13	70.28	55.17
C/1100	1.37	0.44	14.05	15.86	6.72	4.88
C/1200	10.07	1.44	5.29	16.80	61.62	56.37
C/1300	11.60	5.35	3.71	20.66	63.67	53.25
<i>C/1400</i>	<i>4.12</i>	<i>0.44</i>	<i>14.74</i>	<i>19.30</i>	<i>19.62</i>	<i>18.22</i>
<i>D/1100</i>	<i><0.50</i>	<i>0.11</i>	<i>20.20</i>	<i>20.31</i>	<i><0.50</i>	<i><0.50</i>
<i>D/1200</i>	<i><0.50</i>	<i>0.10</i>	<i>19.90</i>	<i>20.00</i>	<i><0.50</i>	<i><0.50</i>
D/1300	11.46	0.11	8.74	20.31	55.24	53.49
<i>D/1400</i>	<i>14.56</i>	<i>1.24</i>	<i>4.74</i>	<i>20.55</i>	<i>72.03</i>	<i>67.96</i>

<0.5 : indicates that the analyte content is below the 0.5% detection limit of the analytical method for the specific analyte. **Italics**: Represents repeated tests

The trend observed from the results was that, the degree of reduction increased with increasing reaction temperature for all the reductants, except for Reductant C where the %DOR was low at 1400°C. The anomalous behaviour was re-evaluated by repeating the test at 1400°C. As shown in Appendix F (Table 9.11), though the overall %DOR was a bit higher compared to the previous result, it still does not fit the trend.

Reductants D and B1 at 1400°C resulted in the highest %DOR and %DOM. For the unconventional Reductant D to have the high %DOR and %DOM at 1400°C, despite that it had a low overall mass loss, concurred with the view described above about the possible inconsistencies in the TGA operations. This might however be ascribed to the high reactivity of Reductant D.

5.1.1.2 Degree of reduction for chromium in chromite

The %DOR, %DOM and speciation results for Cr are given in Table 5.2. Again for simplicity, the degree of reduction of chromium in chromite was calculated using the procedure described under section 5.1.1.

Table 5.2: Chromium Speciation (mass% Cr^x) and %DOR and %DOM.

Test (°C)	Cr ⁰	Cr ³⁺	Cr total	%DOR	%DOM
<i>A/1100</i>	<0.2	20.93	20.93	0.00	0.00
A/1200	0.39	21.90	22.30	0.55	0.20
A/1300	2.06	22.90	24.97	7.12	6.85
A/1400	1.49	26.92	28.41	4.08	4.02
<i>B/1100</i>	<0.2	19.90	19.90	0.00	0.00
B/1200	0.36	20.61	20.96	0.50	0.04
B/1300	1.28	22.66	23.94	4.20	3.90
B/1400	0.80	24.87	25.67	1.90	1.74
B1/1100	0.58	26.37	26.95	0.94	0.85
B1/1200	0.60	26.55	27.15	1.00	0.92
B1/1300	0.52	28.76	29.28	0.56	0.58
B1/1400	1.80	27.82	29.62	4.92	4.90
<i>C/1100</i>	<0.2	<0.2	19.43	<0.2	<0.2
C/1200	0.48	20.17	20.66	1.14	0.65
C/1300	2.90	23.26	26.16	10.00	9.76
C/1400	1.22	21.69	22.91	4.15	3.80
<i>D/1100</i>	<0.2	28.39	28.39	0.00	0.00
<i>D/1200</i>	<0.2	27.98	27.98	0.00	0.00
D/1300	1.87	27.88	29.75	5.13	5.11
D/1400	8.24	20.63	28.86	27.66	27.33

<0.2: indicates an analyte content below the 0.2% detection limit of the analytical method for the specific analyte. **Italics:** Represents repeated tests.

The assumption made was that Cr⁰ and Cr³⁺ were the only chromite species present in the sample – and that Cr⁶⁺ and Cr²⁺ were not part of the sample. The values for the Cr³⁺ were calculated by difference between the Cr total in the sample and the metallic Cr. For the tests that had Cr⁰ content of less than 0.2% or below detection limit, it was assumed that no metallisation occurred in those tests.

The results did not present a clear relationship between the %DOR and %DOM with temperature. As observed in the case of iron in Figure 5.1, unconventional reductant D had the highest %DOR and %DOM at 1400°C.

Further repeat tests done following the repeats for repeatability are given in Appendix F, (Table 9.12). There was a notable change in both the speciation tests results and the calculated degree of reduction and metallisation.

5.2. Comparison of Reactivity at 1100°C, 1200°C, 1300°C & 1400°C.

The reactivity of reductants during solid-state reduction of chromite was evaluated by studying the reaction rate and extent of reduction. This was interpreted from the slope of mass loss curves (Isotherms) and overall decrease in mass at the end of the holding period. The higher the slope or steeper the mass loss curve, the more reactive was a reductant. The isotherms were split into two stages for each temperature as it was evident that the initial reaction phase was always accompanied by a mass reduction, which gradually slowed down in most instances. Figure 5.1 and Figure 5.2, Figure 5.4 and Figure 5.5, Figure 5.7 and Figure 5.8 and lastly Figure 5.10 and Figure 5.11 showed the test sample mass reduction plotted in two phases as a function of reaction time for tests conducted at 1100°C, 1200°C, 1300°C and 1400°C, respectively.

Furthermore, differential time analysis graphs (Figure 5.3, Figure 5.6, Figure 5.9 and Figure 5.12) are plotted. They portrayed the typical decrease in mass experienced with increasing test temperature for each reductant, during the TGA test. This also assisted in highlighting the time or stage at which most of the mass reduction was incurred, when saturation point was reached and finally to quantify the decrease in mass experienced.

5.2.1 Comparison of Reductant Reactivity at 1100°C

5.2.1.1 First Stage

The first stage was represented by 25 minutes of the total reaction time. At 1100°C, corresponding isotherms (Figure 5.1) for the reductants showed that unconventional Reductant D and conventional Reductant C had almost similar reactivity rates. Both reductants were significantly more superior with regards overall mass decrease incurred, compared to the other reductants. This was quite evident during the initial stages of the test. After nearly 10 minutes Reductant C became slightly superior to the unconventional reductant in terms of reactivity and overall mass reduction. Reductant C recorded a decrease in mass of 7.22%, compared to Reductant D with 5.59%. This was followed by Reductants A, B and B1 that consecutively recorded 13.20%, 3.54% and 2.58%.

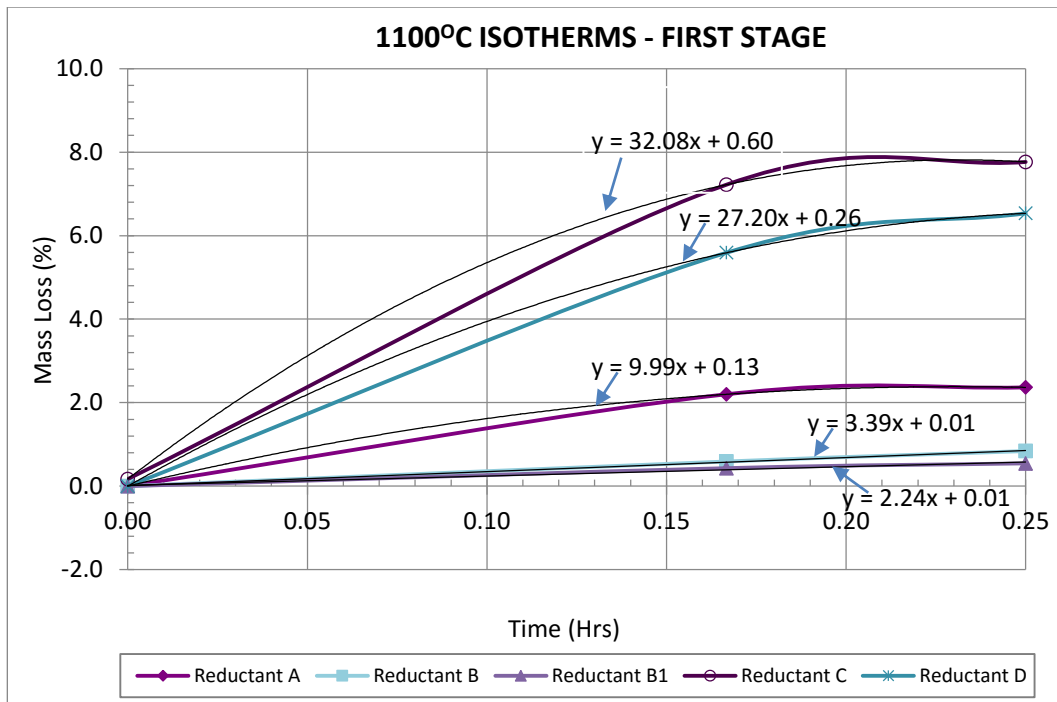


Figure 5.1: Reductants A, B, B1, C and D Isotherms at 1100°C – First Stage.

The high reactivity in this stage was represented by a gradient of 32.08, 27.20, 9.99, 3.39 and 2.24 for the Reductants C, D, A, B and B1 respectively. This corresponds to the total mass reduction recorded.

5.2.1.2 Second Stage

Figure 5.2 shows a second stage that started from 12 minutes until the end of reaction. Reductant C followed by Reductant D continued to have the highest reactivity, followed by reductants B, A and lastly B1. This was clearly illustrated by the slope of corresponding isotherms. However, all the reductants reactivity is relatively subdued than observed in the first stage, with Reductant C having a slope of 2.84, Reductant D = 2.68, Reductant B=1.57, Reductant A=0.54 and finally Reductant B1=0.60.

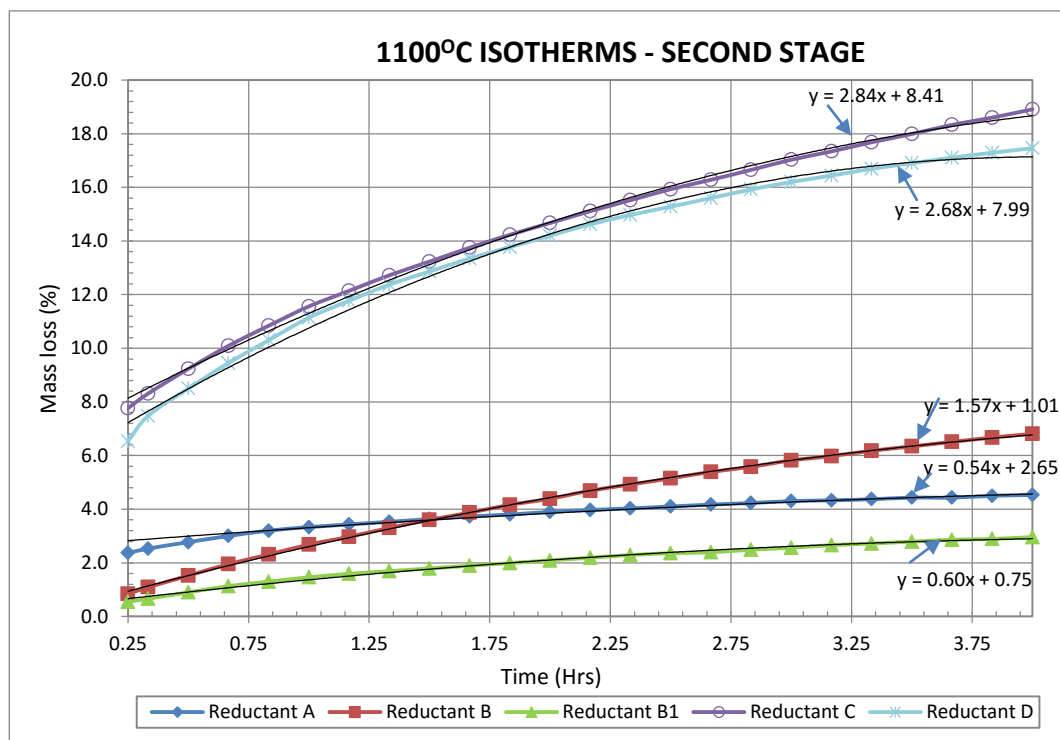


Figure 5.2: Reductants A, B, B1, C and D Isotherms at 1100°C – Second Stage.

Reductant C with the highest rate in both stages dropped from a gradient of 42.30 in 12 minutes (first stage) to 2.86 in the remaining 3 hours and 48 minutes (second stage). However, Reductant B was to substitute Reductant A as third within 90 minutes. It demonstrated a tendency or potential to react further after the 4 hours, compared to the latter that was almost slowing down to reach saturation. Reductants C and D recorded an overall mass reduction of 17.46% and 18.91% respectively. The two had not reached saturation point at 1100°C after 4 hours. Reductant B was the third highest in terms of decrease in mass with a total 6.81% recorded. Reductant B finished with a total decrease in mass of 6.81% compared to Reductant A that recorded 4.53%. The least mass reduction and reactivity was noted in conventional reductant B1, which completed with 2.96% within 4 hours.

5.2.1.3 Differential Time Analysis

The differential time analysis graph of mass reduction (Figure 5.3) portrayed that Reductant C had the highest decrease in mass.

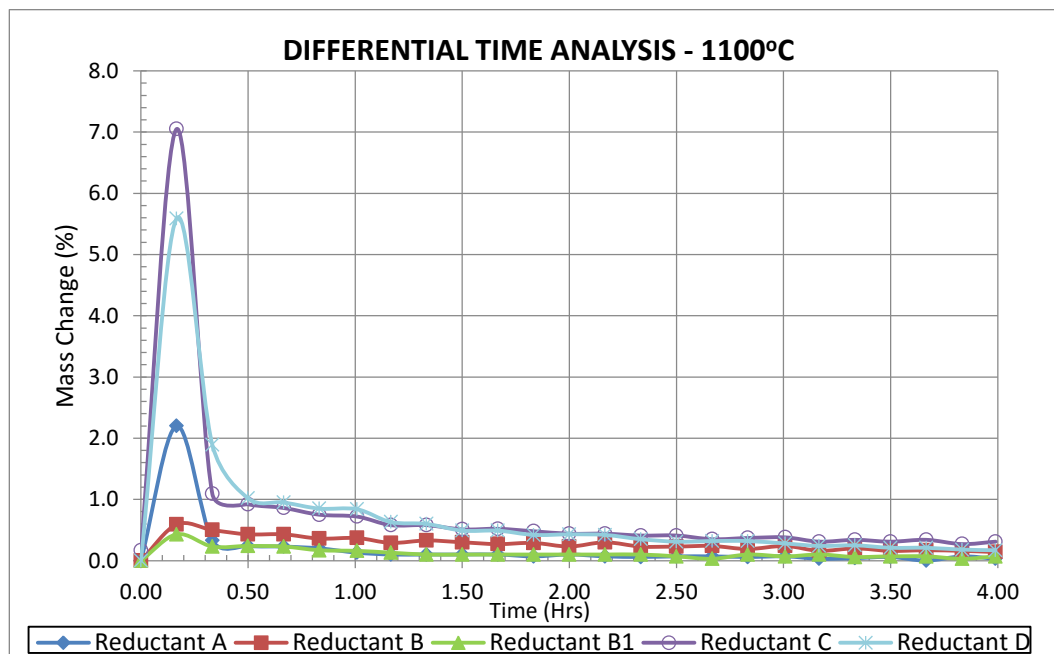


Figure 5.3: Reductant A, B, B1, C and D Change in Mass at 1100°C.

This was 7.05% in 15 minutes, followed by Reductants D (5.59%) then A (2.20%), B (0.59%) and finally B1 (0.43%), within the same time period.

All Reductants had a gradual decrease in mass reduction that relatively flattened within 2.5 hours. Except Reductants B1 and A, the rest still showed potential for continued decrease in mass, at the end of the 4 hour holding period.

5.2.2 Comparison of Reductant Reactivity at 1200°C

5.2.2.1 First Stage

In this region of up to an hour (Figure 5.4), the unconventional Reductant (D) had the highest reactivity. This was followed by the conventional reductants in the following order –Reductants C, B, A and lastly B1. The reductants had a trend line gradient of 10.02, 6.19, 4.07, 3.86, and 2.96 consecutively for Reductants D, C, B, A and B1.

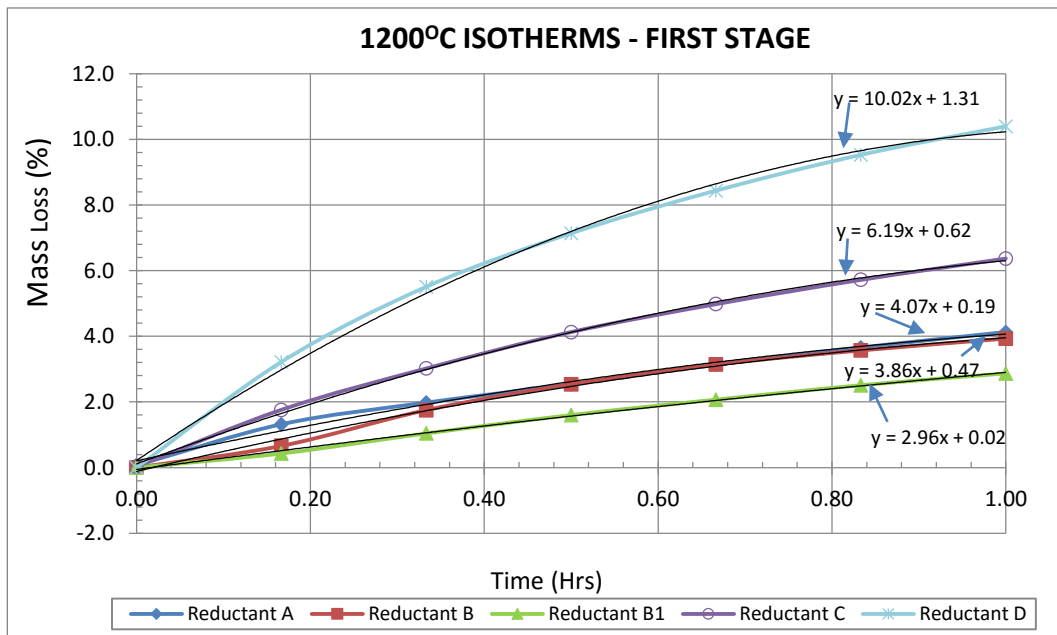


Figure 5.4: Reductants A, B, B1, C and D Isotherms at 1200°C – First Stage.

However, in terms of mass reduction at the end of the first stage the highest recorded was Reductant D, followed by Reductants C and A instead of B, with Reductant B1 maintaining the last position. This was mainly as a result of Reductant A having superior reactivity within the first 24 minutes, during which a significant mass reduction took place, before Reductant B just slightly surpassed Reductant A, in terms of reactivity.

5.2.2.2 Second Stage

This stage (see Figure 5.5) was from an hour till the end of the holding period. Despite the unconventional Reductant D starting off with the highest reactivity, it gradually lost momentum and from 2.67 hours it reached saturation point but was observed to gain in mass until the end of the test.

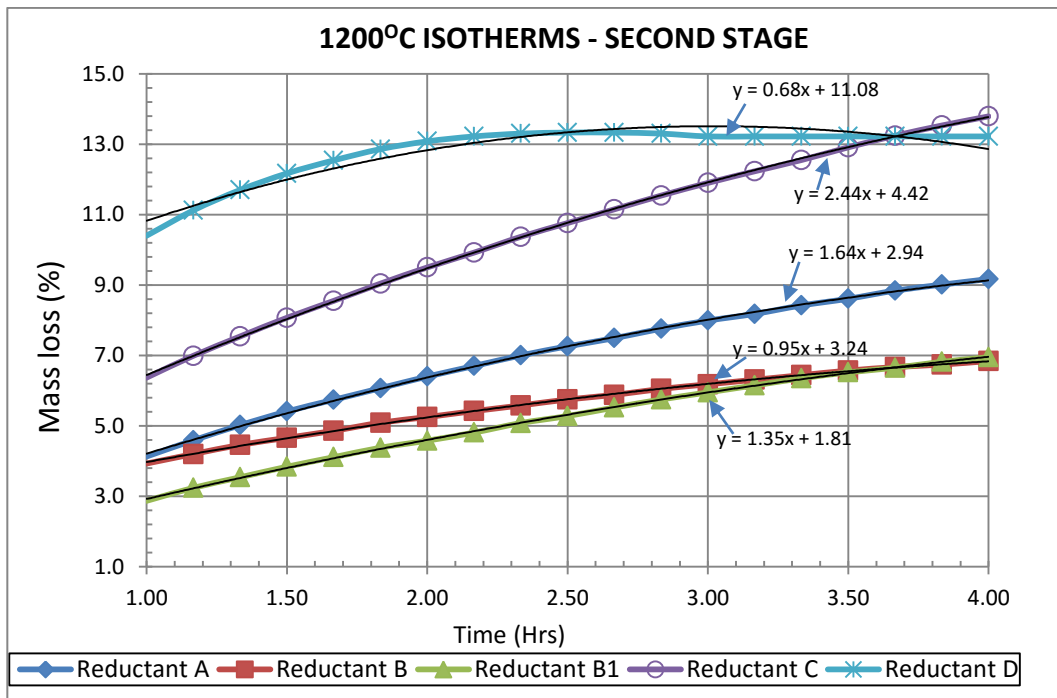


Figure 5.5: Reductants A, B, B1, C and D Isotherms at 1200°C – Second Stage.

Reductant D had the least reactivity during this stage, with Reductant C surpassing it within 2.33 hours, to end up with the highest reactivity. This was followed by Reductants A, B1 and finally B. Reductant B1 was also noted to react past B within 3.50 hours, although the latter had been superior during the first stage. Despite unconventional Reductant D having had the most reactive trend within the first 2 hours, it finished with a mass reduction of 12.39% compared to Reductant C with 13.79%, that also had a higher apparent reactivity (Slope:2.44) compared to Reductant D (Slope:0.68). This was slightly more than twice the reactivity displayed by the reductant with least mass loss, Reductant B (Slope:0.95).

All the conventional reductants demonstrated capacity to continue reacting, after 4 hours.

5.2.2.3 Differential Time Analysis at 1200°C

Figure 5.6 showed that the highest mass reduction occurred within 20 minutes for the reductants D, C and A, whilst for B and B1, this was within an hour.

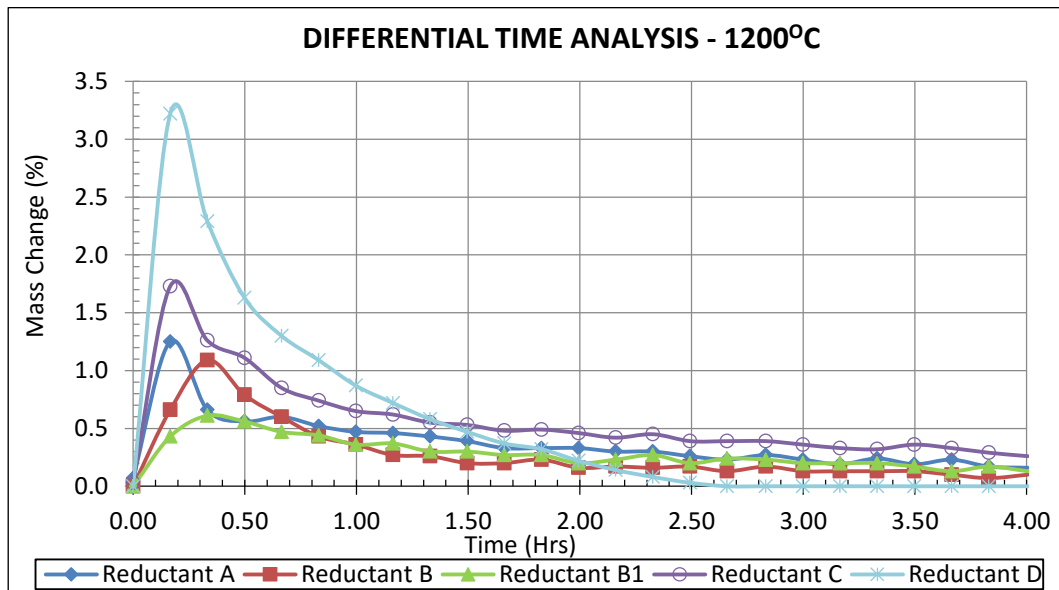


Figure 5.6: Reductant A, B, B1, C and D Change in Mass at 1200°C.

The highest change in mass reduction for Reductants B and B1 within 1 hour was 1.09% and 0.61% respectively. This was still correspondingly lower than the highest mass change for Reductants D, C and A that took place within the first 20 minutes of reaction time.

After the first hour, all reductants gradually reduced in mass change and flattened, with the unconventional reductant experiencing a gain in mass after 2.5 hours. Reductant D finished with a 0.18% mass gain, whilst the rest were still losing mass in minute quantities as follows, Reductant C (0.26%), Reductant A (0.16%), Reductant B (0.13%) and Reductant B (0.10%). The gain in mass could be a result of the buoyancy effect explained as in the slight or partial suspension of light and friable material due to a high rate of volatiles being driven off (quote) or to TGA instability.

5.2.3 Comparison of Reductant Reactivity at 1300°C

5.2.3.1 First Stage

Figure 5.7 portrayed the reactivity at 1300°C for the first 20 minutes. This segment had the highest mass reduction recorded for all reductants. This was linked to the most reactive reductant, which are the unconventional Reductant D, followed by conventional Reductants A, C, B1 and B.

Reactivity was represented by the trend line slope, which was 46.09 for Reductant D, 17.81 Reductant A, 17.27 Reductant C, 11.34, Reductant B1 and lastly 11.16 Reductant B.

This translated into the unconventional Reductant D being about 4 times as reactive as the least conventional Reductant B, and more than twice as reactive as the highest of the conventional reductants, A.

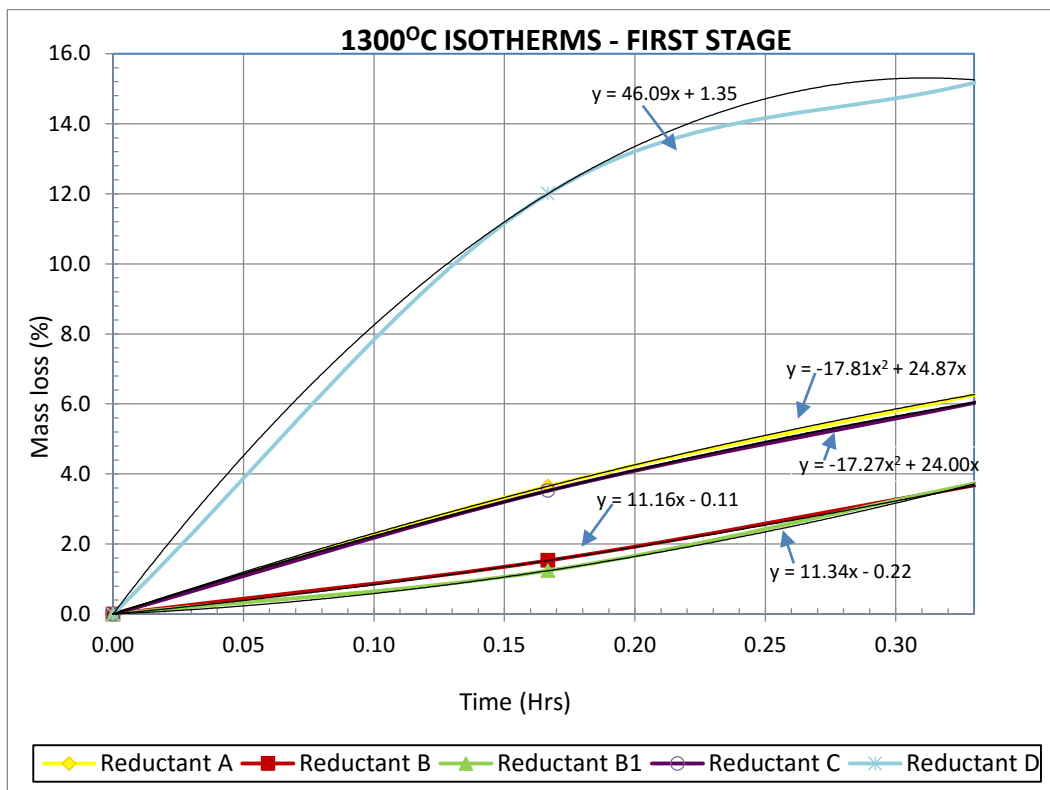


Figure 5.7: Reductants A, B, B1, C and D Isotherms at 1300°C – First Stage

The mass loss realised at the end of the first stage was in the order Reductant D (15.23%), Reductant A (6.31%), Reductant C (6.08%), Reductant B1 (3.78%) and Reductant B (3.72%), with the least mass loss. Despite Reductant B starting off with a slightly higher reactivity and mass loss than Reductant B1, the latter reacted more from 25 minutes to finish off the stage with a slightly higher mass loss.

5.2.3.2 Second Stage

The second stage (Figure 5.8) was from 20 minutes until the end of test (4 hours). Unconventional Reductant D and conventional Reductant B had the least reactivity rates, with Isotherm slopes of 2.61 and 2.58, respectively. In this stage the highest reactivity is demonstrated by Reductant B1 followed by

Reductants C and A that were represented by trend line gradients 4.08, 3.93 and 3.38, respectively.

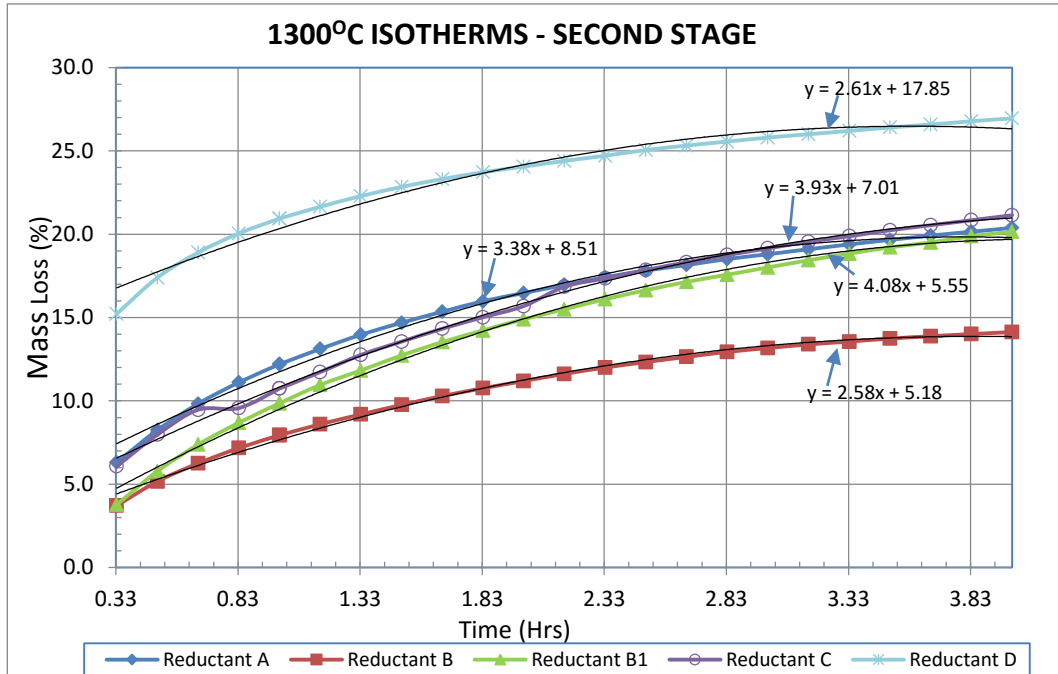


Figure 5.8: Reductants A, B, B1, C and D Isotherms at 1300°C – Second Stage.

At the end of the test, conventional Reductant D had the highest mass loss of 26.95%, although it had the second least reactivity rate during the second stage. Reductant B1 that had the greatest reactivity rate was the fourth in terms of total mass loss (20.15%). Second, third and fifth were Reductants C (21.14%), A (20.38%) and lastly B (14.13%).

5.2.3.3 Differential Time Analysis at 1300°C

The change in mass loss incurred with time is illustrated in Figure 5.9. This clearly showed that Reductant D had the highest change in mass experienced within the first 10 minutes.

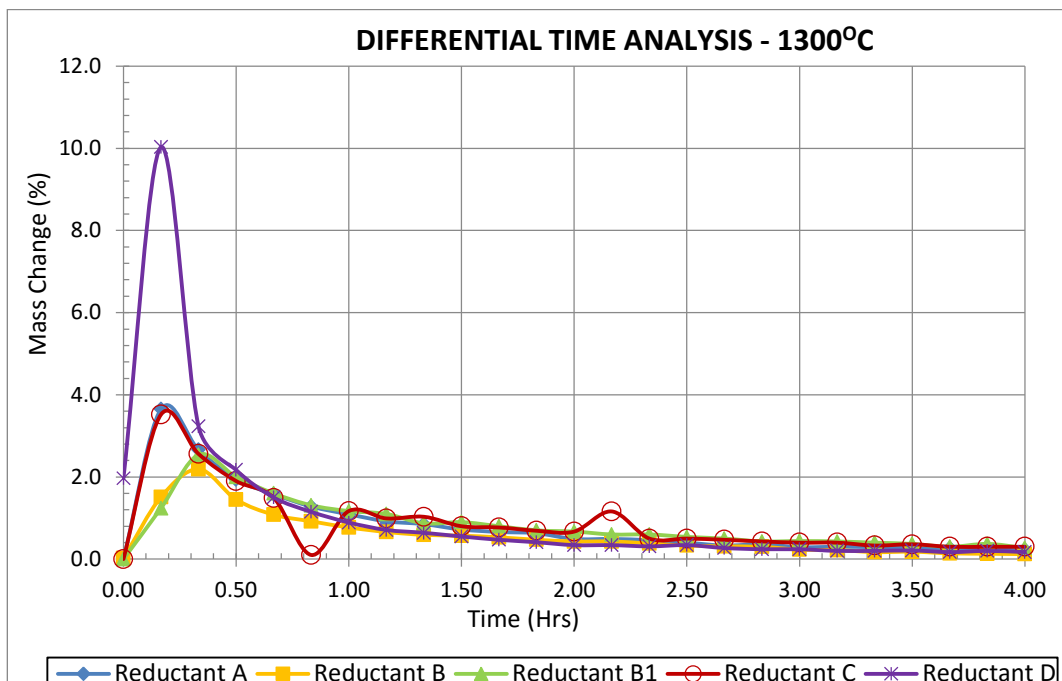


Figure 5.9: Reductants A, B, B1, C and D Change in Mass at 1300°C.

Reductant D had a change in mass of 10.03%, followed by Reductants A (3.65%), C (3.52%), with B1 having 1.51% and the least B (1.24%) within the first 10 minutes. However, Reductants B and B1 had the highest change in mass within 20 minutes of 2.19% and 2.54%, respectively. Reductant B1 was noted to have an increased mass loss to eventually supersede Reductant B. All the reductants then had a gradually decreasing change in mass, which noticeably flattened after 3.0 hours. Prior to this, Reductant C was seen to fluctuate between mass gain (0.83 and 1.17 hours) and mass loss (1.00, 1.33 and 2.17 hours). This could be a result of buoyancy, TGA instability and or leakages.

5.2.4 Comparison of Reductant Reactivity at 1400°C

5.2.4.1 First Stage

At 1400°C, the reactivity of all the reductants (Figure 5.10) showed that Reductant D was slightly the most reactive, closely followed by Reductants C, A and B with B1 lagging behind, within the first 10 minutes. The first stage was represented by the period from the start, up to 40 minutes of reaction time. All the reductants in the first stage portrayed an extremely high reactivity for an extended period. Although Reductant D started off with the highest mass loss within the first 20 minutes, it slackened. Reductant C, which was the second most reactive became the highest reactive until the end.

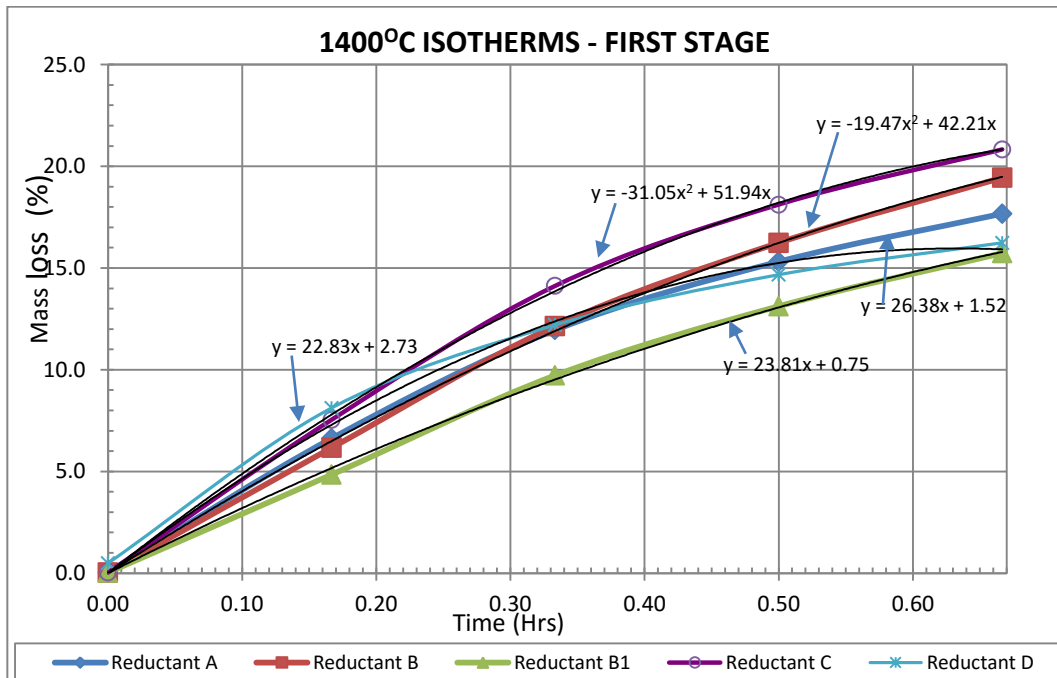


Figure 5.10: Reductant A, B, B1, C and D Isotherms at 1400°C – First Stage.

A similar trend was also experienced with Reductants B and A. They surpass Reductant D within 20 minutes and 25 minutes, to consecutively finish as the second and third most reactive, with Reductant D finishing off as the fourth.

During the first stage, Reductant B1 starts off and finished with the least mass loss.

In terms of mass loss Reductant D lost 16.24% compared to 15.73% for B1, despite having an average gradient of 22.83 that was less than B1 (23.81) in the first stage. This is attributed to the low mass loss experienced with Reductant B1 compared to D within the first 20minutes. The latter lost almost double the mass (8.12%) more than that recorded by the former (4.84%) during the period.

5.2.4.2 Second Stage

Figure 5.11 portrayed the mass loss and reactivity reported for all reductants during the last segment of the test, from 40 minutes until the end.

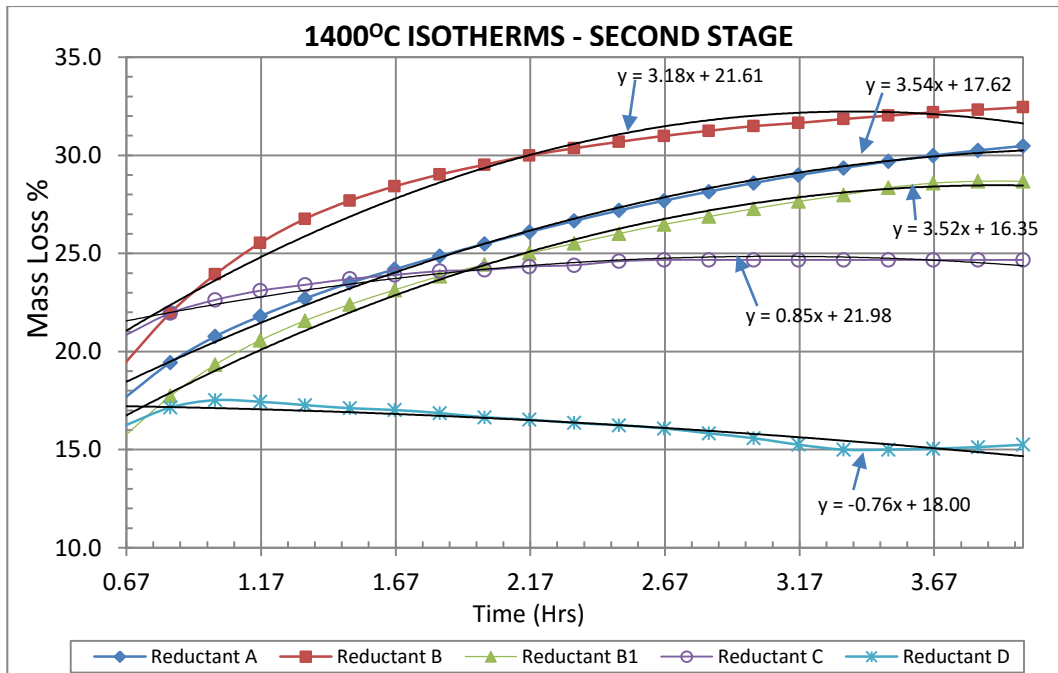


Figure 5.11: Reductant A, B, B1, C and D Isotherms at 1400°C – Second Stage

Reductant C that ended the first stage as the most reactive was now seen to slow down. Reductant B instead progressed within 50 minutes, to become the most reactive. Reductant C continued to slow down and was also surpassed by Reductant A, within 100 minutes that became the second most reactive and by Reductant B within 105 minutes, which finished as the third most reactive. Reductants C and D finished off as fourth and fifth, with both displaying some mass gained towards the end of the second stage. During this stage all reductants had a significantly reduced gradient compared to the first stage.

In terms of mass reduction, Reductant D notably reached saturation within an hour, followed by Reductant C, which had then begun to decrease and also reached saturation within 2 hours. Both finished with an overall mass reduction of 15.25% and 20.66%, respectively. As Reductant C began slowing down before saturation, Reductant B sturdily became the most reactive, followed by Reductants A and B. Reductant B followed by Reductants A, B1, C and D, consecutively had the highest mass loss in the end of 32.45%, 30.48%, 28.68%, 20.66% and 15.21%, at 1400°C. Besides Reductants C and D, the rest of the reductants did not reach saturation point and showed potential to continue losing mass at reduced rates.

5.2.4.3 Differential Time Analysis at 1400°C

Shown in Figure 5.12, is the change in mass loss reported during the 1400°C test. This demonstrated that, Reductant D had the most mass change within the first stage (40 minutes), with the highest change in mass loss of 8.12% in 10 minutes. It was followed by Reductant C, with 7.54, Reductant A with 6.59%, Reductant B with 6.16% and lastly Reductant B1 with 4.84%.

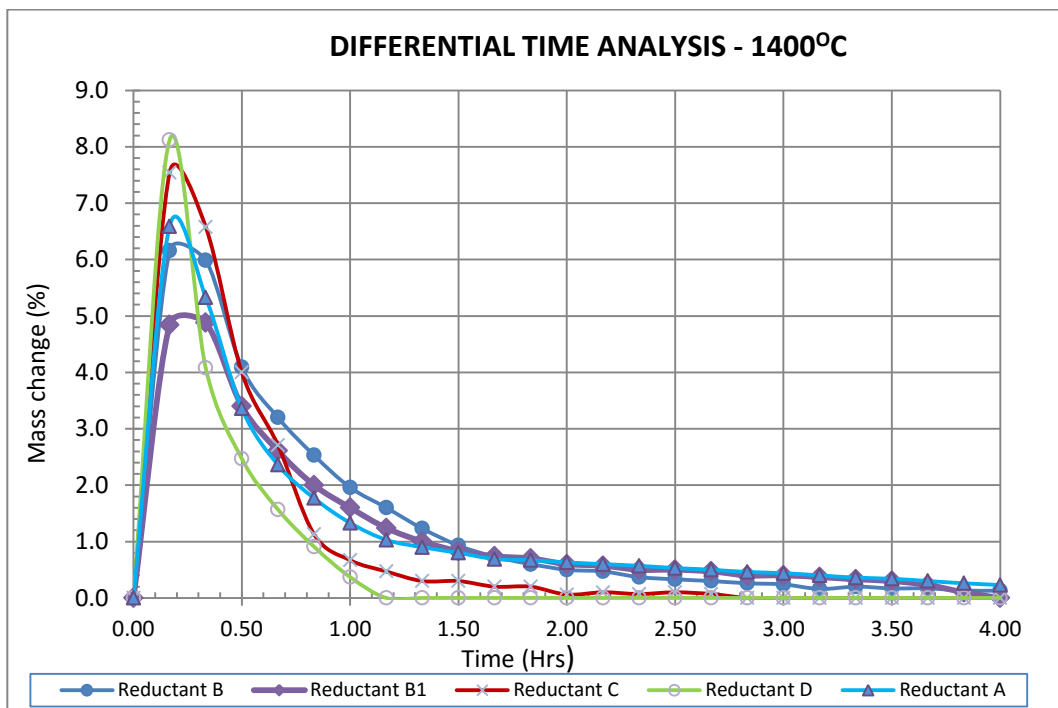


Figure 5.12: Reductant A, B, B1, C and D Change in Mass at 1400°C

This significantly decreased in 40 minutes for the rest of the reductants, with a change in mass loss of less than 3% being experienced. Within 70 minutes, Reductant D began to experience a negative mass loss change (gain in mass) that continuously fluctuated until the end. An almost similar trend was also recorded for Reductant C, which had a massive increase at about 3.83 hours and recorded 2.7% mass gained. All the other reductants gradually reduced in change of mass loss in 60 minutes, until the end.

5.3. Comparison between Speciation and Quantitative XRD Results

Quantitative X-Ray Diffraction (XRD) was conducted on selected samples. This was done to validate the %DOR and %DOM, calculated by the oxygen removal method described in section 5.1. The unconventional Reductant D and the conventional Reductants A, B and C products at 1400°C were subjected to XRD characterisation.

5.3.1 Comparison between Speciation and Quantitative XRD Results for Iron and Chromium

The speciation compositions obtained from ICP-OES were compared to the ones obtained from quantitative XRD for the Fe and Cr species. The comparison of results is presented in Table 5.3 and Table 5.4. The Fe and Cr speciation in the XRD data was manually calculated from the respective mineral phases.

Table 5.3: XRD and speciation compositions of Iron (1400°C).

Sample	Quantitative XRD				Speciation		
	Fe ⁰	Fe ²⁺	Fe ³⁺	Fe Total	Fe ⁰	Fe ²⁺	Fe Total
A	5.60	12.02	-	17.62	11.70	11.17	22.86
B	10.02	5.27	0.09	15.38	9.81	10.64	20.46
C	0.40	6.04	12.30	18.74	7.40	11.36	18.75
D	24.30	16.26	2.17	42.72	14.56	5.88	20.44

'-' Means the analyte was not detected.

As shown in these tables, the Fe and Cr speciation analysis results obtained by selective leaching coupled with ICP-OES and quantitative XRD are significantly different.

Table 5.4: XRD and speciation compositions of Chromium (1400°C)

Sample	Quantitative XRD			Speciation		
	Cr ⁰	Cr ³⁺	Cr Total	Cr ⁰	Cr ³⁺	Cr Total
A	-	3.39	3.39	1.49	26.92	28.41
B	0.5	5.97	6.47	0.80	24.87	25.67
C	-	11.24	11.24	1.22	21.69	22.91
D	3.80	27.09	30.89	8.24	20.63	28.86

'-' Means the analyte was not detected

The quantitative XRD results did not show a specific trend related to recorded isotherms, hence the chemical speciation results were adopted as giving true data for the Fe and Cr species in the reduced materials.

5.4. Comparison of SEM-EDS for Selected 1400°C Products

For the evaluation of phase relations, the reduced materials at 1400°C with unconventional Reductant D and conventional Reductant B were analysed by SEM-EDS. Six phases were identified in both samples (micro-graphs in figures 4.17 and 4.20). As shown in Table 5.5, the phases identified include spinel, chromite, iron-chrome, chrome-iron, olivine and glass. Two modes of iron-chrome occurrence were observed *i.e.* flakes of Fe-Cr that were embedded in the spinel phase and discrete Fe-Cr phase that occurred along the margins of the spinel phase. Chrome-iron phase occurred as regular blebs scattered in the glass phase. Olivine phase was sporadically scattered throughout the glass phase.

Table 5.5: Chemical Analysis of Phases Present (mass %)

Phases	O	Cr	Fe	Al	Si	Mg	Ti	Ca	
1	33.01	48.56	6.92	10.64	-	0.05	0.82	-	spinel
2	0.05	13.44	86.51	-	-	-	-	-	iron-chrome
3	0.07	11.72	88.22	-	-	-	-	-	iron-chrome
4	0.48	39.38	58.45	-	1.69	-	-	-	iron-chrome
5	49.50	6.64	-	16.74	12.07	0.06	3.20	11.78	glass
6	0.66	86.77	12.57	-	-	-	-	-	chrome-iron
7	-	88.71	11.29	-	-	-	-	-	chrome-iron
8		35.74	62.75		1.52	-	-		iron-chrome
9	30.69	35.28	23.94	9.14	-	0.04	0.91	-	chromite
10	0.53	58.31	39.54		1.58	0.03		-	chrome-iron
11	48.97	8.90	0.39	39.90	-	0.18	1.66	-	spinel
12	-	75.29	24.71	-	-	-	-	-	chrome-iron
13	30.95	35.12	23.34	9.68	-	0.04	0.87	-	chromite
14	-	70.95	27.30	-	1.04	-	0.71	-	chrome-iron
15	60.18	2.69	5.29	1.36	30.42	0.07	-	-	silicate
16	46.28	-	-	15.74	25.82	0.04	-	12.11	glass

⁻Means analyte was not detected

The SEM results showed that the dominant phases present in both samples were the Iron-chrome and Chrome-iron phases. This means that these samples were substantially reduced as the dominant phases were metallic.

5.5. Factors Affecting Metallisation and Reduction Degree

Several factors ranging from the test conditions or set-up to material properties exist and are reviewed.

5.5.1 Effect of Temperature on %DOR and %DOM

The general effect of temperature has been illustrated in the previous chapter with isothermal curves obtained for each individual reductant. This should bear resemblance with the effect on both the degrees of reduction and metallisation. The degree of metallisation was seen to increase with temperature, especially for the conventional Reductants A, B and B1 from 1100°C to 1300°C.

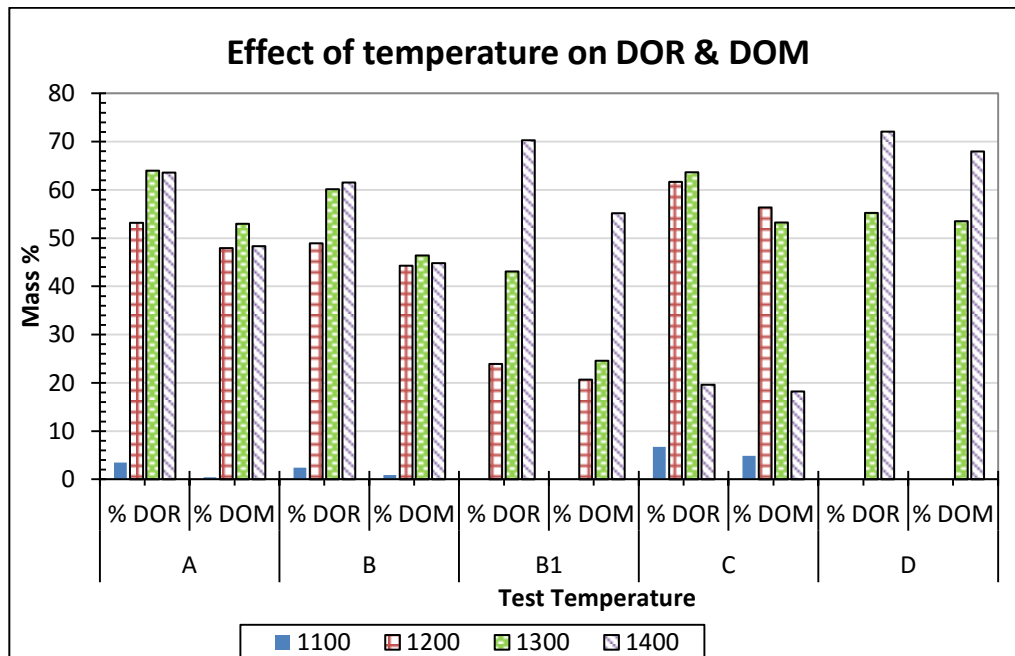


Figure 5.13: Reductant Changes in %DOR and %DOM with Temperature

Figure 5.13 demonstrated the effect of temperature on both the %DOR and %DOM. There was a general increase in %DOR with increasing temperature for the conventional reductants, where relevant measurements were found within detection limits of apparatus used. However, for %DOM, this trend was only valid for the first three temperatures (1100°C – 1300°C) with regards the conventional Reductants A, B and B1. At 1400°C, this trend was still visible but with Reductant A having almost the same %DOR at 1300°C (63.97%) and 1400°C (63.57%) and Reductant C having a significant decrease from 63.67% at 1300°C to 19.62% at 1400°C. Significant increases in %DOR were noted with reductants B1 and D with increasing temperature. The %DOR trend with unconventional reductant was only detectable at 1300°C and 1400°C, which increased from 55.24% to 75.03%, respectively.

There was an anomaly in the %DOM for conventional Reductant C, decreasing at 1300°C and 1400°C from 56.37% at 1200°C to 53.25% and 18.22%, respectively. Unconventional Reductant D was only having detectable results at 1300°C and 1400°C, indicating an increase from 53.49% to 67.96% in metallisation.

5.5.2 Effect of Reductant Rank on % DOR and %DOM

The relationship between reductant rank and the degrees of reduction and metallisation based on random reflective data was summarised in Figure 5.14.

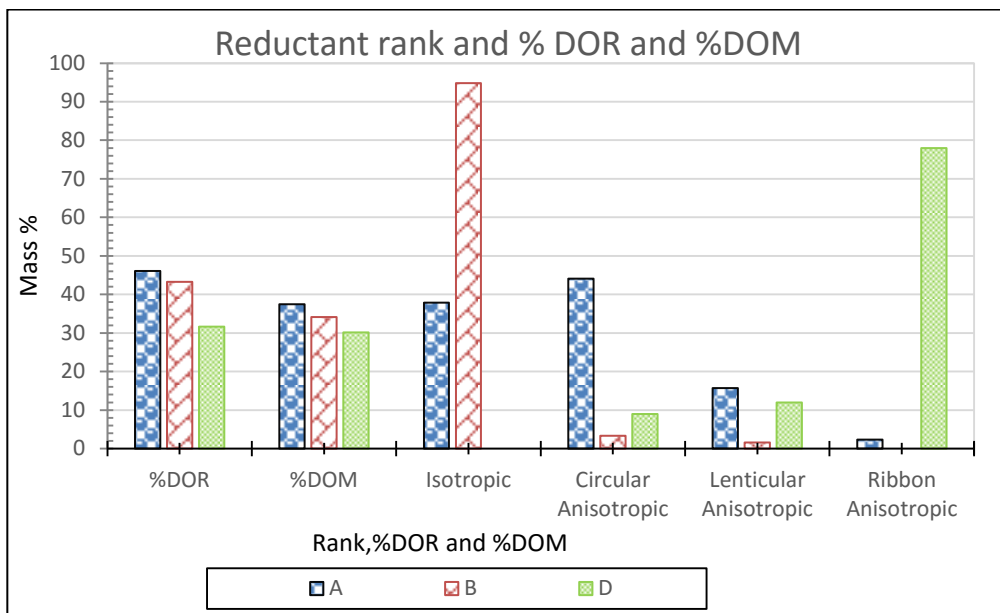


Figure 5.14: Changes in %DOR and %DOM with Reductant Rank.

There was a clear distinction in that the unconventional Reductant D was essentially anisotropic. The major component was ribbon anisotropic (79%) followed by lenticular anisotropic (12%) and the least was circular anisotropic (9%). There were no isotropic components in its structure. In comparison, the selected conventional Reductants A and B had significant isotropic components. Reductants B and A had isotropic components totalling 94.8% and 37.9%, respectively, in the binder phase.

Both conventional Reductants A and B had higher degrees of reduction and less metallisation compared to the unconventional reductant. However, Reductant A had more superior performance and this could mean that being more isotropic may not translate to a high performance but rather a combination of isotropic and anisotropic nature a requirement. Isotropic structure means a more structured and strong structure but the anisotropic structure was generally linked to a highly reactive nature as noted with the unconventional Reductant D.

5.5.3 Effect of Reductant Quality (Fixed Carbon, Ash and volatiles)

Figure 5.15 illustrates the relationship between selected reductant chemical parameters and both calculated degrees of reduction and metallisation.

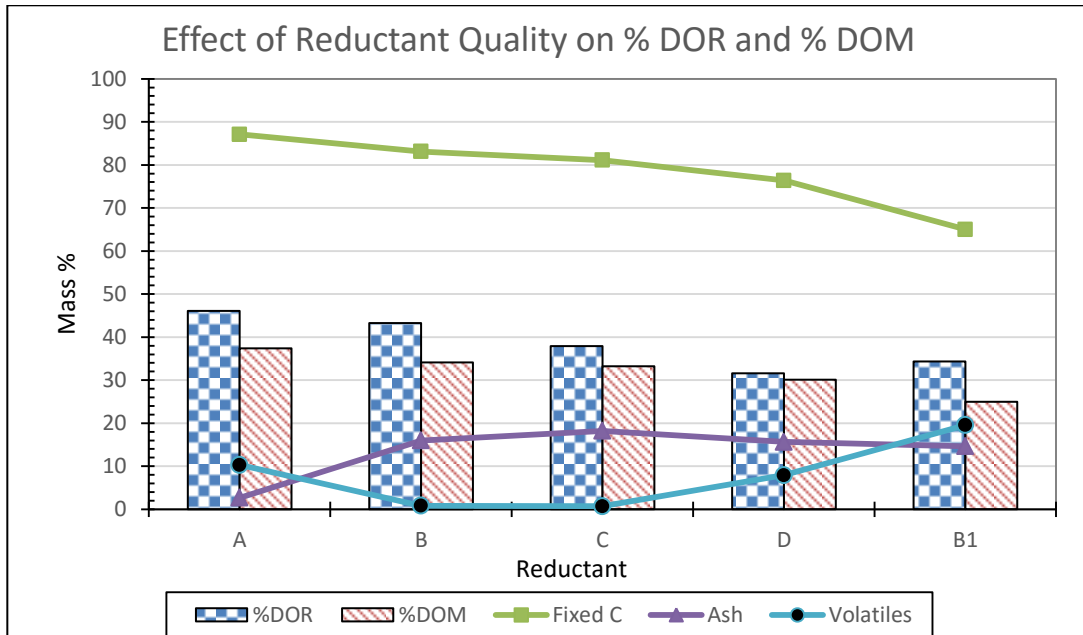


Figure 5.15: Changes in %DOR and %DOM with Reductants Ash, Volatiles and Fixed Carbon Content

5.5.3.1 Effect of Reductant Fixed Carbon Content

There was an almost distinct continuous trend within the convectional reductants of decreasing %DOR and %DOM, with decreasing fixed carbon. This was clearly demonstrated in the graph for Reductants A, B, C and B1. This trend (Table 5.15), however, is somehow inverted by the unconventional reductant with regards degree of reduction. Reductant D (76.1%) has a higher fixed carbon content compared to B (65%), but the latter has a higher degree of reduction (34.32%) than D with 31.6%.

Table 5.6: Reductant Fixed Carbon, %DOR and %DOM (mass %)

Reductant	Fixed Carbon	%DOR	%DOM
A	87.1	46.05	37.41
B	83.1	43.24	34.11
B1	65.0	34.32	24.97
C	81.1	37.90	33.18
D	76.1	31.60	30.11

However, Reductant D had a higher degree of metallisation (30.11%) than Reductant B1 (24.97%) and this conformed to the trend established for the conventional reductants.

A higher fixed carbon content thus indicated increased potential for reducing the metal oxides and hence resulting in increased degrees of both reduction and metallisation. The abnormal behaviour with regards to degree of reduction seen with the unconventional Reductant was possibly a result of the reductant reaching saturation much earlier than all the conventional reductants. This was more pronounced at higher temperatures.

5.5.3.2 Effect of Reductant Ash Content on %DOR and %DOM

A, somewhat opposite trend found with fixed carbon was almost true for the ash content of conventional reductants. Except for Reductant B1, as the fixed carbon decreased, the ash content increased with a corresponding reduction in degrees of reduction and metallisation. Reductants A, B and C had an ash content of 2.7%, 16.0% and 18.2%, compared to a fixed carbon content 87.1%, 83.1% and 81.1%, respectively. However, as noted with the trend in fixed carbon content earlier, Reductant B1 again contained a low ash content of 14% compared to Reductants C and B, despite having the lowest fixed carbon content of 65%. This remained the case even after repeat tests were done for reductant B1.

Although the unconventional reductant having a lower fixed carbon (76.4%) compared to B and C, it almost has the same ash content (15.7%) with B and even slightly less content compared to C. This implies that as the ash content increases and fixed carbon content decreases, expected is a corresponding reduction in the attained degrees of reduction as well as metallisation. The reductants selected did not strictly conform to this expectation.

5.6. Relationship of Reductant Characterization, Reactivity and Product Analysis

The performance of a reductant was directly linked to the degree of “graphitisation”, which directly influenced the performance of the materials as carbon reductants in metallurgical processes. Despite the differences in petrographic composition, all conventional reductants samples were overwhelmingly isotropic with regards to forms of carbon. Thus, a high volatile coal of low rank was mainly used as feed material.

Also of great significance was the reflectance of the reductant sample. The narrow distribution in range of reflectance further gives emphasis to this assumption. In general, the samples (Reductants B and C) displayed relatively high macro-porosity, with cell walls less than 500 microns in width, which was slightly greater than those of Reductant A. The higher porosity values and low index of compactness suggested that the sample had comparatively low strength but high reactivity. In contrast, porosity of Reductant A was considerably lower (~51%) resulting in a significantly higher index of compactness (0.95), pointing to a coke of higher strength but low reactivity.

The TGA reactivity results obtained indicated that unconventional Reductant D was relatively more reactive than the conventional reductants up to a temperature of 1300°C. All Isotherms for the reductants clearly illustrated

that the unconventional Reductant D was the most reactive at low temperatures. This was seen within the first hour of reduction, as supported by the steep curve. The overall mass loss of the unconventional Reductant D was about 90% (up to 1300°C) relative to conventional reductants with Reductant C (73%), Reductant A (44%), Reductant B (39%) and Reductant B1 (37%), respectively.

A review of the isotherms revealed that there was a common relationship found between reductant structure and the mass loss experienced. Reductants that were more isotropic were more consistent in mass loss through-out the holding period, with a potential to continue reacting further. In comparison, a more anisotropic reductant was accompanied by initial bursts of increased reactivity, followed by a well pronounced slackening. Also when past the first reactive phase, the isotherm was not linear and smooth but rather rugged, possibly as a results of remnant reactive pockets/areas within the reductant. This was more evident with unconventional Reductant D, at temperatures between 1100°C to 1300°C.

Further comparison of metallisation (Speciation) and nature or rank of the reductant demonstrated that the anisotropic unconventional reductant and most reactive, resulted-in the highest metallisation levels. This result was surprising given that the unconventional reductant had low fixed carbon content compared to the rest. However, the high volatiles content is believed to have greatly contributed to Reductant D's performance.

In summary the two major test results (TGA and Speciation/Metallisation, indicated that the unconventional reductant was;

- a. More reactive (TGA), and

- b. Provided greater metallisation than other conventional reductants, but performed superior in lower temperatures and over shorter spans of time.

Whilst excellent in terms of reduction properties, the limited time and temperature in which the unconventional reductant operated in may have negative implications for industrial processes requiring longer reaction periods at higher temperature. However, conventional reductants provided physical strength, sustained carbon content for longer times and higher temperatures.

6. CONCLUSIONS

The main objective of this research project was to study and compare the reactivity of commonly used reductants (conventional) with that of available new and sustainable carbon materials (unconventional), for use in the solid state reduction of natural chromite (UG2). This chapter summarises the main findings from the testwork done. According to set objectives, the following was established during the study:

6.1. Characterization of Selected Reductants

Five reductants were chosen and tested in terms of their structures, composition, rates of reaction and suitability with respect to solid state chromite reduction.

The characterization results performed included the following:

- Conventional reductants B and B1 displayed characteristics closer to Reductant A (the Standard Ferroalloys reductant) compared to Reductants C and D with regards to ;
 1. Macro-porosity.
 2. Petrographic composition.
 3. Forms of carbon.
 4. And reactivity to chromite reduction that had a similar profile but with less intensity (mass loss) than the standard reductant as shown by the DTI graphs and the average mass losses recorded -Reductant A (22.9%), Reductant B (22.6%) and Reductant B1 (20.18%)
- Conventional reductants were shown to possess spherulitic and pyrolytic carbon forms that served to increase the coke strength.

However, such materials also resulted in considerably reduced and controlled reactivity rate.

- Reductant D (the unconventional reductant) proved to be highly friable, porous and consisted of a mixture of both petrographically defined lower ranking and mature carbon, subsequently with some areas reacting faster than others and undergoing complex phase changes.
- The highly friable nature of Reductant D resulted in complications during sample preparation. This was especially difficult when preparing for petrographic analyses, thus greater reliance was put on photomicrograph analysis as well as the results of physical and chemical composition tests.
- Conventional reductants were found to be more isotropic in nature whereas the unconventional reductant was anisotropic according to petrographic ranking. The difference in such molecular structure correlated with the reactivity of the reductants, with the anisotropic more reactive in the first stage and showed to be exhausted within the 4 hour period than the isotropic form, which had a consistent but gradually increasing reactivity and continued reacting past the holding period.

6.2. Reactivity Tests

Reactivity tests in terms of carbon dioxide generated during chromite reduction quantified by the mass loss in a TGA furnace provided the following outcomes:

- Unconventional Reductant D was overall best performing with the highest average mass loss (30.5%) followed by Reductants C (28.2%), A (22.9%), B (22.6%) and B1 (20.18%), consecutively in reducing order.
- Despite low fixed carbon content, reactivity of unconventional Reductant D was higher than all the conventional reductants at low temperature (1100°C -1300°C).
- Notably all conventional reductants performed adequately at the highest test temperatures compared to the unconventional reductant.
- Conventional reductants displayed a well-controlled and consistently increasing trend in reactivity throughout the tests, with none that reached saturation (complete consumption) at the end of the 4 hour holding period.
- There was clear evidence of a generally positive response to changes in temperature for most reductants, with only a few occasions when an increase in temperature was not accompanied with an increase in reactivity (*i.e. Reductants D and C both lost less mass at 1200°C compared to mass lost at 1100°C, similarly Reductant D lost less mass at 1400°C compared to that incurred at 1300°C*).
- Greatest mass loss was experienced within the first stage for all the reductants.
- All the reactions taking place displayed a pronounced effect of chemical control within the first stage compared to diffusion control, seen in the second stage.

6.3.Relevancy and Sustainability Of Reductants Currently In Use For The Ferrochrome Process In South Africa

With regards to relevancy and sustainability of reductants used in the South African Ferrochrome industry, it was established from the test-work that;

- Significant solid state reduction or pre-reduction levels of ferrochrome were attained as shown by the following results:
 - With regard to iron oxide(s) reduction, the highest degree of reduction produced by the conventional reductants was found to be in the range of 63.97% – 70.28% whereas the unconventional Reductant D produced 72.03% reduction of iron at 1400°C. Reductant A produced the highest reduction of 63.97% at 1300°C. Reductant B the highest reduction of 61.51% at 1400°C, B1 the highest reduction of 70.28% at 1400°C, and C the highest reduction of 63.67% at 1300°C
 - With regard to metallisation, correspondingly the conventional reductants produced the following highest degrees of metallisation: Reductant A produced 52.97% degree of metallisation at 1300°C, Reductant B produced 46.42% at 1300°C, Reductant B1 produced 55.17% at 1400°C and Reductant C produced 56.37% at 1200°C. The unconventional reductant D was superior with the highest degree of metallisation, namely, 67.96% at 1400°C.
- Further support of successful pre-reduction was seen from the SEM-EDS results. These showed that the dominant phases present in the TGA products for both conventional and unconventional reductants were the iron-chrome and chrome-iron phases. This was also supported by the results generated from speciation tests.

- The potential reason for the higher metallisation and reactivity results when testing the unconventional Reductant D was considered to be the highly macro-porous nature of this material. This would have resulted in better diffusion of reaction gases as well as improved contact with the chromite ore to give the reported higher levels of reactivity.

- Notwithstanding conventional reductants being readily available, these carry a high cost element due to the use of imported coal as part of the cokemaking components. In this manner, the unconventional Reductant D would be a more sustainable (locally produced) and less expensive alternative. However, the friable nature indicates that this reductant should be produced on site in order to mitigate transport decrepitation.

- The key properties in characterizing reductants for the successful pre-reduction of chromite fines were confirmed to be the following:
 - ✓ Chemical Composition: viz Fixed Carbon, Moisture, Volatiles, Ash, Sulphur and Phosphorus
 - ✓ Macro-porosity related to Cell Wall Width
 - ✓ Rank (level of maturity of coal) and Petrographic Composition
 - ✓ Friability

- The critical process and quality control parameters to measure success in the metallisation process in the ferrochrome industry were identified to be the following:
 - ✓ **Degree of reduction** of chromium and iron oxides in chromite ore or production rate measured by correlating the quantity of oxides remaining with the initial amount(s).

- ✓ ***Degree of metallisation*** or metal recovery with regards the target metal composition (in this case chrome and iron for the Ferrochrome industry).
- ✓ ***Rate of reductant consumption***, or amount of reductant utilised, per tonne of chromium recovered as well as cost per tonne of chromium recovered relative to reductant used.

The SEM-EDS results showed that the dominant phases present when using both conventional and unconventional reductants were the iron-chrome and chrome-iron phases. The presence of these metallic phases not only confirms that substantial iron and chrome reduction were obtained in all cases but also that the unconventional Reductant D provided the highest reduction and at the fastest rate relative to the conventional reductants within the 4 hour holding period. The presence of iron-chrome and chrome-iron phases was further supported by the chemical speciation results.

The calculated percentage (%) DOR and percentage (%) DOM were in-line with what results reported by previous investigators with regards to chromite reduction. In terms of process, it was confirmed (as is well established) that iron is easily reduced and is thus the first to metallise, after which chromite reduction begins. In this study, the quantities of metallic iron obtained were shown to be correspondingly greater than chromium, also that the reduction of both iron and chromium increases significantly with temperature.

The benefits of unconventional reductants were outlined and it was proposed that such reductants may well prove more sustainable and cost effective for the ferrochrome industry in future. The study demonstrated a procedure on how ranking of the various reductants can be undertaken.

7. RECOMMENDATIONS

This includes but is not limited to;

7.1. Further Investigations in Unconventional Reductants

This study confirmed that in South Africa conventional reductants are available and widely utilised. However, most of these conventional reductants although readily available, have as part of their feed material a component of imported quality coal and this carries a considerable cost implication. This research project has shown that there is great potential in using an unconventional reductant. This material also has the benefit of a reduced carbon footprint. The unconventional reductant currently finds application in the local Silicon smelting industry, with the original source (eucalyptus tree) also widely used in the pulp industry. Consequently, the scaling-up of current infrastructure and introduction of the reductant into the ferrochrome or ferroalloys industry at pilot plant level should be practically possible and is justified.

Recommendations are thus based on opportunities that exist for:

- experimenting with a variety of unconventional reductants in addition to the known forms,
- developing related process innovations,
- learning from lessons learnt and, finally,
- Improving the sustainability and competitiveness of the South African Ferrochrome industry.

7.2. Cost Implications

In South Africa, imminent introduction of a carbon tax in the foreseeable future is a reality. This will inevitably cause a rise in the cost of ferrochrome,

given the coal-based reductants currently being used. This will impact negatively on ferrochrome production unit costs. Depending on the scale of substitution implemented with unconventional (or bioforms of) reductants, use of such reductant material is likely to reduce carbon tax penalties (given the neutral connotations when using growing vegetation). However, care should be taken to proceed sustainably to ensure that there are no negative environmental consequences (e.g. deforestation and related issues when obtaining the basic plant materials for the bioforms of reductants).

7.3. Process Innovation

Apart from developments related to the capacity and use of readily available unconventional reductants in the local timber industry, further investigations into related process technologies are required. This in turn, will serve as a driving force to encourage increased sustainability and competitiveness in the ferrochrome industry as the country possesses the largest chromite ore resources in the world. A combination of the established facts that, *e.g. competent reductant resources locally are continuously depleting while the related costs of importing quality reductant feed (coal) keep increasing*, amplifies the paramount need for further experimenting, both in available carbonaceous materials as well as investigating areas in the handling of materials, process operations and design aspects of the ferrochrome plants in that industry. Some suggestions are outlined below:

- a) Testing the smelting of ore fines without prior agglomeration, *i.e.* using pre-reduction processes with bioform reductants.

- b) Blending of more mechanically competent expensive reductants (conventional) with highly reactive, cheaper, friable and porous unconventional reductants .

- c) Production of a lower-cost minimised-CO₂-emitting process by substitution of *carbon-intensive* conventional reductants by *carbon-neutral* unconventional reductants. Environmental laws are progressively becoming more stringent.
- d) Testing of poorer coking coal resources (rather than best quality coking coals) with unconventional bioform reductants in order to investigate potential beneficial properties of both in ferrochrome processing.
- e) Testing other unconventional reductants coal quality such as (i) those currently being used locally in the pulp industry (e.g. Eucalyptus) and (ii) those woody/plant forms not yet commercially produced but which are under consideration for development in South Africa (e.g. Bamboo plantations on mine rehabilitated lands).

Additional fundamental studies are also proposed:

1. Investigations into the reaction mechanisms and feasibility of agglomerating/pelletizing of chromite ore with unconventional reductants.
2. Determination of the reasons for the anomalous behaviour reported in this research study, *i.e.* (1400 °C test results have less % DOR and/or % DOM compared to the 1300 °C) through SEM-EDS phase relation analysis.
3. Establishing the typical CSR and CRI of Charcoal to confirm typical quantities that can be used in conjunction with competent

conventional reductants in submerged arc furnaces without compromising furnace charge or burden porosity.

4. Confirming the saturation point in most of the reactions that demonstrated potential to continue reacting beyond the current 4 hour holding period.
5. Optimising the reactivity efficiency by blending the conventional and unconventional reductants to boost metal recoveries and reduce reaction time.
6. Characterizing further the unconventional reductant in terms of all typical ferrochrome smelting requirements in submerged furnaces *e.g.*
 - As with the porosity investigation, more tests are required to determine the exact nature of the carbon phase changes.
 - Full Micum drum strength (M40, M20, M10) plus CSR and CRI for the carbon forms (bioform or charcoal) to be done.
 - Sulphur and Phosphorus deportation to ferrochrome.
 - Electrical resistivity of the reductant and its relevance.
 - Impact of the caloric value of a reductant.
7. Studying the behaviour of this reductant in *liquid state processing of chromite* to simulate the chromite smelting operations. This would represent the final step in the ferroalloy process and the most important one.

8. REFERENCES

1. American Society for Testing and Materials (1993), ASTM D 5341 93, Standard Test Method for Measuring Coke Reactivity Index (CRI) and Coke Strength after Reaction (CSR)
2. Babich, A., Senk, D and Gudenau, H.W. (2006), Coke quality for a modern blast furnace, *Proceedings of 4th International Congress on the Science and Technology of Ironmaking*, Osaka, Japan, pp.351–354
3. Babich, A., Senk, D., Gudenau, H.W. (2009), Effect of coke reactivity and nut coke on the blast furnace operation', *Ironmaking and Steelmaking Journal*, vol. 36, no3, pp.222–229
4. Barcza, N.A., Jochens, P.R and Howat, D. D. (1971), The Mechanism and Kinetics of Reduction of Transvaal Chromite Ores, *Electric Furnace Proceedings*, Vol.29, pp.88-93
5. Barnes, A. R., Finn, C.W.P., Algie, S.H. (1983), The pre-reduction and smelting of Chromite concentrate of low chromium-to-iron ratio, *Journal Of The South African Institute Of Mining And Metallurgy*. pp.49-54
6. Barnes, A. R and Eric R.H. (1995), The relative reducibilities of Chromite ores and relative reactivity of carbonaceous reductants, *Proceedings of the 7th International Ferroalloys Congress INFACON XII: Trondheim, Norway*, pp.231-238
7. Barnes, A., Muinonen, M and Lavigne, M. J. (2015), Reducing energy consumption by alternative processing routes to produce ferrochromium alloys from chromite ore, *The Conference Of Metallurgists hosting*

AMCAA, Published by the Canadian Institute of Mining, Metallurgy and Petroleum, pp.1-22. INTERNET.<http://www.metsoc.org> Cited 15 October 2015

8. Basson, J., Curr, T.R and Gericke, W. A. (2007), South Africa's Ferroalloys Industry – Present Status and Future Outlook, *Proceedings of the 11th International Ferroalloys Congress, INFACON XI*, India, pp.3-24
9. Bonte, L., Sergeant, R., Daelman, A., Dauwels, G and Huysse, K. (2005), Influence of the coke and burden quality on the productivity of the blast furnace, *Stahl und Eisen*, vol. 125, no.6, pp.5–10
10. Bronnikov, V.K and Eidelman, E.Y. (1973), Effect of the moisture content of the charge on physical and mechanical properties of coke, *Coke and Chemistry*, no.10, pp. 15-18
11. Brügemann, L and Gerndt, E.K.R. (2004). Detectors for X-ray diffraction and scattering: a user's overview, *Nuclear Instruments and Methods in Physics Research A* 531, pp 292–301
12. Buchanan, D.L. (1979), Platinum-group metal production from the Bushveld Complex and its relationship to world markets, *Johannesburg, Bureau for Mineral Studies*, Report no.4, pp.35
13. Chakraborty, D., Ranganathan, S and Sinha, S.N. (2007), Reduction of Chromite Ore at different flow rates of inert gas, *Proceedings of the 11th International Ferroalloys Congress, INFACON XI: India*, pp.53-158

14. Cramer, L.A., Basson, J and Nelson, L.R. (2007), The Impact of Platinum Production from UG2 Ore on Ferrochrome Production in South Africa, *Proceedings of the 6th International Ferroalloys Congress, INFACON XI: Cape Town*, Vol.1, pp.47-59
15. Curr, T. R. (1996), A Review of Ferrochromium Smelting Technologies. *Presentation at ICDA (International Chrome Development Association)*, Spring Meeting, Cape Town, South Africa, pp.1-8
16. Diessel, C. and Pickel, W. (2012), Carbonisation and coke petrology. 5th International Committee for Coal and Organic Petrology Course in Organic Petrology, *International Committee for Coal and Organic Petrology (ICCP)*, Brisbane. Vol.2, pp.53-129
17. Diez, M.A., Alvarez, R and Barriocanal, T. (2002), Coal for metallurgical coke production : predictions of coke quality and future requirements for Cokemaking, *International Journal of Coal Geology*, vol.50, pp.389-412
18. EPA. (1998), Bituminous and Subbituminous Coal Combustion – External Combustion Sources. AP Vol.42, pp.1.1-53, INTERNET. <http://www.epa.gov>. Cited 10 April 2015
19. Farjadi, M.H and Azari, J (2004), Effect Of Chrome Ore Quality On Ferrochrome Production Efficiency, *Proceedings of the 10th International Ferroalloys Congress, INFACON X: 'Transformation through Technology'*, Cape Town, South Africa, pp.103-107

20. Ferrochrome Technologies, INTERNET. <http://www.outokumpu.com>.
Cited 01 March 03 2015
21. Gibson, J. (1979), Carbonization and coking. *In: Coal and modern coal processing: An introduction*. Eds. Pitt & Milliard, Academic Press, London, Chapt.3, pp.51-67
22. Given, P.H., Weldon, D and Zoeller, J.H. (1986), Calculation of calorific values of coals from ultimate analysis: theoretical basis and geochemical implications. *Fuel*, vol.65, pp.849-854
23. Gudenau, H. W., Mulanza, J. P and Sharma, R. (1990), Carburisation of cast iron by industrial cokes. *Steel Research*, Vol.61(6), pp. 97–104.
24. Holappa, L and Xiao, Y. (2004), Slags in ferroalloys production – review of present knowledge, *The South African Institute of Mining and Metallurgy*, Proceedings of the V11th International Conference on Molten Slags Fluxes and Salts, pp.641-649
25. ICCP. (2012), Course in Organic Petrology, *International Committee for Coal and Organic Petrology*, Brisbane, Vol. 2, pp.53-129
26. International Organization for Standardization (1992), ISO 5061 – 92. Standard for Coke Petrographic Analysis
27. International Organization for Standardization (1994), ISO 7404 – 5, 1994 , Standard for Rank Determination
28. International Organization for Standardization (2001), ISO 13909-5:2001, Hard Coal and Coke, Mechanical Sampling

29. International Organization for Standardization (2005), ISO 11769-2005, Standard for Reflectance Measurement
30. Jones, H. V and Kruse, C. W. (1982), Proposed techniques for evaluating chars made from high-sulphur Illinois coals for manufacture of formed coke, *State Geological Survey Division*, Illinois Department of Energy and Natural Resources
31. Jordan, P and Falcon. R.M.S. (2010), Coke Quality Prediction Models Evaluated by Coal Characterization Techniques, pp.1-11
32. Kumar, PP, Barman, S, Ranjan, M, Ghosh, S, Raju, VVS. (2008), Maximisation of non-coking coals in coke production from non-recovery coke ovens. *Ironmaking and Steelmaking*, vol.35, no.1, pp.33-37
33. Kwiecińska, B. and Petersen H.I (2004), Graphite, semi-graphite, natural coke, and natural char Classification—ICCP system. *International Journal of Coal Geology*, vol.57, pp.99–116
34. Li, W, Zhu, Y, Chen, S, Zhou, Y. (2013), Research on the structural characteristics of vitrinite in different coal ranks. *Fuel*, vol.107, pp.647-652
35. Lintumaa, T., Krogerus, H and Jokinen, P. (2007), Factors Affecting the Reducibility of Sintered Chromite Pellets and Chromite Lumpy Ore. *Proceedings of the 11th International Ferroalloys Congress*, INFACON XI: India, pp.

36. Lu, L., Devasahayam, S., and Sahajwalla, V. (2013), Evaluation of coal for metallurgical applications in *The Coal Handbook: Towards Cleaner Production. Woodhead Publishing Limited*, vol.2: Coal Utilisation, pp. 352-386
37. Majumder, AK, Jain, R., Banerjee, P., Bernwall, A. (2008), Development of a new proximate analysis based correlation to predict calorific value of coal. *Fuel*, vol.87, pp.3077-3081
38. Menéndez, J.A., Álvarez, R., Pis, J. J. (1999), Determination of metallurgical coke reactivity at INCAR : NSC and ECE-INCAR reactivity tests. *Ironmaking and Steelmaking*, vol.26, No.2, pp.117–121
39. Mitchell, G. D. (1999a), Selecting coals for quality coke. Part V: introduction to the coal to coke transformation, *Iron and Steel Maker*, pp. 49–50
40. Mitchell, G.D. (2014), Coal utilization in the steel industry. *American Iron and Steel Institute*, INTERNET. <http://www.steel.org> Cited 25 November 2014
41. Munson, E.J. (2001), Analytical Techniques in Solid-state Characterization, *Theories and Techniques in The characterization of Drug Substances and Excipients*, Chap 3, pp.
42. Myrvågnes, V. and Lindstad, T. (2007), The Importance of Coal – And Coke Properties in the Production of High Silicon alloys, *Proceedings of the 11th International Ferroalloys Congress*, INFACON XI: India, pp.402-413

43. Naiker, O., Riley, T., V. and Lindstad, T. (2006), Xstrata Alloys in Profile – Southern African Pyrometallurgy, *SAIMM*, Johannesburg, pp.297-306
44. Neuschutz, D. (1992), Kinetic Aspects of Chromite Ore Reduction with Coal at 1200°C to 1550°C, *Proceedings of the 6th International Ferroalloys Congress*, INFACON VI: Cape Town, Vol.1, pp.65-70.
45. Nightingale, R.J., Chew, S.J., Austin, P.R., Mathieson, J.G. (2002), Assessment of blast furnace Deadman condition, *Proc. Int. Blast Furnace Lower Zone Symposium*, Wollongong, Australia.
46. Ng, K. W., MacPhee, J.A., Giroux, L and Todoschuk, Ted (2011), Reactivity of bio-coke with CO₂, *Fuel Processing Technology*, vol.92, pp. 801-804
47. Nurmukhanbhetov, Zh., Privalov O., Prokopiyeu L. (2013), Reducibility and Electric Resistance of Carbonaceous Material within Ferroalloys Smelting Processes, *The Thirteenth International Ferroalloys Congress – ‘Efficient technologies in ferroalloy industry’*, Almaty, Kazakhstan, pp.
48. Oberholzer, J. and Daly, K. (2014), SA Chrome & Ferrochrome Tug-of-war with a giant, *Macquarie First South Securities (Pty) Ltd*
49. Peters, M., Schmöle, P., Janhsen, U., Wolny, H.J. (2011), Investigation of blast furnace coke using optical particle analysis, *6th European Coke and Ironmaking Congress*, Düsseldorf, Germany, pp.14
50. Pistorius P.C (2002), Reductant selection in Ferro-alloy production: The case for the importance of dissolution in the metal, *Journal of South African Institute of Mining and Metallurgy*, pp.33-36

51. Ruiters, (Dr) A. (2012), The South African Ferrochrome Industry – Has it lost its shine? *International Chromium Development Association*, The Rukki Group. INTERNET. <http://www.icdacr.com>. Cited 03 March 2015
52. Sahajwalla, V., Dubikova, M. and Khanna, R. (2004), Reductant characterization and selection: Implications for ferroalloys industry, *INFACON X: 'Transformation through Technology'*, Cape Town, South Africa, pp.351-362
53. Sanders, J., Goldsworthy, P., Woolard, J., Juniper, L. and Dale, L. (2010), The Handy Coal Book, *Ultra Systems Technology Pvt. Ltd*, Australia
54. Slatter, D. de L. (1980), The Composition of Zimbabwean chromium ores and the derivation of chemical and physicochemical ratings for smelting the ores to high-carbon ferrochromium. *Zimbabwe Institute of Mining Research*, University of Rhodesia, Salisbury, Report no.173, pp. 79
55. Soykan, O., Eric, R.H and King, R.P. (1991), The Reduction Mechanism of a Natural Chromite at 1416°C, *Metallurgical Transactions B*, Vol.22B, pp.53-62
56. Speight, J.G. (2013), Handbook of coal analysis, *Published by John Wiley & Sons, Inc.*, Hoboken, New Jersey
57. Stankevich, A.S, Kruglov, V.N and Vorsina, D.V. (2001), Effect of petrographic inhomogeneity and degree of oxidation of coals on coke strength. *Coke and Chemistry*, USSR, no.4, pp. 1-16

58. Steyn, J. G. D and Smith, W. H. (1977), Coal petrography in the evaluation of S. A. Coals, *Coal, Gold and Base Minerals of Southern Africa*, Vol.25, no.9, pg.107-11
59. Strakhov, V.M. (2009), Alternative Carbon Reducing agents for Ferroalloy Production, *Published in Coke and Chemistry*, Kuznetsk Center, Eastern Coal- Chemistry Institute, Russia. Vol.52, No.1, pp.19-22
60. Sundar Murti, N.S and Seshadri, V. (1981), Kinetics of Reduction of Synthetic Chromite with Carbon. *Transactions ISIJ*, Vol.22, pp.925-933
61. Typical DC- Arc Furnace, INTERNET. <http://www.bateman-dc.com/>. Cited 03 March 2015
62. UNEP (2006), Coal- Fuels & Combustion Energy Efficiency Guide for Industry in Asia. INTERNET. <http://www.energyefficiencyasia.org>. Cited 08 April 2015
63. Valia, HS. (2010), Coke Production, Coal Selection, and Coal Quality Monitoring, *Keystone Coal Industry Manual*, pp.176-181
64. Weber. P and Eric, R.H. (2006), The reduction of chromite in the presence of silica flux, *Minerals Engineering*, vol.19, pp. 318–324
65. Wilkinson, HC. (1984), Correspondence between the composition and plastic properties of British coals and the structural properties and reactivity of the corresponding cokes, *Fuel*, vol.63, pp.101-108

- 66.Xiao, Y., Yang, Y., Holappa, L and Boom, R. (2007), Microstructure Changes of Chromite Reduced with CO Gas, *Proceedings of INFACON XI: 'Innovation in Ferro Alloy industry'*, India, pp.
- 67.Xiao, Z and Laplante, A.R. (2004), Characterizing and recovering the platinum group minerals – a review, *Minerals Engineering*, vol.17,pp. 961–979

9. APPENDICES

9.1. Appendix A: Chrome Ore Samples

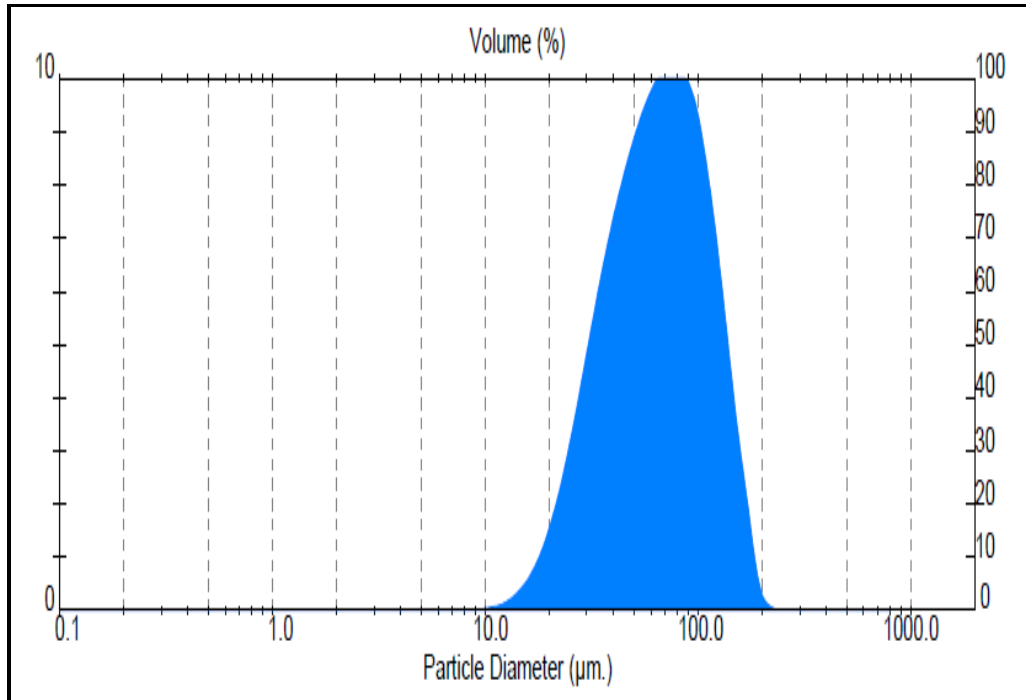


Figure 9.1 : Chromite Ore Concentrate Particle Size Distribution (Source: Mintek 2015)

9.2. Appendix B: Reductant Samples



Figure 9.2 : Reductant Samples – As Received

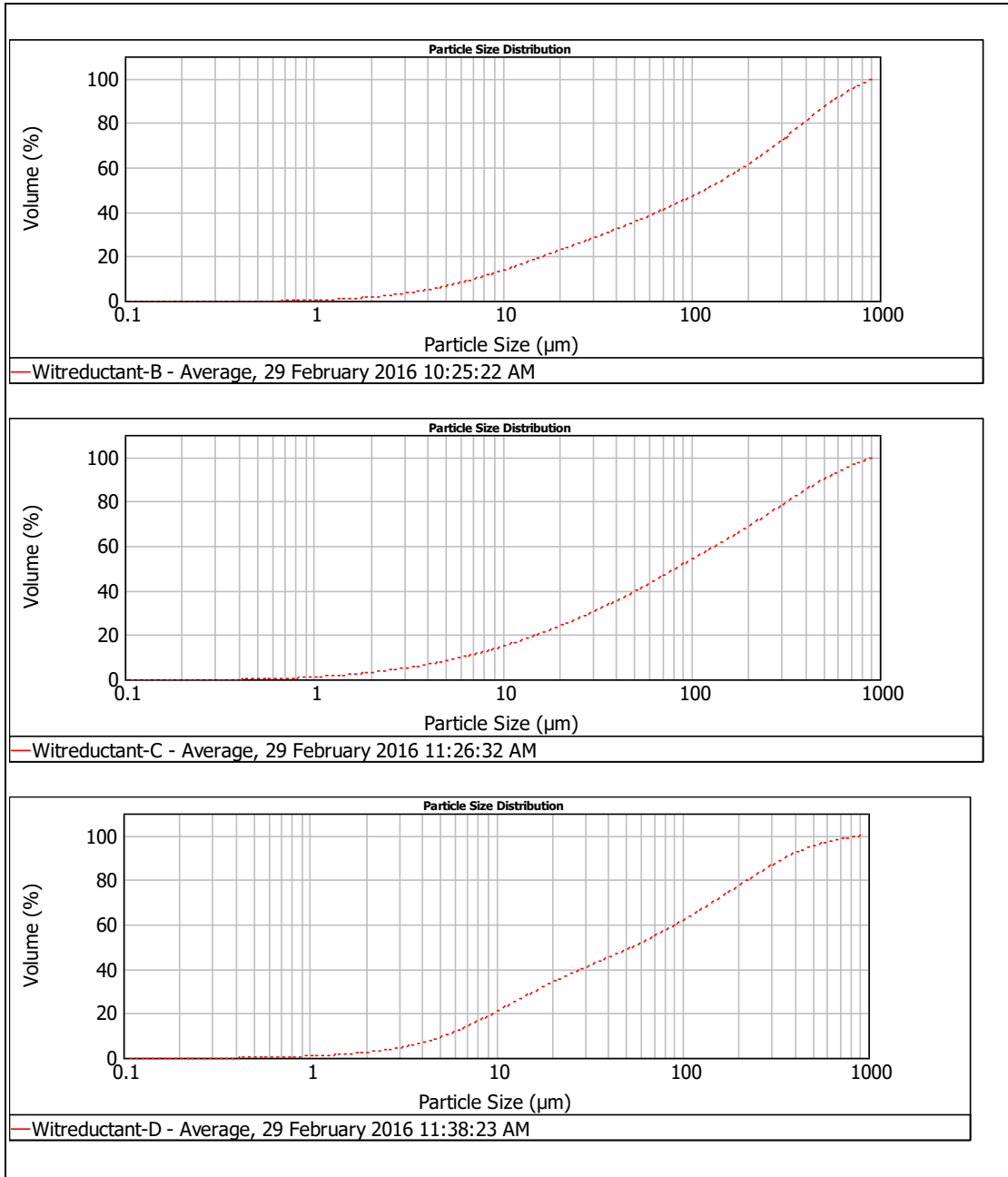


Figure 9.3 : Reductants Particle Size distribution, (Mintek 2016)

9.3. Appendix C: TGA Furnace Feed Material Charge Calculation

Table 9.1 : Typical Reaction Mix of Reductant and Chromite Ore

Reductant Type	Reaction Mix	Fixed Carbon (%)	Reductant Mass (g)	Chromite Ore Mass (g)
Reductant B	I	83.0	120.91	500
Reductant A	II	87.1	115.22	500
Reductant C	III	76.4	131.36	500
Reductant D	IV	65.0	154.39	500
Reductant B1	V	73.0	137.47	500

Nb. Calculations based on ore and reductant oven-dried to 0 % moisture.

Typical Feed calculation:

Chrome Reduction based on Reductant A

UG2 Chromite Cr₂O₃ =41.94% and FeO = 26.42%

Ratio (1) 2Cr:Cr₂O₃ = 0.6842

Molecular mass Cr = 52, Oxygen =16, Carbon =12.



$$2[(52*2) + 3(16)] + 3(12) = 4(52) + 3[12 + (16*2)]$$

$$2(104 + 48) + 36 = 208 + 3(44)$$

$$2(152) + 36 = 208 + 142$$

$$304 + 36 = 340$$

Iron Reduction

Based on 2Moles of FeO reacts with a Mole of Carbon to give 2moles of Iron metal (equation 2)



Ratio (2) Fe: FeO = 0.7778

$$2(56 + 16) + 12 = 2(56) + 12 + (16+16)$$

$$2(72) + 12 = 112 + 12 + 32$$

$$114 + 12 = 156$$

Reductant Requirements for 500grams of UG2 Chromite Concentrate

TGA Feed for Reductant A (Fixed Carbon Content = 87.1%, Volatiles = 2.29%, Moisture =0%)

a.) Based on 2 Moles of Cr_2O_3 reacts with 3 Moles of Carbon to give 4moles of Chromium

Metal (Equation 1);

2moles of 100% Cr_2O_3 react with 3 Moles 100% Carbon

1 mole 100% Cr_2O_3 react with $3/2$ moles of Carbon (100% Fixed Carbon)

1gram 100% Cr_2O_3 react with $3/2 * (100/87.1)$ grams Carbon (87.1% Fixed carbon)

Requirements for 41.94% Cr_2O_3 at 40% excess Carbon:

1 gram mole of 42% Cr_2O_3 react with $0.4194 * [3/2 * (100/87.1)]$ grams Carbon

At 40% Excess Carbon = $1.40 * 0.4194 * [3/2 * (100/87.1)]$ grams Carbon

Requirements for 500grams of 42% Cr_2O_3 = $500(1.40 * 0.4194 * [3/2 * (100/87.1)])$ grams Carbon

b.) Based on 2Moles of FeO reacts with a Mole of Carbon to give 2moles of Iron metal

(Equation 2)

2moles of 100% FeO react with 1 Mole 100% Carbon

1 mole 100% FeO react with $1/2$ mole of Carbon (100% Fixed Carbon)

c.) Total Reductant Requirements

$c = a + b$

Table 9.2: Typical Reaction Outputs Calculated

Outputs					
Stream	Species	Mass %	Mass (kg)	Kmoles	M (kgkmol-1)
Charge Chrome	Fe	36.00	36.00	0.64	55.85
	Cr	56.00	56.00	1.08	52.00
	Si	2.00	2.00	0.07	28.09
	C	6.00	6.00	0.50	12.00
Total		100.00	100.00		
Off-gas	CO		38.57	1.38	28.00
Total			268.57		

9.4. Appendix D: Reductant Characterization Results

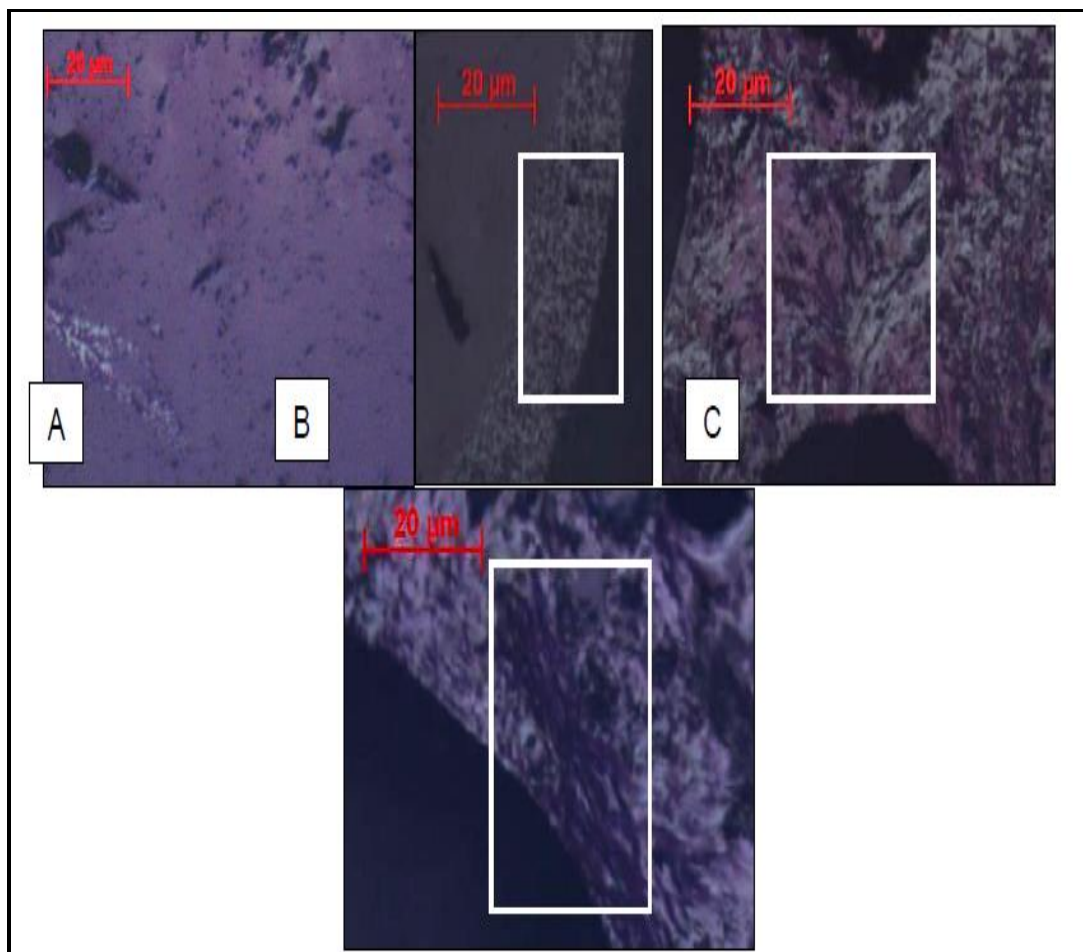


Figure 9.4: Photomicrographs of Conventional Reductants (A) coarse circular. (B), coarse lenticular and (C) medium ribbon anisotropic carbon, as indicated by the boxed areas.

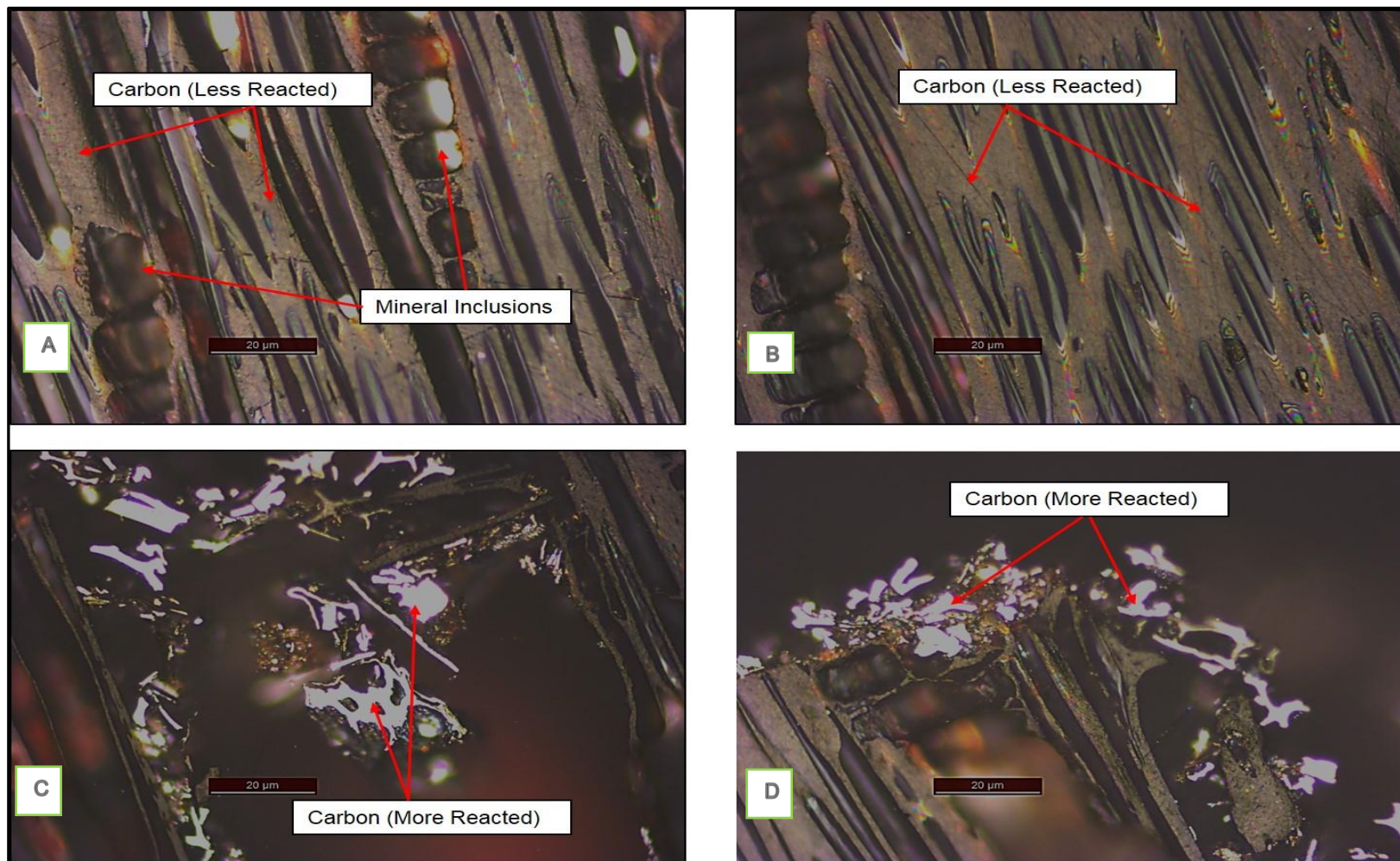


Figure 9.5: Photomicrographs of Unconventional Reductant (D) Particle 1(A, B, C & D).

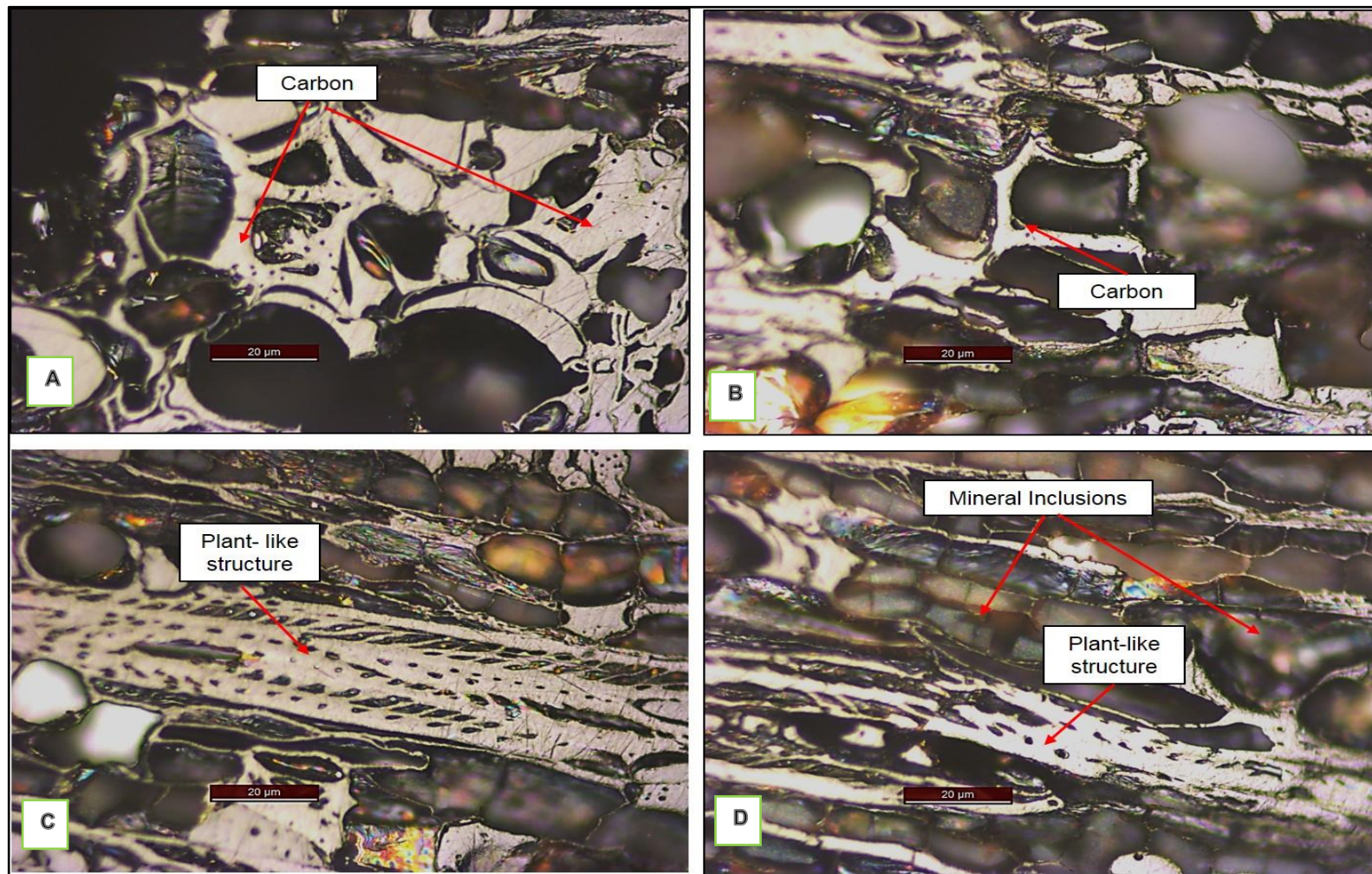


Figure 9.6: Photomicrographs of Unconventional Reductant (D) Particle 2(A, B, C & D).

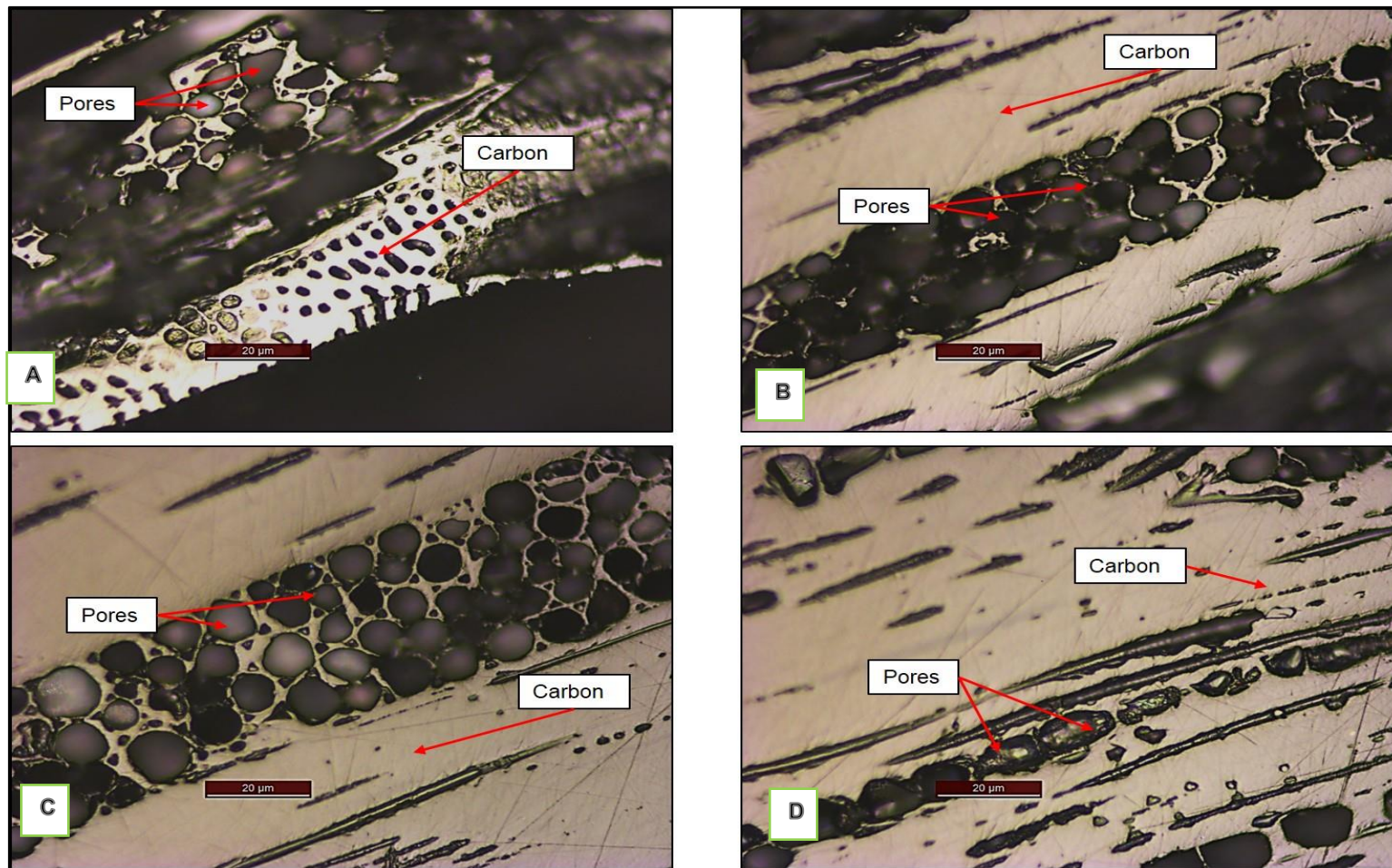


Figure 9.7: Photomicrographs of Unconventional Reductant (D) Particle 3(A, B, C & D).

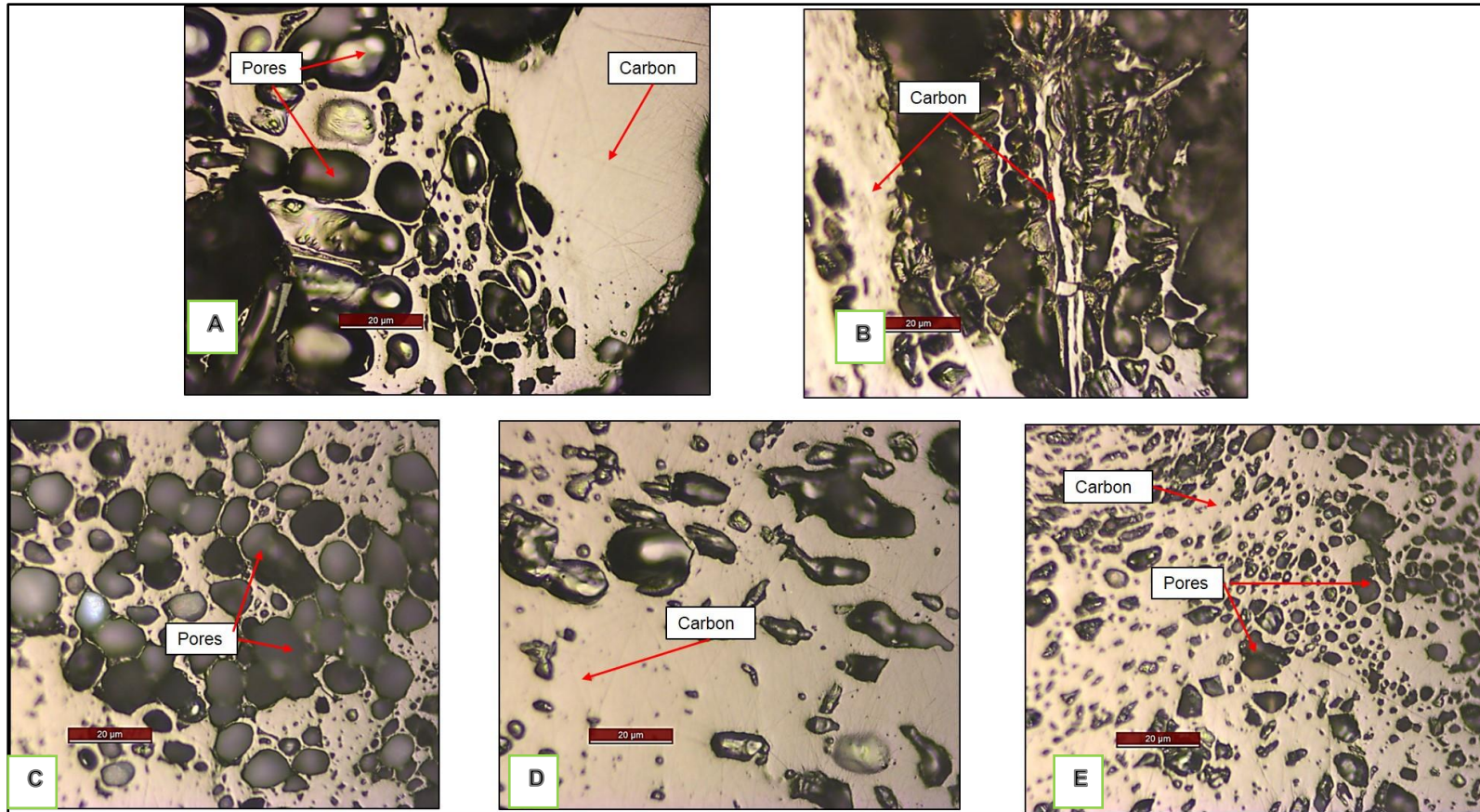


Figure 9.8: Photomicrographs of Unconventional Reductant (D) Particle 5(A, B, C, D & E)

8.5 Appendix E: TGA Raw Data

Table 9.3: 1100°C TGA Test Raw Data

TGA Isothermal Test-1100°C										
Time(Hr)	Reductant A		Reductant B		Reductant B1		Reductant C		Reductant D	
	%mass loss	% mass	%mass loss	% mass	%mass loss	% mass	%mass loss	% mass	%mass loss	% mass
0.00	0.00	100.00	0.00	100.00	0.00	100.00	0.17	99.83	0.00	100.00
0.17	2.20	97.80	0.59	99.41	0.43	99.57	7.22	92.78	5.59	94.41
0.33	2.53	97.47	1.09	98.91	0.66	99.34	8.31	91.69	7.48	92.52
0.50	2.77	97.23	1.52	98.48	0.90	99.10	9.23	90.77	8.50	91.50
0.67	3.00	97.00	1.95	98.05	1.13	98.87	10.09	89.91	9.45	90.55
0.83	3.20	96.80	2.31	97.69	1.30	98.70	10.84	89.16	10.30	89.70
1.01	3.33	96.67	2.68	97.32	1.46	98.54	11.56	88.44	11.14	88.86
1.17	3.43	96.57	2.97	97.03	1.59	98.41	12.14	87.86	11.77	88.23
1.33	3.53	96.47	3.30	96.70	1.69	98.31	12.72	87.28	12.37	87.63
1.50	3.63	96.37	3.60	96.40	1.79	98.21	13.23	86.77	12.86	87.14
1.67	3.73	96.27	3.87	96.13	1.89	98.11	13.75	86.25	13.35	86.65
1.83	3.80	96.20	4.16	95.84	1.99	98.01	14.23	85.77	13.77	86.23
2.00	3.90	96.10	4.39	95.61	2.09	97.91	14.67	85.33	14.20	85.80
2.17	3.97	96.03	4.69	95.31	2.19	97.81	15.11	84.89	14.62	85.38
2.33	4.03	95.97	4.92	95.08	2.29	97.71	15.52	84.48	14.97	85.03
2.50	4.10	95.90	5.15	94.85	2.36	97.64	15.93	84.07	15.28	84.72
2.67	4.17	95.83	5.39	94.61	2.39	97.61	16.28	83.72	15.60	84.40
2.83	4.23	95.77	5.58	94.42	2.49	97.51	16.65	83.35	15.92	84.08
3.01	4.30	95.70	5.82	94.18	2.56	97.44	17.03	82.97	16.20	83.80
3.17	4.33	95.67	5.98	94.02	2.66	97.34	17.34	82.66	16.44	83.56
3.33	4.37	95.63	6.18	93.82	2.72	97.28	17.68	82.32	16.69	83.31
3.50	4.43	95.57	6.34	93.66	2.79	97.21	17.99	82.01	16.90	83.10
3.67	4.43	95.57	6.51	93.49	2.86	97.14	18.33	81.67	17.11	82.89
3.83	4.50	95.50	6.67	93.33	2.89	97.11	18.60	81.40	17.29	82.71
3.99	4.53	95.47	6.81	93.19	2.96	97.04	18.91	81.09	17.46	82.54

Table 9.4: 1200°C TGA Test Raw Data

TGA Isothermal Test -1200°C										
Time(HR)	Reductant A		Reductant B		Reductant B1		Reductant C		Reductant D	
	%mass loss	% mass	%mass loss	% mass	%mass loss	% mass	%mass loss	% mass	%mass loss	% mass
0.00	0.07	99.93	0.00	100.00	0.00	100.00	0.03	99.97	0.00	100.00
0.17	1.32	98.68	0.66	99.34	0.43	99.57	1.76	98.24	3.22	96.78
0.33	1.98	98.02	1.75	98.25	1.04	98.96	3.02	96.98	5.51	94.49
0.50	2.54	97.46	2.54	97.46	1.60	98.40	4.13	95.87	7.14	92.86
0.66	3.14	96.86	3.14	96.86	2.07	97.93	4.98	95.02	8.44	91.56
0.83	3.66	96.34	3.57	96.43	2.51	97.49	5.72	94.28	9.53	90.47
1.00	4.13	95.87	3.93	96.07	2.87	97.13	6.37	93.63	10.40	89.60
1.16	4.59	95.41	4.20	95.80	3.24	96.76	6.99	93.01	11.12	88.88
1.33	5.02	94.98	4.46	95.54	3.54	96.46	7.54	92.46	11.70	88.30
1.50	5.41	94.59	4.66	95.34	3.84	96.16	8.07	91.93	12.17	87.83
1.66	5.74	94.26	4.86	95.14	4.11	95.89	8.55	91.45	12.54	87.46
1.83	6.07	93.93	5.09	94.91	4.38	95.62	9.04	90.96	12.86	87.14
1.99	6.40	93.60	5.25	94.75	4.58	95.42	9.50	90.50	13.08	86.92
2.16	6.70	93.30	5.42	94.58	4.81	95.19	9.92	90.08	13.22	86.78
2.33	7.00	93.00	5.58	94.42	5.08	94.92	10.37	89.63	13.30	86.70
2.49	7.26	92.74	5.75	94.25	5.28	94.72	10.76	89.24	13.33	86.67
2.66	7.49	92.51	5.88	94.12	5.52	94.48	11.15	88.85	13.33	86.67
2.83	7.76	92.24	6.05	93.95	5.75	94.25	11.54	88.46	13.30	86.70
3.00	7.99	92.01	6.18	93.82	5.95	94.05	11.90	88.10	13.22	86.78
3.17	8.18	91.82	6.31	93.69	6.15	93.85	12.23	87.77	13.12	86.88
3.33	8.42	91.58	6.44	93.56	6.35	93.65	12.55	87.45	13.01	86.99
3.50	8.61	91.39	6.57	93.43	6.52	93.48	12.91	87.09	12.90	87.10
3.66	8.84	91.16	6.67	93.33	6.65	93.35	13.24	86.76	12.75	87.25
3.83	9.01	90.99	6.74	93.26	6.82	93.18	13.53	86.47	12.57	87.43
4.00	9.17	90.83	6.84	93.16	6.95	93.05	13.79	86.21	12.39	87.61

Table 9.5: 1300°C TGA Test Raw Data

TG Isothermal Test -1300°C										
Time(Hr)	Reductant A		Reductant B		Reductant B1		Reductant C		Reductant D	
	%mass loss	% mass	%mass loss	% mass	%mass loss	% mass	%mass loss	% mass	%mass loss	% mass
0.00	0.00	100.00	0.02	99.98	0.00	100.00	0.00	100.00	0.03	99.97
0.17	3.65	96.35	1.53	98.47	1.24	98.76	3.52	96.48	12.00	88.00
0.33	6.31	93.69	3.72	96.28	3.78	96.22	6.08	93.92	15.23	84.77
0.50	8.25	91.75	5.17	94.83	5.78	94.22	7.98	92.02	17.40	82.60
0.67	9.83	90.17	6.25	93.75	7.38	92.62	9.47	90.53	18.90	81.10
0.83	11.11	88.89	7.17	92.83	8.69	91.31	9.57	90.43	20.05	79.95
1.00	12.20	87.80	7.94	92.06	9.86	90.14	10.74	89.26	20.94	79.06
1.17	13.12	86.88	8.60	91.40	10.96	89.04	11.73	88.27	21.65	78.35
1.33	13.97	86.03	9.19	90.81	11.83	88.17	12.76	87.24	22.29	77.71
1.50	14.69	85.31	9.76	90.24	12.73	87.27	13.56	86.44	22.84	77.16
1.67	15.35	84.65	10.29	89.71	13.53	86.47	14.33	85.67	23.31	76.69
1.83	15.98	84.02	10.76	89.24	14.23	85.77	15.02	84.98	23.72	76.28
2.00	16.47	83.53	11.19	88.81	14.90	85.10	15.69	84.31	24.06	75.94
2.17	16.96	83.04	11.62	88.38	15.50	84.50	16.85	83.15	24.40	75.60
2.33	17.42	82.58	12.00	88.00	16.10	83.90	17.35	82.65	24.71	75.29
2.50	17.82	82.18	12.33	87.67	16.64	83.36	17.85	82.15	25.05	74.95
2.67	18.15	81.85	12.64	87.36	17.14	82.86	18.32	81.68	25.32	74.68
2.83	18.51	81.49	12.94	87.06	17.57	82.43	18.75	81.25	25.56	74.44
3.00	18.80	81.20	13.17	86.83	18.01	81.99	19.15	80.85	25.80	74.20
3.17	19.10	80.90	13.39	86.61	18.44	81.56	19.55	80.45	26.00	74.00
3.33	19.39	80.61	13.56	86.44	18.84	81.16	19.88	80.12	26.20	73.80
3.50	19.66	80.34	13.74	86.26	19.21	80.79	20.24	79.76	26.41	73.59
3.67	19.92	80.08	13.88	86.12	19.51	80.49	20.54	79.46	26.58	73.42
3.83	20.15	79.85	14.01	85.99	19.88	80.12	20.84	79.16	26.78	73.22
4.00	20.38	79.62	14.13	85.87	20.15	79.85	21.14	78.86	26.95	73.05

Table 9.6: 1400°C TGA Test Raw Data

TGA Isothermal Test -1400°C										
Time(hr)	Sample ID									
	Reductant A		Reductant B		Reductant B1		Reductant C		Reductant D	
	%mass loss	% mass	%mass loss	% mass	%mass loss	% mass	%mass loss	% mass	%mass loss	% mass
0.00	0.03	99.97	0.03	99.97	0.03	99.97	0.03	99.97	0.49	99.51
0.17	6.62	93.38	6.16	93.84	4.84	95.16	7.54	92.46	8.12	91.88
0.33	11.95	88.05	12.15	87.85	9.72	90.28	14.12	85.88	12.20	87.80
0.50	15.31	84.69	16.24	83.76	13.12	86.88	18.12	81.88	14.67	85.33
0.67	17.67	82.33	19.44	80.56	15.73	84.27	20.83	79.17	16.24	83.76
0.83	19.44	80.56	21.97	78.03	17.73	82.27	21.96	78.04	17.15	82.85
1.00	20.77	79.23	23.93	76.07	19.33	80.67	22.63	77.37	17.52	82.48
1.17	21.80	78.20	25.53	74.47	20.57	79.43	23.10	76.90	17.44	82.56
1.33	22.70	77.30	26.76	73.24	21.57	78.43	23.40	76.60	17.27	82.73
1.50	23.50	76.50	27.69	72.31	22.40	77.60	23.70	76.30	17.11	82.89
1.67	24.19	75.81	28.42	71.58	23.14	76.86	23.90	76.10	17.02	82.98
1.83	24.86	75.14	29.02	70.98	23.84	76.16	24.10	75.90	16.86	83.14
2.00	25.49	74.51	29.52	70.48	24.44	75.56	24.16	75.84	16.65	83.35
2.17	26.09	73.91	29.99	70.01	25.01	74.99	24.33	75.67	16.53	83.47
2.33	26.66	73.34	30.36	69.64	25.51	74.49	24.40	75.60	16.36	83.64
2.50	27.19	72.81	30.69	69.31	26.01	73.99	24.60	75.40	16.24	83.76
2.67	27.69	72.31	30.99	69.01	26.48	73.52	24.67	75.33	16.08	83.92
2.83	28.15	71.85	31.25	68.75	26.88	73.12	24.47	75.53	15.83	84.17
3.00	28.59	71.41	31.49	68.51	27.28	72.72	24.13	75.87	15.58	84.42
3.17	28.99	71.01	31.65	68.35	27.65	72.35	24.06	75.94	15.25	84.75
3.33	29.35	70.65	31.85	68.15	27.98	72.02	23.80	76.20	15.00	85.00
3.50	29.69	70.31	32.02	67.98	28.35	71.65	23.70	76.30	15.00	85.00
3.67	29.99	70.01	32.19	67.81	28.58	71.42	23.60	76.40	15.05	84.95
3.83	30.25	69.75	32.32	67.68	28.68	71.32	23.36	76.64	15.13	84.87
4.00	30.48	69.52	32.45	67.55	28.68	71.32	20.66	79.34	15.25	84.75

8.6 Appendix F: TGA Product Analysis Results

Table 9.7: TGA Products Chemical Speciation Results (% mass- Oxides)

TGA Test	Al ₂ O ₃	CaO	Cr ₂ O ₃	FeO	MgO	MnO	SiO ₂
A/ 1100°C	11.40	0.79	30.50	22.10	10.8	0.19	10.00
A/ 1200°C	11.60	0.80	30.70	22.40	11.00	0.19	10.00
A/ 1300°C	12.10	0.90	32.60	23.70	11.30	0.21	10.50
A/ 1400°C	13.60	0.93	36.50	26.00	12.00	0.23	11.40
B/ 1100°C	11.50	0.81	29.10	21.40	10.50	0.19	12.10
B/ 1200°C	12.20	0.80	30.90	22.40	11.20	0.20	12.60
B/ 1300°C	13.50	0.97	35.00	25.00	12.10	0.24	13.70
C/ 1100°C	11.80	1.01	28.40	20.30	10.90	0.18	11.60
C/ 1200°C	12.50	1.02	30.20	21.50	11.30	0.19	12.10
C/ 1400°C	13.90	1.11	33.50	24.70	12.30	0.21	6.55
D/ 1100°C	13.00	0.99	41.50	26.00	9.79	0.23	6.36
D/ 1100°C	13.10	1.54	40.90	25.60	9.82	0.24	6.92
D/ 1100°C	13.30	1.17	43.50	26.00	10.00	0.25	6.40
D/ 1100°C	13.50	1.31	42.20	26.30	10.30	0.26	6.15

Table 9.8: TGA Products Chemical Speciation Results (Oxides)

FECR_SLAGS

Type	(°C)	Al ₂ O ₃	CaO	Cr ₂ O ₃	FeO	MgO	MnO	SiO ₂	TiO ₂
A	1100	11.50	0.80	30.60	22.25	10.90	0.19	10.00	0.60
A	1200	12.10	0.90	32.60	23.70	11.30	0.21	10.50	0.62
A	1300	13.60	0.93	36.50	26.00	12.00	0.23	11.40	0.71
A	1400	15.47	0.91	41.54	29.41	14.26	0.26	13.51	0.78
B	1100	11.50	0.81	29.10	21.40	10.50	0.19	12.10	0.61
B	1200	12.15	0.80	30.65	22.35	11.30	0.20	12.70	0.65
B	1300	13.50	0.97	35.00	25.00	12.10	0.24	13.70	0.74
B	1400	15.10	0.95	37.52	26.32	13.56	0.26	15.11	0.78
C	1100	11.80	1.01	28.40	20.30	10.90	0.18	11.60	0.61
C	1200	12.50	1.02	30.20	21.50	11.30	0.19	12.10	0.64
C	1300	15.74	1.13	38.25	26.45	13.50	0.25	13.93	0.78
C	1400	13.90	1.11	33.50	24.70	12.30	0.21	6.55	0.71
D	1100	13.00	0.99	41.50	26.00	9.79	0.23	6.36	0.69
D	1200	13.10	1.54	40.90	25.60	9.82	0.24	6.92	0.69
D	1300	13.30	1.17	43.50	26.00	10.00	0.25	6.40	0.75
D	1400	13.50	1.31	42.20	26.30	10.30	0.26	6.15	0.71
B1	1100	13.60	0.40	39.40	23.50	9.68	0.20	5.94	0.72
B1	1200	13.50	0.53	39.70	24.20	10.00	0.21	5.54	0.74
B1	1300	14.40	0.53	42.80	24.80	10.60	0.22	5.98	0.80
B1	1400	14.70	0.58	43.30	23.20	10.50	0.22	6.51	0.82

Table 9.9: TGA Products XRD results (mass %)

Phase	Ideal Chemical Formula	A	B	C	D
Chromite	FeCr ₂ O ₄	7.3	12.85	24.2	58.3
Iron	Fe	5.6	10.02	0.4	24.3
Chromium	Cr	-	0.09	-	3.8
Mullite	3Al ₂ O ₃ 2SiO ₂ / 2Al ₂ O ₃ SiO ₂	2.6	-	-	5.6
Wüstite	FeO	0.5	-	<0.1	2.2
Graphite	C	46	15.52	4.1	-
Olivine	(Fe, Mg) ₂ SiO ₄	17.9	-	-	-
Spinel	MgAl ₂ O ₄	20.1	21.9	43.3	-
Hematite	Fe ₂ O ₃	-	0.13	17.6	3.1
Cristobalite	SiO ₂	-	-	10.5	2.6
Tridymite	SiO ₂	-	-	-	-
Quartz	SiO ₂	-	0.61	-	-
Carbon	C	-	18.74	-	-
Fosterite	Mg ₂ SiO ₄	-	16.75	-	-
Iron chromium-carbide	FeCrC	-	0.94	-	-
Suessite	Fe, Ni ₃ Si	-	2.44	-	-
Total		100	100	100	100

Table 9.10: TGA Products Chemical Analysis of SEM Phases Present (mass %).

Phases	O	Cr	Fe	Al	Si	Mg	Ti	Ca	
1	33.0	48.6	6.9	10.6	-	0.1	0.8	-	spinel
2	0.1	13.4	86.5	-	-	-	-	-	Iron-chrome
3	0.1	11.7	88.2	-	-	-	-	-	Iron-chrome
4	0.5	39.4	58.5	-	1.7	-	-	-	Iron-chrome
5	49.5	6.6	-	16.7	12.1	0.1	3.2	11.8	glass
6	0.7	86.8	12.5	-	-	-	-	-	chrome-iron
7	-	88.7	11.3	-	-	-	-	-	chrome-iron
8		35.8	62.8		1.5	-	-		Iron-chrome
9	30.7	35.2	23.9	9.1	-	-	0.9	-	chromite
10	0.57	58.3	39.5		1.6	-		-	chrome-iron
11	49.0	8.9	0.4	39.9	-	0.2	1.7	-	spinel
12	-	75.3	24.7	-	-	-	-	-	chrome-iron
13	30.9	35.1	23.4	9.7	-	-	0.9	-	chromite
14	-	70.9	27.3	-	1.0	-	0.7	-	chrome-iron
15	60.2	2.7	5.2	1.4	30.4	0.1	-	-	silicate
16	46.3	-	-	15.8	25.8	-	-	12.1	glass

-: Analyte was not detected

Table 9.11: TGA Products Iron Speciation (mass %) and %DOR & %DOM for repeats

Test (°C)	Fe ⁰	Fe ²⁺	Fe ³⁺	Fe total	%DOR	%DOM
C/1400	7.40	0.80	10.56	18.75	38.99	39.44
B1/1100	<0.05	0.26	17.52	18.28	0.14	2.74
D/1100	0.58	0.28	18.44	19.30	0.43	3.01
D/1200	2.38	0.56	16.51	19.45	10.44	12.23

<0.05: the analyte content is below the 0.05% detection limit of the analytical method for the particular analyte

Table 9.12: TGA Products Chromium Speciation (mass %) and %DOR & %DOM for repeats

Test (°C)	Cr ⁰	Cr ³⁺	Cr total	%DOR	%DOM
A/1100	0.58	26.37	26.95	0.94	0.85
B/1100	0.60	26.55	27.15	1.00	0.92
C/1100	0.52	28.76	29.28	0.56	0.58
D/1200	1.80	27.82	29.62	4.92	4.90